UNIVERSITÉ DU QUÉBEC

MÉMOIRE PRÉSENTÉ À

L'UNIVERSITÉ DU QUÉBEC À CHICOUTIMI

COMME EXIGENCE PARTIELLE

DE LA MAÎTRISE EN INGÉNIERIE

Par

Afet Ayşegül Osma

Modélisation mathématique du traitement thermique du bois à haute température

(Mathematical Modelling of the Thermal Treatment of Wood at High Temperatures)

Avril 2005

Canım Anneme
ve
Canım Babama

RÉSUMÉ

Dans un procédé de traitement thermique du bois à haute température, le bois est chauffé à des températures entre 180°C et 250°C et ce, selon l'essence à traiter et les propriétés physico-mecaniques désirées. Le procédé a pour but de diminuer le comportement hydrophile du bois par une modification tridimensionnelle de sa structure chimique à l'aide d'un traitement thermique dans une atmosphère contrôlée. Le traitement du bois à haute température fut développé en Europe et récemment introduit en Amérique du Nord. La technologie est par conséquent très nouvelle au Canada et plusieurs activités de recherches furent amorcées afin de mieux comprendre et d'améliorer le procédé et ces différents facteurs d'influence.

L'objectif de la recherche consiste en la réalisation d'un modèle mathématique, basé sur des principes physiques et chimiques fondamentaux, permettant de simuler l'évolution et l'interaction des différents paramètres du procédé, de même que des propriétés finales du bois lors d'un traitement à haute température. Le modèle simule le transfert de quantité de mouvement, de chaleur et de masse et ce, de façon simultanée, en régime transitoire. Il permet de prédire les changements d'humidité et de température aux points désirés d'un maillage dans le bois lors d'un traitement. Le principal avantage du modèle est de permettre une foule de simulations en vue d'optimiser les différents paramètres du procédé tout en ayant une idée de l'impact sur les propriétés finales du bois sans pour autant avoir à réaliser l'ensemble de ces essais en laboratoire.

La première étape dans la réalisation du projet a consisté en une recherche bibliographique sur la structure et les propriétés du bois, sur la relation entre l'humidité et le bois, sur les changements chimiques favorisés par le traitement à haute température et sur le transfert de chaleur et de mass couplé. Un modèle préliminaire d'écoulement de gaz en régime permanent (3D), où l'accent a été mis sur les configurations des injecteurs et du

bois dans le four, a permis de mettre en évidence les vitesses d'écoulement entre les rangées de bois. Un autre modèle d'écoulement (3D) a permis de mettre en évidence la distribution des gaz dans le four. À l'aide de ce modèle, différentes configurations furent simulées (vitesses et angles d'injection des gaz, géométrie du four) afin d'obtenir des conditions d'écoulement plus uniformes. Le changement de design des injecteurs a permis une nette amélioration quant aux régimes d'écoulement dans le four. Un modèle transitoire unidimensionnel de transfert de chaleur dans le bois fut combiné avec un modèle tridimensionnel de transfert de quantité de mouvement et de chaleur dans les gaz. La distribution modélisée de température dans le bois fut comparée avec des mesures industrielles. La dernière étape de modélisation fut de réaliser un modèle couplé unidimensionnel de transfert de chaleur et de masse dans le bois en simulant comme conditions environnante, un modèle tridimensionnel en régime transitoire de transfert de quantité de mouvement, de chaleur et de masse. Cette modélisation a permis de simuler la distribution de la température et de l'humidité dans le bois et dans le gaz.

La présente étude a permis de conclure que la distribution des gaz dans le four n'est pas uniforme. Cette conclusion a pour conséquence que la distribution des températures et de l'humidité dans les gaz et dans le bois n'est également pas uniforme. Les résultats du modèle furent validés avec des données de l'industrie et démontrent une bonne représentativité.

Les modifications géométriques et opérationnelles suggérés tendent à améliorer l'uniformité de produit finale. D'autres projets de recherche ont permis et permettront de valider expérimentalement l'ensemble des concepts d'optimisation suggérés dans cette étude.

ABSTRACT

In the high temperature heat treatment process, wood is subjected to temperatures ranging from approximately 180°C to 250°C depending the type of the species and desired physico-mechanical characteristics. The process aims to reduce the hydrophilic behavior of wood by the three-dimensional modification of its chemical structure through heat treatment in a controlled atmosphere. The high temperature heat treatment of wood was previously developed in Europe and recently introduced to the North America. The technology is new in Canada and several research activities have been started in order to better understand the process and its parameters and to improve them.

This research work's objective is to develop a mathematical model based on fundamental engineering principles and to analyze the process parameters and the final properties of wood in order to establish a relationship between them during the high temperature heat treatment of wood. The model simulates the unsteady state flow, heat and mass transport phenomena occurring simultaneously in the heat treatment unit and predicts the change of moisture content and temperature at designated mesh points in the wood during the treatment. The main advantage of the model is that the effect of the possible modifications in the process parameters on the final properties of wood can be determined without extensive experimentation.

As a first step of the project, a detailed literature research was carried out on wood structure, properties, moisture relations, chemical changes caused by the treatment and coupled heat and mass transfer. The preliminary 3D steady-state flow models focusing on the gas injection and wood packing configuration gave a good idea of the gas velocity at injection and between the wood channels. Then a 3D steady state flow model of the furnace predicts the distribution of the gas in the whole furnace. Different injection velocities, angles, and furnace modifications were modelled in order to obtain uniform flow

conditions. The best gas distribution was obtained with the new injection geometry. A 1D unsteady-state heat transfer model of wood was introduced into the 3D unsteady-state heat transfer and flow model of gas; and the temperature distribution in the wood was calculated. Finally the 1D unsteady-state coupled heat and mass transfer model of wood is added to the 3D unsteady-state flow, heat and mass transfer model of gas. The temperature and humidity distributions in the wood and in the gas were obtained.

This study showed that the distribution of the gas is not uniform in the furnace. As a result of the non-uniform flow, the temperature and humidity distributions in the gas and in the wood are not uniform. The model results are validated with the available plant data. The results, temperature profile in the wood and the final moisture content of the wood, are in good agreement with the experimental results.

The considered and suggested modifications in this work became the subject of other research activities and tested experimentally. The geometrical and operational modifications seemed to improve the final product uniformity.

ACKNOWLEDGEMENTS

I wish to express my sincere thanks to my advisor Dr. Duygu Kocaefe, and co-advisor Dr. Yaşar Kocaefe for their scientific and personnel teachings, suggestions, criticism, and supports. Their office door was always open, and I learnt a lot from them. My gratitude is also given to the other members of my committee; Dr. Andre Charette and Mr. Peter Waite for their valuable time and feedback.

I am also indebted to Dr. Marcel Paquet and Dr. László Kiss for their interest and advices. I would like to thank Andre Falgueyret, Danny Ouellet, Gaetane Grenon, and Madeleine Potvin for their technical support and guidance. Thanks are also given to all members of CURAL and GRTB. The financial support of the University of Québec at Chicoutimi and PCI Industries is greatly appreciated.

I am very grateful to all the friends in the university: Dominique, Vincent, Sophie, Zafer, Çağla, Alex, Simon, Mathieu, Saska, Omid, Shahrooz, Dominic, Sándor, Géza, László, France, Bushra, Cristina, and Güvenç. You are the source of motivation and happiness. My gratitude is also extended to Jean. His endless support, encouragement, and motivation helped me through all the difficult times.

There are no words to adequately describe the feeling of gratitude I have for my mother and father, for their continuing encouragement, patience, support, understanding, enthusiasm, affection, and inspiration.

TABLE OF CONTENTS

LIST OF FIGURES

LIST OF TABLES

NOMENCLEATURE

a_m : mass diffusion coefficient (m^2/s)

a_q : thermal diffusivity (m^2/s)

B : body force

Bi : Biot number

C : constants

c_m : moisture capacity ($kg_m/kg_{db}°M$)

c_p : coefficient of humid air capacity (kg/kg.P)

c_q: heat capacity (J/kgK)

E_b : activation energy for water diffusion (J/mole)

D : diffusivity

Fo : Fourrier number

G :specific Gibbs free energy of water in the state under consideration (J/kg_w)

G_O :specific Gibbs free energy of water in the standard reference state (J/kg_w)

G_{BF} : production due to the body force

G_{SG} : specific gravity of wood

H : enthalpy (J/kg)

h : relative humidity

j : mass flux (kg/m^2s)

j_q : heat flux (J/m^2s)

k : turbulence kinetic energy

K(M,T) : effective water conductivity tensor

k_m: moisture conductivity (kg/ms°M)

k_p : moisture filtration coefficient

k_q: thermal conductivity (W/mK)

L : thickness of a wood slab (m)

M : moisture content

M_{MW} : Molecular weight of water (kg_w/mole)

n_n : total number of nodes

n_t : total number of time steps

P : pressure (atm)

P_{prod} : shear production

q_m : moisture flux (kg/ms)

R : universal gas constant

S : volume saturation

Sv : the molar entropy (J/molK)

T : temperature (°C,K)

t : time (s)

U : moisture potential (°M)

v : velocity (m/s)

V : volume

w_0 : the oven dry mass

x, y, z : coordinate axis

Greek Letters

α_m : convective mass transfer coefficient (kg/m^2sK)

α_q : convective heat transfer coefficient (W/m^2K)

β : turbulence dissipation rate

γ : volume fraction

δ (δ') : thermal gradient coefficient (°M/K) ($\delta = \delta'/c_m$)

ε : ratio of vapor diffusion coefficient to coefficient of total moisture diffusion

θ: permeability

κ : chemical potential (L/mol)

λ : latent heat (J/kg)

μ : viscosity (kg/ms)

ξ : exchange coefficient

ρ : density (kg/m^3)

σ : stress tensor (N/m)

φ : phase potential

φ : general variable

χ : depth scalar (m)

ψ : water potential (J/kg)

ψ_g : gravitational potential

ψ_M : matric potential

ψ_o : osmotic potential

ψ_p : pressure potential

ω : mass fraction

Matrix Notation

$[\overline{A}]$: the system matrix

$[X]_m^{p+1}$: the solution matrix

$[\overline{B}]_m$: the limiting matrix

Subscripts and Exponent

a : ambient

app : apparent

eff : effective

g : gravitational

m : mass

M : Matric

moist : moist

o : osmotic

p : previous time step

P : pressure

S :surface

q : heat

w : water

CHAPTER 1

INTRODUCTION

1.1 Background

It has been known for a long time that different intrinsic wood properties are changed due to treatment at high temperatures [1,2,3]. However, only recently in Europe several attempts were made to develop industrially applicable technology for the thermal treatment of wood. Developments mainly took place in France, Finland, Germany, and Netherlands [2,3]. What all the European heat treatment processes have in common is that wood is subjected to temperatures close to or above 200°C for several hours. The main differences between the processes are essentially in the process conditions (process steps, heating mediums, steaming, wet or dry process, use of oils, initial wood properties, etc.).

Recently, high temperature heat treatment of wood has gained a great interest in North America [3]. This interest has lead to the development of several treatment processes presently introduced to the Canadian market.

Comprehensive research on the important wood properties showed an improved durability and dimensional stability of wood [2,3,4]. These improvements are due to severe changes of the intrinsic wood chemistry, caused by the high temperatures without any additional chemicals. By this thermal modification some mechanical properties are reduced.

"Bois Perdure" is one of the wood treatment technologies based on the thermal treatment of wood at high temperature [1,2]. The heat treatment is carried out in a furnace by contacting the wood with hot combustion gases. A uniform distribution of the hot gases in the furnace is necessary to obtain good quality product with uniform properties.

1.2 Project Description

This study is aimed at developing a mathematical model of the high temperature heat treatment furnace of the Perdure Technology. The mathematical model solves the equation of motion, heat, and mass transfer simultaneously. The mathematical model is a useful tool for the simulation of heat treatment processes as well as for the monitoring and control of the following process parameters:

- flow of the hot gas (the source of heat for the wood) in the furnace,
- temperature and humidity profiles of hot gas in the treatment furnace,
- temperature and humidity profiles of wood during the treatment,
- effects of changes in furnace geometry, wood properties, and hot gas properties.

The model can be used to optimize the process in order to have a better end product.

1.3 Objectives

The global objective of the project is the modelling and simulation of the wood treatment process at high temperatures in order to understand and improve the process and the operation.

The specific objectives are:

- to examine existing heat treatment process, transfer mechanisms, and models,
- to develop a mathematical model of the furnace,
- to study the flow, heat transfer, and mass transfer occurring during operation,
- to build a numerical procedure for the solution,
- to interpret model results,
- to find geometry of the furnace and wood piles and operation conditions which will lead to better wood properties.

CHAPTER 2

LITERATURE REVIEW

2.1 Wood Treatment

Forestry is one of the major industries in North America, especially in Canada. It is also very important for the economy of the Saguenay-Lac-St.Jean region. Chemically treated wood constitutes 98% of the wood used in America for the constructional purposes [5].

This treatment which uses chromated copper arsenate (CCA) is aimed at preventing infestation by insects and other microorganisms that can cause decay and structural problems. However, CCA is classified as a known human carcinogen by Environmental Protection Agency and World Health Organization. Arsenic-treated wood has been banned in some countries, such as Switzerland, Vietnam, and Indonesia. In Canada and United States, it is also banned effective in 2005 in all the residential settings except at harbors. Now, industry is looking for safer alternatives. Heat treatment at high temperature seems to be a viable alternative to chemical treatment.

2.1.1 Chemical Treatment

Wood can be protected from the attack of decay due to fungi, harmful insects, or marine borers by applying chemical preservatives. The degree of protection achieved depends on the preservative used and the proper penetration and retention of the chemicals. Some preservatives are more effective than others, and some are more adaptable to specific application requirements. The EPA regulates pesticides, and wood preservatives are one type of pesticide. Preservatives that are not restricted by EPA are available to the general consumer for non-pressure treatments, and the sale of others is restricted to certified pesticide applicators. Wood preservatives can be divided into two general classes [6]: (1) oil-borne preservatives, such as creosote and petroleum solutions of pentachlorophenol and (2) water-borne preservatives that are applied as water solutions. Many different chemicals are present in each of these classes, and each has different effectiveness in various exposure conditions.

Oil-borne preservatives are coal-tar creosote, pentachlorophenol solutions, copper naphthenate, chlorothalonil, chlorothalonil/chlorpyrifos, oxine copper (copper-8-quinolinolate), zinc naphthenate, bis(tri-n-butyltin) oxide, 3-iodo-2-propynyl butyl carbamate, alkyl ammonium compound propiconazole, 4,5-dichloro-2-n-octyl-4-isothiazolin-3-one, tebuconazole, chlorpyrifos.

Waterborne preservatives are acid copper chromate, ammoniacal copper zinc arsenate, chromated copper arsenate, ammoniacal copper quat, copper bis (dimethyldithiocarbamate).

2.1.2 Heat Treatment

Heat treatment offers an extremely interesting ecological alternative to the chemical treatment. Wood is a renewable material, however; it is handicapped by its dimensional unstability with changing moisture content and degradation under the influence of fungi. Most water contained in a freshly cut tree must be removed before useful products can be made from the wood.

In traditional heat treatment, which is called drying, only the water is removed by heating the wood up to 120°C. Consequently, the water evaporates. Newly developed high temperature heat treatment process reduces the hydrophilic behavior of the wood by the three-dimensional modification of the chemical structure of some of its components through controlled atmosphere without the use of any chemical substance of external origin.

2.1.3 High Temperature Heat Treatment

This process was initiated in Europe. Many methods of thermal modification of wood have been developed in France, Finland, Germany, and Netherlands. Since the processes were complicated in large scale production because of the high temperature, the treatment has not been commercialized for a long time [2, 3, 4,].

High temperatures over 150°C alter the physical and chemical properties of wood permanently in such way that;

- the shrinkage and swelling of the wood are reduced,
- the equilibrium moisture content of the wood is improved,
- the strength properties start to weaken,
- the resistance to rot is improved,
- the susceptibility to fungal decay is reduced, and
- the color of the wood darkens.

Different heat treatment processes [2, 3] developed mainly in Europe are presented in the following sections.

Heat Treatment in France:

In France, there are two process developed: "Retification" and "Bois Perdure" **[1, 2, 3, 4]** . Main differences between these processes are initial humidity requirement of the wood and the heating medium. What both treatments have in common is that solid wood is subjected to temperatures close to or above 200˚C for several hours in an atmosphere with low oxygen content.

In the retification process, the previously dried wood (around 12%) is heated slowly up to 210-240ºC in a nitrogen atmosphere with less than 2% oxygen.

The process "Bois Perdure" can be started with fresh wood. After an artificial drying period, the wood is heated up to 230ºC under steam atmosphere.

Four-stage treatment (7-16 hours) is as follows:

- Preheating (→ 100-120˚C);
- Drying at constant temperature;
- Heating (→ 200-230˚C);
- Cooling.

In North America, the Pluri Capital Industries (PCI) is the owner of this technology.

Heat Treatment in Finland:

The technology is called ThermoWood. Today in Finland, eight heat treatment plants with 35,000 m^3/year production (2000) are operating **[1, 2, 3, 4]**. Wood load is heated with air (<3.5%) and steam which prevents the wood from burning. Gas circulation is achieved with fans with 10m/s velocity.

Three steps of the process are;

- Temperature increase period (48 hours); Preliminary warm up (→ 100°C), kiln drying (100-150°C), temperature rise (150°C→);
- Actual heat treatment period (0.5-4 hours); temperature is kept between 150°C to 240°C. Temperature and duration are important for final product;
- Cooling and stabilizing period (24 hours); temperature decreases to room temperature.

During the process, it is important for the quality of the final product that there is not a large temperature difference between the wood and gas. Water vapor content in the gas acts as a protective atmosphere. The duration of the process and the initial humidity content affect also the quality.

There are three Finnish equipment supplier companies, which are members of "Finnish ThermoWood Association"; *Tekmaheat Oy, Stellac Oy, and Valutec Oy.*

Heat Treatment in Germany:

The heat treatment takes place in vegetal oil instead of air and steam. That is why this technology is called Oil Heat Treatment [2, 3, 4]. The purpose is to supply 100% oxygen free atmosphere and a fast heat transfer. The oil temperature is around 200-230°C during the treatment. The wood load size determines the treatment period. For 2 inch x 4 inch woods, heating is one hour, actual treatment is 3-4 hours, and cooling is 2 hours. For 4 inch x 4 inch woods, the whole procedure takes 18-24 hours.

Heat Treatment in Netherlands:

In Plato Process, wood is treated in water vapor at the pressure of 6-8 bars [2, 3, 4]. Wood is pre-dried.

The stages of the treatment process are as follows:

- Hydrotermolysis (4-5 hours); heat treatment of wood at temperatures between 160°C-190°C at super-atmospheric pressure;
- An intermediate drying process (3-5 hours); drying of the treated wood to lower the moisture content (10%);
- Curing (14-16 hours); heat treatment of wood at temperatures between 170°C-190°C;
- Conditioning (2-3 days).

Heat Treatment in Austria:

The Thermoholz Process [2, 3, 4] treats pre-dried wood (8-12%) in air at five stages:

- Temperature increase period (3-10 hours) (→ 100°C);
- Drying at constant temperature (3-24 hours);
- Second temperature increase period (3-10 hours) (→ 160-220°C);
- Thermo treatment at constant temperature (2-10 hours);
- Cooling (3-10 hours).

Heat Treatment in Switzerland:

The Intemporis Process [2, 3, 4] is based on heating pre-dried wood at high temperatures, 200°C, by using air. Water vapor is used as shielding gas.

The process steps are:

- Temperature increase period I (8 hours) (→ 140°C);
- Temperature increase period II (4 hours) (→ 160°C);
- Temperature increase period III (2 hours) (→ 180°C);
- Temperature increase period IV (1 hours) (→ 200°C);
- Temperature stabilization period at 200°C and 80 bars (3 hours);
- Cooling (2 hours).

Heat Treatment in Denmark:

The Iwotech Process [2, 3, 4] is the heat treatment of wood in air + water vapor atmosphere at high pressure for 3-6 hours.

In Table 2.1 patent number for each one of the technology is given with the patent titles. The existing high temperature heat treatments are summarized in Table 2.2.

Table 2.1 *Patents Titles and Numbers for Different Technologies* [4]

Patent No	**Patent Title**	**Technology**
FR 2604942	Methods for manufacturing a lignocellulosic material by heat treatment and material obtained by this method	Retification
CA 2232971	Method for treating wood at the lass transition temperature thereof	Retification
CA 2232974	Wood curing method	Retification
CA 2269904	Method for heating wood by impregnation	Retification
CA 2274944	Apparatus and process for the heat treatment of lignocellulosic material	Bois Perdure
CA 2162374	Method for improving biodegradation resistance and dimensional stability of cellulosic products	ThermoWood
CA 2289867	Wood treatment process	Oil Heat Treat.
CA 2112937	Process for upgrading low-quality wood	Plato Process
CA 2224031	Process for preparing cellulosic fibrous aggregates	Plato Process
FR 0308259	Apparatus and process for the high temperature heat treatment of lignocellulosic material	Imtemporis
CA 2392159	Method and device for treating wood and similar materials	Iwotech

Table 2.2 *Summary of High Temperature Heat Treatments* [3]

Process	Pre-Drying	Type of Energy For Heating	Type of Installation	Treatment Temperature	Heating Medium	Pressure Change	Duration	Capacity	Investment for One Unit of Treatment
ThermoWood	Preferred	Electricity/Oil Thermal/Vapor	Furnace	230°C	Air+Steam	No	~3 Days	Medium/Large	++/+++
Perdure	Preferred	Gas	Furnace	220°C	Air+Steam	No	7-16 Hours	Weak	++
Retification	Yes	Electricity/Gas	Furnace	245°C	Air	No	8-10 Hours	Weak	++
Plato	Yes	Steam	Autoclave/ Dryer/Furnace	180°C	Air+Steam	Yes	16-21 Hours	Large	++++
OHT	Yes	Electricity/Oil Thermal/Vapor	Impregnation unit	220°C	Vegetal Oil	Yes	~8 Hours	Weak	++
Thermoholz	Yes	Oil Thermal	Furnace	220°C	Air	No	25-27 Hours	Weak/Medium	++
Intemporis	Yes	Gas	Furnace	200°C	Air	Yes	20-25 Hours	Weak	++
Iwotech	Yes	Steam	Impregnation unit	210°C	Air+Steam	Yes	3-6 Hours	Weak	++

\+ Order of several hundred thousands CAD

++ Order of million CAD

+++ Order of ten millions CAD

++++ Order of several millions CAD

More detailed description of "Bois Perdure" technology is given in the following section since the research work is mainly focused on the modeling of the Perdure technology furnace.

2.1.4 Bois Perdure

Perdure Technology is new in North America. There was one furnace constructed at the end of 2002 at St. Ambroise, Quebec for production. Another furnace was constructed at the end of 2003 at UQAC for research purposes. Now there are more high temperature treatment furnaces (Rivière-du-Loup, Dolbeau), and constructions of others are being considered. In Figure 2.1, a heat treatment furnace from France is seen [7].

Figure 2.1 *Wood Heat Treatment Furnace* [7]

In Figure 2.2, a Perdure Technology furnace is shown [1] in more detail.

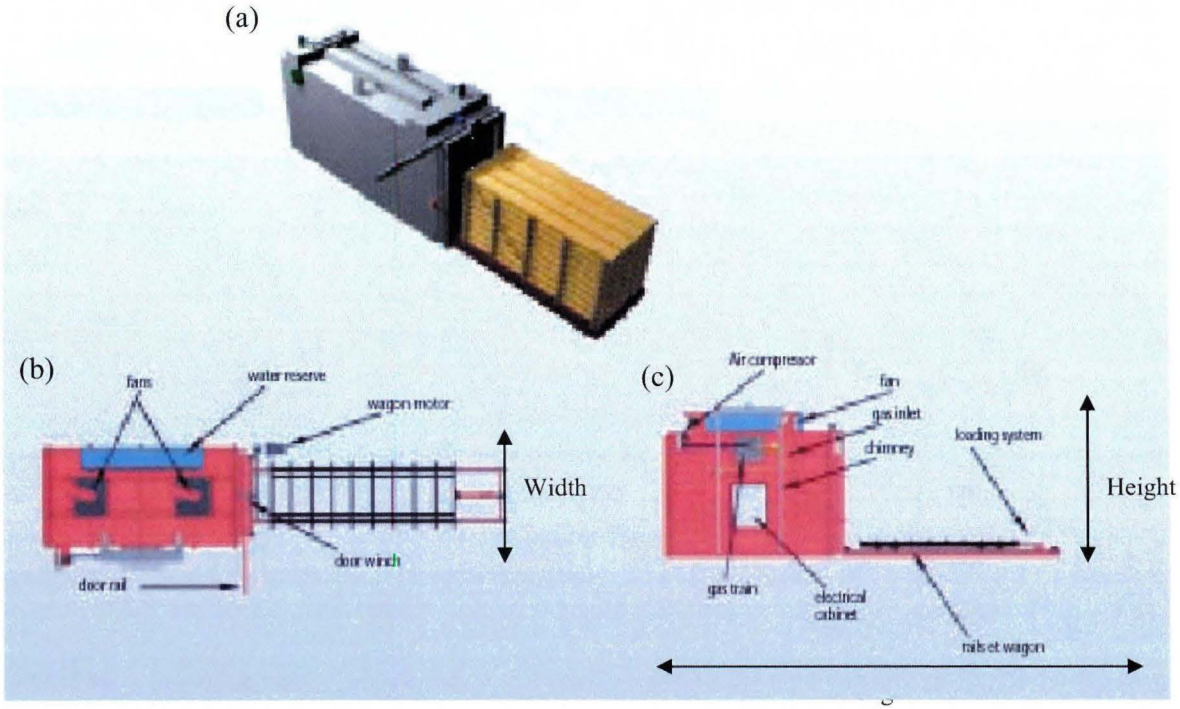

Figure 2.2 *a) Furnace General View, b) Furnace Top View, c) Furnace Side View* **[1]**

The dimensions of two treatment units are given in Table 2.3.

Table 2.3 *Furnace Dimensions* [1]

		PC5	PC6
Exterior Dimensions	Length	16,315 mm	17,315 mm
	Width	2,595 mm	2,595 mm
	Height	5,300 mm	5,300 mm
Interior Dimensions	Length	5,500 mm	6,500 mm
	Width	1,543 mm	1,543 mm
	Height	2,500 mm	2,500 mm
Dimensions of the Load	Length	5,250 mm	6,250 mm
	Width	1,250 mm	1,250 mm
	Height	2,000 mm	2,000 mm
Wagon	Length	5,250 mm	6,250 mm
	Width	1,350 mm	1,350 mm
	Height	2,200 mm	2,200 mm
Maximum Theoretical Capacity Per Year		5,250 m3	6,300 m3
Production Capacity by Treatment Cycle		8.75 m3	10.5 m3

The wood slabs are piled on a wagon which carries them into the furnace, as shown in Figure 2.2; 2 inch x 4 inch or 2 inch x 6 inch slabs of wood* can be used and the maximum wood load capacity is 8.75 m^3 for PC5 furnace (see Table 2.3). This means that 26 slabs of wood are placed vertically with 27 mm distance. The load capacity can be increased if the distance between the wood is decreased.

* Change of wood dimensions with treatment is negligible **[14]**.

The furnace at St. Ambroise is equipped with several gas inlets and outlets on the side walls. There are 570 inlets and 570 outlets as given in Table 2.4.

Table 2.4 *Furnace's Inlets and Outlets*

	Inlets			Outlets		
	Horizontal	**Vertical**	**Total on wall**	**Horizontal**	**Vertical**	**Total on wall**
Side Wall 1	30	10	300	30	9	300
Side Wall 2	30	9	270	30	10	270
Total in furnace			570			570

There is 168 mm distance between the inlets (or the outlets) in horizontal direction and 184 mm distance in vertical direction (see Figure 2.3). The gas is injected from 11.89 mm diameter nozzles, whereas it is evacuated from 17.44 mm diameter outlets (inside diameters). If the injection velocity is assumed 3 m/s, total gas flow rate is 683 m^3/h. The inlet and outlet configurations of the opposite walls of the furnace are different. If one side has an inlet, the opposite side has an outlet at the same level as shown in Figure 2.3.

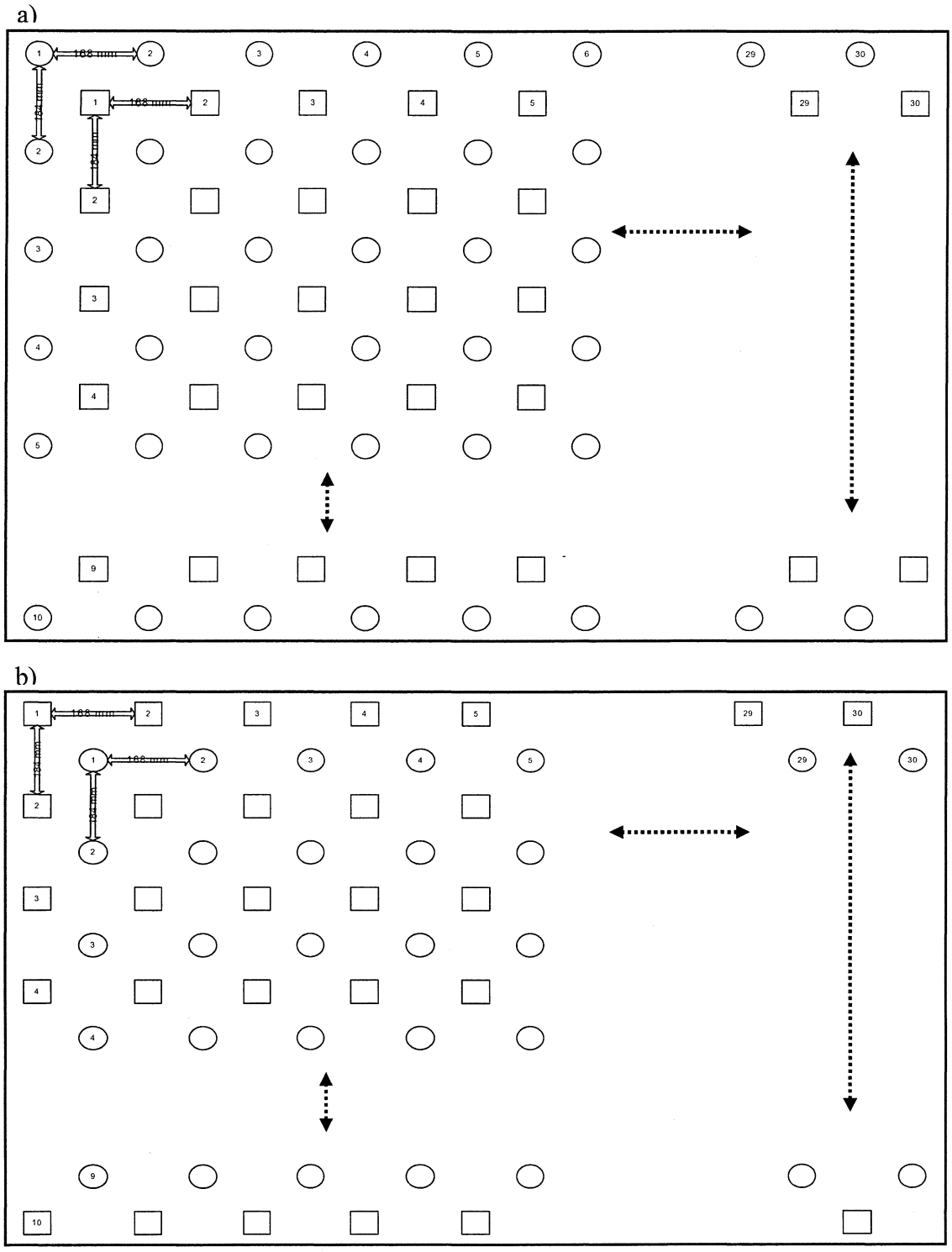

Figure 2.3 *Inlets and Outlets Geometry of the Furnace*

a) *Side Wall 1 with (30*10) inlets* ○ *and (30*9) outlets* □ ,

b) *Side Wall 2 with (30*9) inlets* ○ *and (30*10) outlets* □.

Besides the inlets and outlets, there are 78 water injections nozzles located on the side walls and at the top. These are used for cooling the wood slabs at the end of the treatment.

In a combustion chamber, a fuel such as propane is burnt with excess air. The reaction is :

$$C_3H_8 + 5O_2 \rightarrow 3CO_2 + 4H_2O \qquad (2\text{-}1)$$

As a result, the injection gas mainly contains CO_2, H_2O, O_2, and N_2. Then the hot gases (180°C-230°C) are injected from the nozzles into the furnace with a high velocity. The circulation of the hot gas heats the wood to a temperature as high as 220°C. Temperature of the wood is measured by the three thermocouples placed in the wood at different positions.

The duration of the operation depends on the temperature difference between the hot gas and the wood being treated; in other words, it depends on rate of the heat and mass transfer as well as the initial moisture content of the wood.

The injected gas circulates in the furnace and between the woods. Depending on the relative position of the nozzles and the wood layers, the amount of the gas entering between the layers is significantly different at different positions of the furnace. If the nozzle is placed directly across from the channel between the wood layers, gas will pass through.

Otherwise it will hit the wood creating circulation and the amount of gas entering the channels will be reduced significantly.

The treatment cycle consists of three phases [1]:

- elimination of free water,
- elimination of bound water, and
- modification of wood structure.

The easiest phase is the elimination of free water lodged in the wood's channels. This is achieved by the evaporation of the unbound water in the wood. There are no chemical changes in the wood.

In the second part, bound water contained in the wood cells crosses the cell walls and then it is released. These two phases depend on the initial humidity. Wood with low water content have a relatively short elimination period compared to the freshly cut wood with high water content.

The third phase is the modification of the micromolecular structure of the wood. This is achieved only by subjecting the wood to high temperature. Detailed description of the chemical transformation process is given in the following section (2.2.4) of this chapter.

Treated wood has the following properties [8]:

- Resistance to biodegradation: Humidity content facilitates biodegradation of the wood. Heat treatment improves the resistance of the wood to fungal action.

- Hydrophobic quality: Because of the chemical changes in the wood structure, reabsortion of water by the treated wood is reduced by 40%.

- Dimensional quality: Change of the hydrophobic character improves dimensional stability which can be expressed by reduced contractibility and a lowered fibre saturation point. The material no longer displays any deformation over variable humidification/drying cycles.

- Mechanical properties: Physico-mechanical properties of the wood change. It looses some of its elasticity.

- Handling: The absence of the storage time after treatment in contrast to the chemically treated wood. Heat-treated wood is ready for machining immediately.

- Color and smell: Due to the high temperatures in the treatment unit, treated wood gets a brownish color. The higher the temperature and the longer the duration of the process are, the darker the color becomes. At the end of the treatment, besides the dark color, the wood has a caramellish smell.

2.2 Wood

2.2.1 Structure of Wood

Parts of a tree

A cross section of a tree, given in Figure 2.4, has the following well-defined features:

- Bark (A&B) ;
- The cambium layer (C);
- Sapwood (D) ;
- Heart-wood (E) ;
- Pith (F).

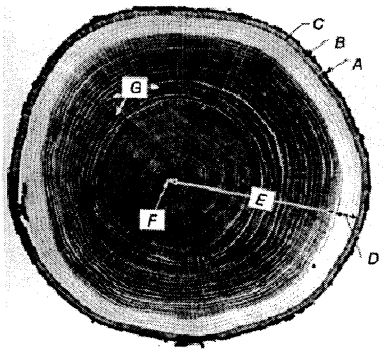

Figure 2.4 *A cross sectional view of a tree* **[6]**

Bark is composed from an outer corky dead part (A) and an inner thin living part (B). The thickness of the dead part varies greatly with species and age of trees. The inner living part carries food from the leaves to the growing parts of the tree.

The cambium layer (C) is found inside the inner bark. It forms wood cells and bark cells and only can be seen with a microscope.

Sapwood (D) contains living and dead cells. There is not any further development at old cells. Sapwood handles primarily the storage of food and the transport of water and sap.

Heartwood (E) is formed by a gradual change in the sapwood and is inactive. Heartwood has more extractive content then sapwood. These extractives affect the color and permeability. The function of heartwood cells are water conduction and food storage. As sapwood changes to heartwood, there are not any changes in cell number and cell shape.

Pith (F) is a small core and located at the center of a tree. Initial wood growth takes place around the pith. The wood rays play a role in food transfer and storage from pith to bark and connect various layers [1].

Growth in the thickness of the bark and wood is the result of the cell division in the cambium. There is growth in radial direction only at the cambial zone by the addition and growth of new cells. New wood cells are formed on the inside of the cambium, whereas new bark cells are formed on the outside. As a result, the diameter of the wood trunk increases since the new wood accumulates at the outside part of the old wood in sapwood region.

Wood Cells

Wood is a cellular material and composed of hollow, elongated, spindle-shaped cells. The complicated wood structure consists of different cell types which have a cell wall surrounding a cell lumen in the center. Most of the cells are arranged parallel to each other in longitudinal direction which is the tree's trunk direction.

The elongated and pointed end cells are called fibers or tracheids. The fibers are smaller than tracheids, only 0.7-3 mm in length and 0.02 mm in diameter. Short, wide cells arranged end to end, forming a system of tubes are called vessel elements (see Figure 2.5).

Both hardwoods and softwoods have cells that are oriented horizontally in the direction from pith toward bark. They are called rays. Fiber cells are dead at maturity and serves as a mechanical support in the plant. Tracheids transport water, sap, and some phytohormones in longitudinal direction. Vessel elements conduct water from roots to the plant. Rays conduct sap radially. Another type of wood cells, known as longitudinal or axial parenchyma cells, function mainly as a storage for food.

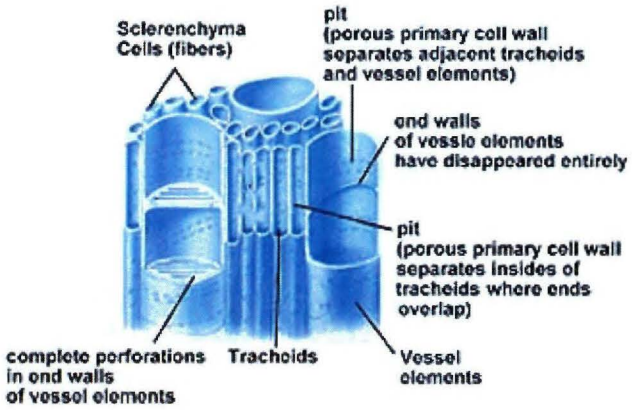

Figure 2.5 *Wood Cell* **[9]**

Hardwoods are trees with broad leaves, and softwoods are trees with needle-like leaves. These terms do not apply to the hardness or density of the woods. The structure of hardwoods is generally more complex than that of softwoods (see Figure 2.6).

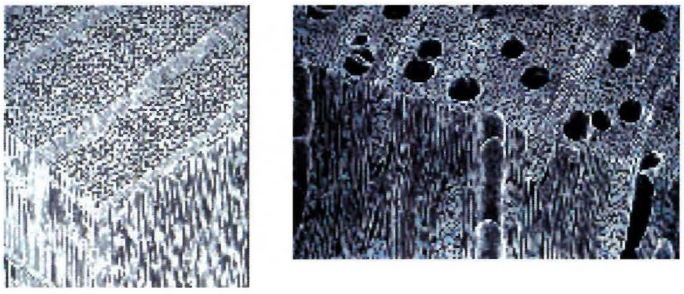

Figure 2.6 *Wood Structure of a) Softwood, b) Hardwood* **[10]**

Chemical Composition

Dry wood is primarily composed of cellulose, lignin, hemicellulose, and minor amounts of extraneous materials (see Figure 2.7). Cellulose and hemicellulose are carbohydrates that are structural components of wood.

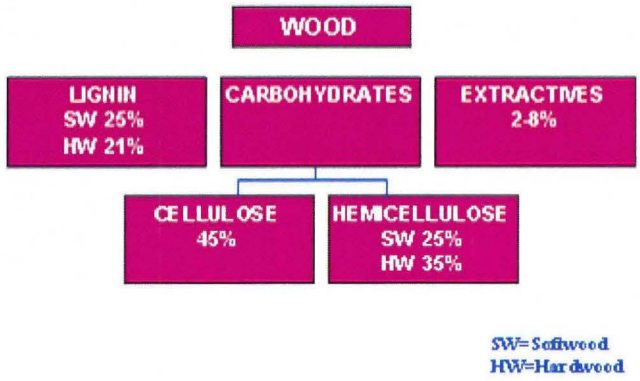

Figure 2.7 *Wood Components* **[10]**

Cellulose, the major component of wood, constitutes approximately 40-50% of wood substance by weight. Through photosynthesis, a tree produces the sugar glucose. Long chain of glucose forms cellulose (DP 5000-10000). Cellulose is a high-molecular-weight linear polymer consisting of chains of β-D-glucopyranoses, joined by (1-4)-glycoside bonds **[11]**. In Figure 2.8 glucose and cellulose structures are given.

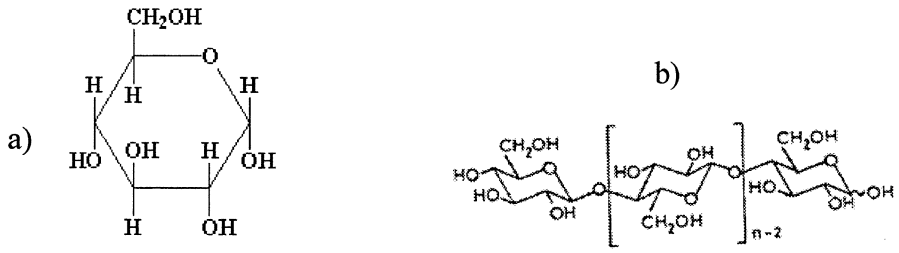

Figure 2.8 *Structure of a) Glucose, b) Cellulose* **[10]**

During growth of a tree, the cellulose molecules are arranged into ordered strands (micro fibrils), which in turn are organized into the larger structural elements that make up the cell wall of wood fibers as in Figure 2.9.

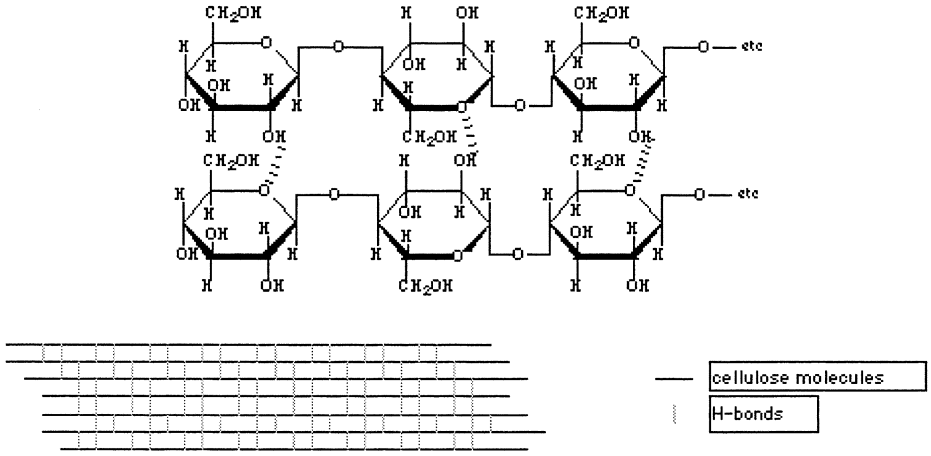

Figure 2.9 *Micro fibrils* **[10]**

Most of the cell wall cellulose is crystalline cellulose fibrils embedded in an amorphous hemicellulose-lignin matrix and is organized in several layers (see Figure 2.10).

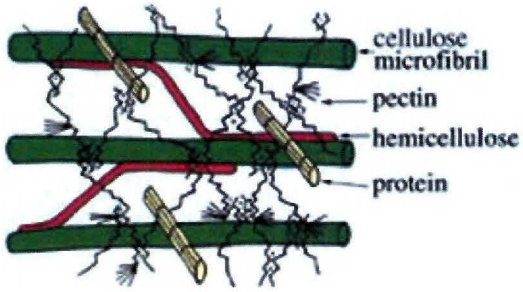

Figure 2.10 *Cell Wall Structure* **[10]**

The hemicellulose (DP 150-200) is associated with cellulose and is branched, low-molecular-weight polymers composed of several different kinds of pentose, hexoses, glucose, mannose and galactose (see Figure 2.11).

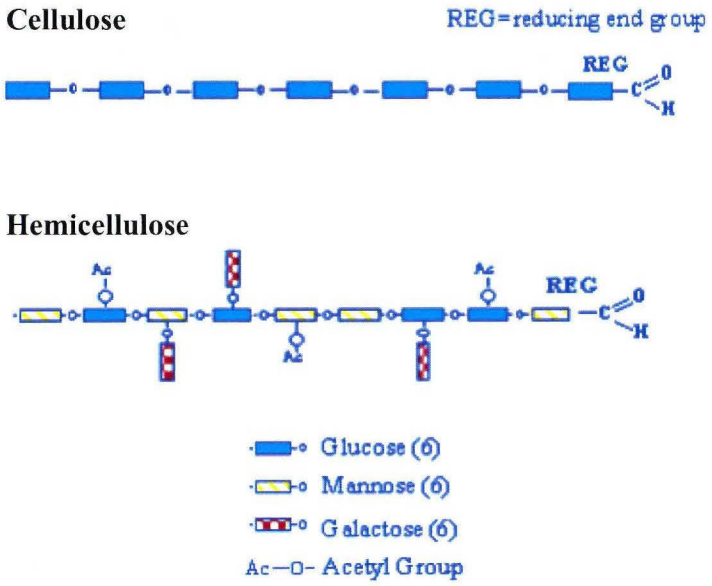

Figure 2.11 *Cellulose and Hemicelluloses Structures* **[10]**

Hemicelluloses are present in larger amounts in hardwood than in softwood. They are joined by (1-4) or (1-6) bonds. The component sugars of hemicellulose are of potential interest for conversion into chemical products.

Lignin constitutes 25% to 30% of the wood substance in softwoods and 20% to 25% in hardwoods. Although lignin occurs in wood throughout the cell wall, it is concentrated toward the outside of the cells and between cells. Lignin is often called the cementing agent that binds individual cells together. Lignin is three-dimensional phenylpropane polymers (see Figure 2.12).

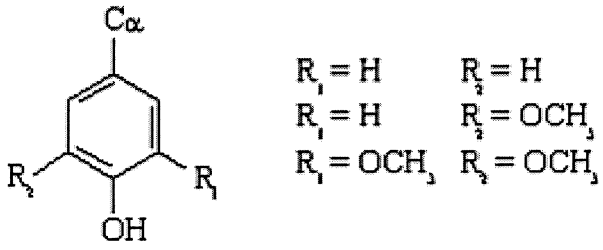

Figure 2.12 *Lignin Monomers* **[10]**

Pneylpropane polymers are joined by ether- and carbon-carbon bound (DP 10-50) as shown in Figure 2.13, and its structure and distribution in wood are still not fully understood.

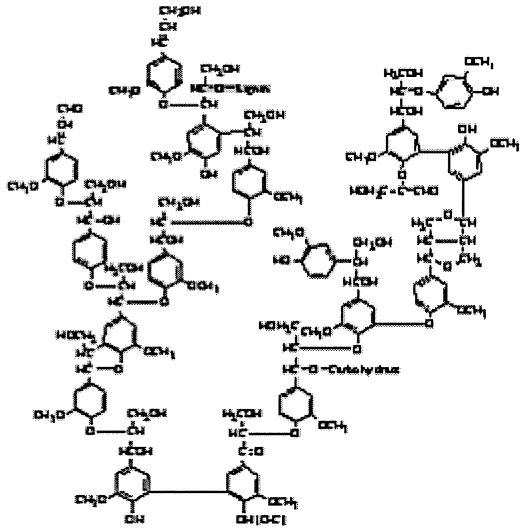

Figure 2.13 *Lignin Structure* **[10]**

On a commercial scale, it is necessary to remove lignin from wood to make high-grade paper or other paper products. Theoretically, lignin might be converted to a variety of chemical products, but in commercial practice a large percentage of the lignin removed from wood during pulping operations is a troublesome byproduct, which is often burned for heat and used in recovery of pulping chemicals.

Unlike the major constituents of wood, extraneous materials are not structural components (around 5%). Both organic and inorganic extraneous materials are found in wood. The organic component takes the form of extractives, which contribute to wood properties such as color, odor, taste, decay resistance, density, hygroscopicity, and flammability. This component is termed extractives because it can be removed from wood by extraction with solvents, such as water, alcohol, acetone, benzene, or ether. Calcium,

potassium, and magnesium are the more abundant elemental constituents. Trace amounts of phosphorus, sodium, iron, silicon, manganese, copper, zinc, and perhaps a few other elements are usually present.

Wood has unique and independent mechanical properties in the directions of three mutually perpendicular axes: longitudinal, radial, and tangential. These axes are shown in Figure 2.14.

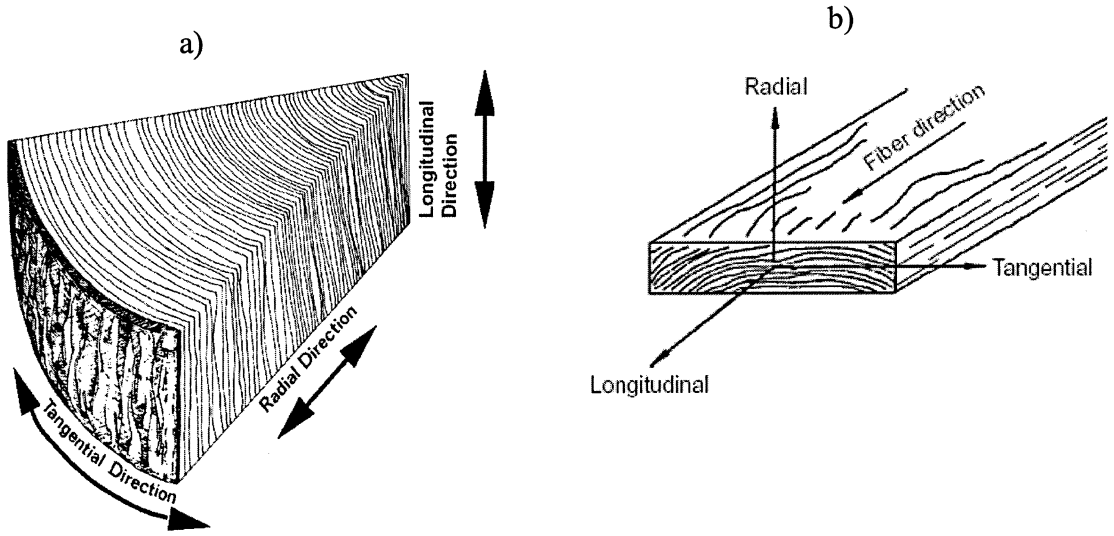

Figure 2.14 *Three Principal Axes of Wood With Respect To Grain Direction and Growth Rings a) For a Trunk, b) For a Slab* [1]

The longitudinal axis *L* is parallel to the fiber (grain); the radial axis *R* is normal to the growth rings (perpendicular to the grain in the radial direction); and the tangential axis *T* is perpendicular to the grain but tangent to the growth rings.

2.2.2 Moisture and Wood

Wood is hygroscopic. This means the attraction between dry wood and water is so strong that it is impossible to prevent moisture gain. Water easily binds with the cellulose fibers (micro fibrils) in the cell wall. Bound water is attracted to and held between micro fibrils in the cell walls by hydrogen bonding (see Figure 2.15)

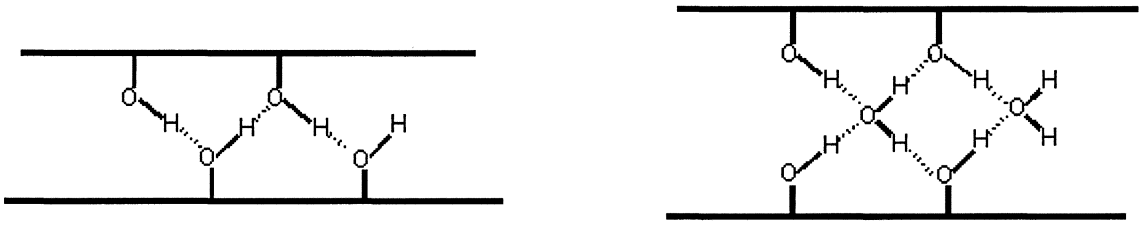

Figure 2.15 *Hydrogen Bonds between Micro Fibrils and Water in the Cell Wall* **[10]**

Moisture content (MC) is a measure of how much water is in a piece of wood relative to the wood itself. MC is expressed as a percentage and is calculated by dividing the weight of water to the weight of oven dried wood. Wood placed in an environment with a stable temperature and relative humidity, will eventually reach a moisture content that yields no vapor pressure difference between the wood cells and the surrounding air. In other words, molecules of water are constantly evaporating and condensing at the wood surface. If the number of molecules evaporating and condensing is equal, an equilibrium condition exists. Wood moisture content will stabilize at a point called the equilibrium moisture content (EMC). If, on the other hand, more molecules of water evaporate than those condense,

drying takes place. Otherwise, wetting takes place and the wood increases in moisture content. The equilibrium moisture content of wood is determined largely by the water content or relative humidity of the surrounding air. If the water vapor content or relative humidity of the air is high, the equilibrium moisture content of the wood will be high. If the relative humidity of the surrounding air is low, the EMC of the wood will be low. Fiber saturation is the level of maximum moisture content. The water absorbed by fibers is first held in the cell walls and called bound water. When they are full, any additional water absorbed by the wood will fill the cavities of tubular cells. Water in the cell cavities is called free water. The free water is relatively accessible, and an accessible source of water is essential for decay causing fungi to grow. The fiber saturation point is also the limit for wood shrinkage. As the wood's moisture content changes, shrinking or swelling takes place (see Figure 2.16). Any change in water content in the cell cavity will have no effect on the dimension of the wood. Therefore, wood only shrinks and swells when the moisture content falls below the fiber saturation point.

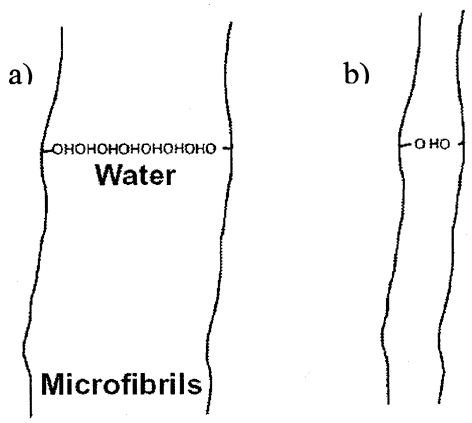

Figure 2.16 *a) Bound Water Causes the Cell Wall to Swell, b) The Lack of Bound Water Causes the Cell Wall to Shrink* **[3]**

The dimensional change occurring due to shrinking and swelling is largest in tangential direction, smallest in longitudinal direction, and intermediate in radial direction. Fiber saturation point is a phenomenon which occurs at the cell level. At any given time, some cells in a wood may reach the fiber saturation while others do not. It would be unreasonable to expect all cells to be at their fiber saturation point in a large piece of wood at the same time. Woods shrinks or swells by different amounts in the three different directions due to its anisotropy and moisture content differences. These differences cause some internal stresses which results in splitting and warp.

Moisture moves through several kinds of passageways in the wood. The principal ones are the cavities in the cells, the pit chambers, and pit membrane openings in the cell walls. Movement of moisture in these passageways occurs not only lengthwise in the cells but also sideways from cell to cell through pit membranes toward the drier surfaces of the wood. When wood dries, several moisture driving forces may be operating to reduce its moisture content. These forces, which may be acting at the same time, include the following:

- Capillary action that causes the free water to move through the cell cavities, pit chambers, and pit membrane openings,
- Differences in relative humidity that cause moisture in the vapor state to flow through cell cavities, pit chambers, pit membrane openings, and intercellular spaces to regions of lower humidity,

- Moisture content differences that cause movement of moisture to regions of lower moisture content through the passageways within the cell walls.

As moisture evaporates from the surface of wet wood the moisture content of the outer layers decrease and moisture begins to move from the wetter interior to the drier surface. In dense hardwoods, the structure of wood offers resistance to the passage of moisture. If the evaporation from the surface occurs at a faster rate than the moisture from the interior zones flows to these surfaces, the moisture gradient within the wood becomes progressively steeper. If the moisture content of the surface is below the fibre saturation point, the tendency of surface to shrink is resisted by the wetter interior. A state of stress develops, between the outer layer in tension and the inner zones in compression. If the tension forces in the surface layer become too large, surface tension can develop. The drying proceeds towards the interior region of wood, which then shrinks. However, the inside shrinkage is restrained by the already dry and set outer layers. The tension develops at the centre of the wood and the surface layers become compressed.

The principal factors that affect rate of decay are moisture and temperature. Wood degrades more rapidly in warm, humid areas than in cool or dry areas. Each wood has different degrees of natural decay resistance. Under decay-producing conditions, untreated sapwood has low resistance to decay and has a short service life. The decay resistance of heartwood is greatly affected by differences in the preservative qualities of the wood extractives, the attacking fungus, and the conditions of exposure. Considerable difference

in service life can be obtained from pieces of wood cut from the same species, even from the same tree, and used under apparently similar conditions. The principal organisms that can degrade wood are fungi, insects, bacteria, and marine borers. Figure 2.17 shows the penetration of fungi in a cross section of wood [6].

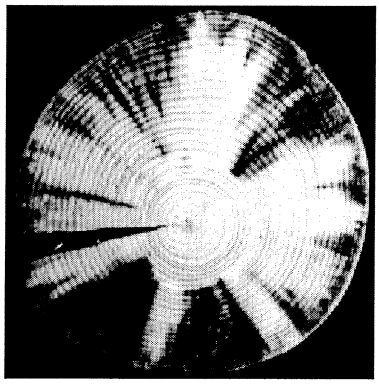

Figure 2.17 *Radial Penetrations of Fungi* [6]

The growth of fungi depends on temperatures, moisture, and air. Insects and bacteria also may damage wood, and in many situations must be considered in protective measures.

Wood is degraded biologically since the organisms recognize the carbohydrate polymers in the cell wall. They have very specific enzyme systems capable of hydrolyzing these polymers into digestible units. Biodegradation of the cell wall matrix and the high molecular weight cellulose weakens the fiber cell. Strength is lost as the cell wall polymers and matrix undergoes degradation through oxidation, hydrolysis, and dehydration reactions.

2.2.3 Chemical Changes in Wood During Heat Treatment

In the case of wood, the cell wall polymers (cellulose, hemicellulose, and lignin) are the components that, if modified, would change the properties of the resource. If the properties of wood are modified, the performance of wood will be changed. This is the basis of chemical modification of wood to change properties and improve performance.

In the heat treatments, the objective is to heat the wood to increase dimensional stability and moisture resistance. Desired changes start to appear already at about 150°C, and the changes continue as the temperature is increased

During the heat treatment, cellulose and hemicellulose undergo changes; however, the main changes occur in hemicellulose because the decomposition temperature of the hemicellulose is lower than the corresponding temperature for cellulose. Hemicellulose content is higher in hardwood than in softwood that is why degradation in hardwood is easier than softwoods. Breaking of cellulose chains reduces the strength of the wood more than the breaking of a hemicellulose chain. During the heat treatment, acetic acid is formed from acetylated hemicellulose by hydrolysis [11]. The released acid is used as a catalyst in the hydrolysis of hemicellulose to soluble sugars, which may undergo reversion reactions to form less hygroscopic, highly branched polysaccharides. Repeated glucose units bonded together by *beta*-linkages form cellulose. Humans and many other animals do not digest cellulose because they lack an enzyme to break the *beta*-linkages. Enzymes found in fungi

hydolyze the beta linkage in celluloses. Cellulose chains are joined by bonds between hydroxylgroups. At temperatures under 300°C, the degree of polymerisation in cellulose decomposition decreases, water is eliminated and free radicals, carbonyl, carboxyl, and hydroperoxide groups, as well, as carbon monoxide, carbon dioxide are generated.

The lignin holds the cellulose fibers together by acting as an adhesive in the cell walls. As the lignin degrades, the surface becomes richer in cellulose content. As wood is heated, ether bonds between phenyl propane units which form lignin are broken. The chemical reactions create a new pseudo-lignin which is more hydrophobic and rigid. Lignin modification and hemicellulose removal prevent fungi enzymes from hydrolyzing the nutrients. There is no generation of toxic chemicals during the process, it is observed that fungi are present in the end product. They are not killed, but they are unable to develop in the wood. Extractives in the wood degrade more easily and evaporate from the wood during the heat treatment.

The chemical changes, during high temperature heating, have the following effects on the wood [11] :

- Degradation of cellulose affects equilibrium moisture and toughness;
- Degradation of hemicelluloses affects equilibrium moisture, biological durability, strength, weather resistancy;
- Degradation of lignin affects biological durability, toughness, paintability;
- Degradation of extractives affects paintability and glueability.

2.3 Mathematical Modelling

Mathematical description of wood drying process has been of great importance for many decades. Development of a mathematical model in order to determine heat and mass transfer phenomena in porous bodies has been an interesting and challenging topic of research for several researchers [14-19]. However, there is no model reported in the literature for the heat treatment of wood. Therefore, in this section, a literature review on wood drying models is given.

To achieve the goal of solving a mathematical problem, three steps are followed:

- Mathematical modeling of the physical problem: definition of the geometry and the computational domain, grid generation, selection of the physical and chemical phenomena, definition of properties, and specifications of initial and boundary conditions.
- Mathematical solution of the model equations: discretisation of the governing equations in space and in time and solution of the algebraic equations by an iterative method.
- Analysis of the results and physical interpretation.

2.3.1 Coupled Heat and Mass Transfer Modelling

Tuttle [12] was the first to propose an equation derived for drying of wood assuming a pure diffusion mechanism; after him, numerous models have been developed.

The interrelation between heat and mass transfer in capillary porous media was established by Luikov [14]. He defined a coupled system of partial differential equations by using the thermodynamics of irreversible process. Several researchers [15-17] worked on the numerical and analytical solutions of Luikov's equations in order to model the heat and mass transfer phenomena in wood drying. Model developments have been based on transfer phenomena approaches, derived from Fourier's and Fick's laws and the principles of irreversible thermodynamics. Traditionally, moisture content gradients have been employed as the driving forces for diffusion. In addition, gradients of chemical potential and water potential have also been used. Thermally induced mass transfer is also taken into account.

The fact that wood is an anisotropic medium leads to some difficulty in modeling wood drying. Modeling is complicated because more than one mechanism may contribute to the total moisture flow and the contribution of different mechanisms may change as the drying process proceeds. Also, in coupled heat and mass diffusion, a gradient in temperature can cause mass transfer (Soret effect) and a gradient in mass concentration can cause heat flow (Dufour effect).

Several parameters are needed to clearly describe the phenomena. Once the problem is successfully formulated in terms of a coupled system of partial differential equations, the analytical solution of these equations presents a major problem and consequently the solutions are given for only the simplest of geometrical configurations and boundary conditions [14]. In general, they have to be solved numerically.

2.3.1.1 Wood Drying Models

A detailed literature research has been carried out to understand and to characterize the physical phenomena taking place in wood during the drying process. Even though it is difficult to classify clearly the approaches used so far, two main categories of wood drying models can be identified: *(a) models based on potential energy term, (b) multi-component model.* Almost all the authors [13-17] neglected the radiation since the temperature of drying is not high. Up to date, no high temperature thermal treatment model is reported in the literature.

a) Models Based on Potential Energy Term

Luikov described an interrelation between heat and mass transfer in porous media by applying the methods of irreversible thermodynamics. The relationship can be described by Luikov's two-way coupled system of partial differential equations [13, 14]. In these equations, the required energy to break-up the hydrogen bounding is neglected.

Models based on a potential energy term can be classified in four groups:

- *Models based on mass transfer potential*
- *Models based on irreversible thermodynamics*
- *Models based on chemical potential*
- *Models based on water potential*

Models Based on Mass Transfer Potential

To model the coupled heat and mass transfer in a porous media, the basic equations given by Luikov were studied by several researchers like Thomas et al, Comini and Lewis, **[15-17]** and simplified into a set of governing differential equations for transient flow in drying as:

$$\rho c_q \frac{\partial T}{\partial t} = \vec{\nabla} \bullet \left[\underbrace{\left(k_q + \varepsilon \lambda k_m \delta\right) \vec{\nabla} T}_{\text{Fourier law}} + \underbrace{\varepsilon \lambda k_m \vec{\nabla} U}_{\text{Non-isothermal diffusion law}} \right] \tag{2-2}$$

$$\rho c_m \frac{\partial U}{\partial t} = \vec{\nabla} \bullet \left[\underbrace{k_m \vec{\nabla} U}_{\text{Fick's law}} + \underbrace{\left(k_m \delta\right) \vec{\nabla} T}_{\text{Soret effect}} \right] \tag{2-3}$$

where T : temperature

U : moisture potential

t : time

ρ : density

c_q: heat capacity

c_m: moisture capacity

k_q: thermal conductivity

k_m: moisture conductivity

ϵ : ratio of vapor diffusion coefficient to coefficient of total moisture diffusion

λ: latent heat

δ : thermal gradient coefficient.

The first term on the right hand side of Equation 2-2 is the heat transfer by conduction (Fourier Law); a term is added for the component of heat transfer due to phase change. The heat transfer takes place due to temperature gradient; however, in the case of coupled heat and mass transfer, it also takes place due to moisture gradient. However, this is considered insignificant for porous capillary bodies. The second term is the component of non-isothermal diffusion.

The first term on the right hand side of Equation 2-3 is the component of mass transfer due to the gradient in moisture concentration (Fick Law) and the second term represents the mass transfer taking place because of the gradient in temperature (Soret effect).

Lui and Cheng based the model on the assumption that pressure was constant throughout the capillary body [18]. The authors summarized Luikov equations under constant pressure and proposed the following boundary and initial conditions for the coupled heat and mass transfer equations 2-2 and 2-3:

$$\rho c_q \frac{\partial T}{\partial t} = \vec{\nabla} \bullet \left[k_q \vec{\nabla} T + \varepsilon \lambda \rho c_m \frac{\partial U}{\partial t} \right]$$

$$\rho c_m \frac{\partial U}{\partial t} = \vec{\nabla} \bullet \left[k_m \vec{\nabla} U + (k_m \delta) \vec{\nabla} T \right]$$

For one dimensional problem, at the surface (x=L), the boundary conditions of the third kind (Luikov 1966) apply. They are :

$$k_q \frac{\partial T}{\partial x} + \alpha_q (T - T_a) + (1-\varepsilon)\lambda\alpha_m (U - U_a) = 0 \qquad (2\text{-}4)$$

$$k_m \frac{\partial U}{\partial x} + k_m \delta \frac{\partial T}{\partial x} + \alpha_m (U - U_a) = 0 \qquad (2\text{-}5)$$

where α_m : convective heat transfer coefficient

α_q : convective mass transfer coefficient

T_a : ambient temperature

U_a : ambient moisture potential

Because of symmetry, at x=0

$$\frac{\partial T}{\partial x} = 0 \quad \text{and} \quad \frac{\partial U}{\partial x} = 0$$

where x=0 the mid-point of the slab.

The initial conditions are assumed to be constant and are represented by :

$$T(x,0) = T_0 \quad \text{and} \quad U(x,0) = U_0$$

Lui and Cheng presented [18], in their study, an analytical method to solve Luikov equations to predict temperature and moisture distributions.

In another study, Lewis and Ferguson assumed that during drying of capillary porous materials, pressure gradient exists due to vapor present in the system, and causes moisture transfer by infiltration in addition to moisture transfer by diffusion. Therefore, the author concluded that Luikov's coupled heat, mass transfer model should include this effect [13, 19].

The partial differential equations given by Luikov are modified and simplified as:

$$\frac{\rho c_q \delta}{c_m}\frac{\partial T}{\partial t} = \left(\frac{(k_q + \varepsilon\lambda k_m)\delta}{c_m}\right)\nabla^2 T + \left(\frac{(\varepsilon\lambda k_m)\delta}{c_m}\right)\nabla^2 U + \left(\frac{(\varepsilon\lambda k_p)\delta}{c_m}\right)\nabla^2 P \qquad (2\text{-}6)$$

$$\varepsilon\lambda\rho c_m \frac{\partial U}{\partial t} = \left(\frac{(\varepsilon\lambda k_m)\delta}{c_m}\right)\nabla^2 T + \varepsilon\lambda k_m \nabla^2 U + \varepsilon\lambda k_p \nabla^2 P \qquad (2\text{-}7)$$

$$\frac{-\lambda\rho c_p k_p}{k_m}\frac{\partial P}{\partial t} = \left(\frac{(\varepsilon\lambda k_p)\delta}{c_m}\right)\nabla^2 T + \varepsilon\lambda k_p \nabla^2 U + \left(-\frac{(\lambda(1-\varepsilon)k_p{}^2)}{k_m}\right)\nabla^2 P \qquad (2\text{-}8)$$

where P : pressure

k_p : moisture filtration coefficient

c_p : coefficient of humid air capacity

In the same study, boundary and initial conditions are given as follows:

$$(k_q + \varepsilon\lambda\rho\delta a_m)\frac{\partial T}{\partial n} + \frac{(k_q + \varepsilon\lambda\rho\delta a_m)\alpha_q}{k_q}(T - T_0) + A_\varepsilon(U - U_0) + J_q = 0 \qquad (2\text{-}9)$$

$$a_m \frac{\partial U}{\partial n} + -\frac{a_m \delta\alpha_q}{k_q}(T - T_0) + \left(\alpha_m - \frac{a_m \alpha_m \rho\lambda\delta}{k_q}(1-\varepsilon)\right)(U - U_0) + J_m = 0 \qquad (2\text{-}10)$$

where $$J_q = \frac{k_q + \varepsilon\lambda\rho\delta a_m}{k_q} \qquad (2\text{-}11)$$

$$J_m = \frac{j_m}{\rho_0} - \frac{a_m \delta j_q}{k_q} \qquad (2\text{-}12)$$

a_m : moisture diffusivity

The authors used finite element model to predict temperature, moisture, and pressure variation. Material properties and variables used in this model are summarized in Appendix 1.

Models Based on Irreversible Thermodynamics

Horacek [20] studied the modeling of coupled moisture and heat transfer during drying. He summarized diffusion equations inspired by Siau and Avramidis [21] who found, using these equations, the best agreement between the experimental data and the results of the thermodynamic model to describe moisture and heat transport phenomena in wood. He

analyzed the non-isothermal diffusion by using a thermodynamic model considering the gradients of both water potential and temperature.

In the model, moisture content and temperature gradients are set as driving forces, since all the other possible factors related to moisture content are applicable only in the hygroscopic region.

The differential unsteady-state equations for a two-dimensional cross-section are

$$c_q \rho \frac{\partial T}{\partial t} = \frac{\partial}{\partial x}\left(k_{q,x} \frac{\partial T}{\partial x} \right) + \frac{\partial}{\partial y}\left(k_{q,y} \frac{\partial T}{\partial y} \right) + \frac{E_b}{1.8c} \frac{\partial M}{\partial t} \tag{2-13}$$

$$\frac{\partial M}{\partial t} = \frac{\partial}{\partial x}\left(a_{m,x} \frac{\partial M}{\partial x} + \phi_x \frac{\partial T}{\partial x} \right) + \frac{\partial}{\partial y}\left(a_{m,y} \frac{\partial M}{\partial y} + \phi_y \frac{\partial T}{\partial y} \right) \tag{2-14}$$

where M : moisture content,

E_b : activation energy for water diffusion.

ϕ is a phenomenological coefficient of the temperature gradient in the mass balance equation derived by Siau and Avramidis. It is a strong function of moisture content and temperature as diffusion coefficient.

$$\phi = F(M,T)$$

$$a_m = F(M,T)$$

Equation 2-14 can be rewritten in the following one-dimensional form by taking into account the above function :

$$\frac{\partial M}{\partial t} = \frac{\partial a_{m,x}}{\partial M}\left(\frac{\partial M}{\partial x}\right)^2 + \frac{\partial a_{m,x}}{\partial T}\frac{\partial T}{\partial x}\frac{\partial M}{\partial x} + a_{m,x}\frac{\partial^2 M}{\partial x^2} + \frac{\partial \phi_x}{\partial M}\frac{\partial M}{\partial x}\frac{\partial T}{\partial x} + \frac{\partial \phi_x}{\partial T}\left(\frac{\partial T}{\partial x}\right)^2 + \phi_x\frac{\partial^2 T}{\partial x^2} \qquad (2\text{-}15)$$

ϕ is defined as follows :

$$\phi = \frac{E_b}{T}\frac{a_m h}{RT}\frac{\partial M}{\partial h}$$

which refers to the *Soret* effect (thermal diffusion) based on slope of the sorption isotherms $\partial M / \partial h$, relative humidity h, and activation energy for water diffusion E_b. In the above equation R is the universal gas constant

Sorption is the ability of a hygroscopic material such as wood to absorb or release water vapor from or into air until a state of equilibrium is reached. The sorption isotherms are the graphic representation of the sorption behavior of the material, in other words, these isotherms represent the relationship between the water content of material and the relative humidity of the ambient air (equilibrium) at a particular temperature. Since the sorption ability of each wood differs, these isotherms are specific to wood specimen.

Horacek [20] described the boundary conditions at the surface of the wood as,

$$-a_m\left(\frac{\partial M}{\partial x}\right)_L = \alpha_m(M(L,t)-M_a) \tag{2-16}$$

$$-k_q\left(\frac{\partial T}{\partial x}\right)_L = \alpha_q(T(L,t)-T_a) \tag{2-17}$$

where L : thickness of a wood slab

The author solved the partial differential equations using the Galerkin finite element method with quadratic or cubic basis functions involving nodal values of system variables only [20].

Models Based on Chemical Potential

Chemical potential model based on irreversible thermodynamics have been proposed both by Siau *et al.* [21]. Siau expressed Fick's law as follows assuming chemical potential as the driving force :

$$\frac{\partial M}{\partial t} = \frac{\partial}{\partial x}\left[-D_\mu \frac{\partial \kappa_v}{\partial x}\right] \tag{2-18}$$

Chemical potential can be expressed as a function of temperature *(T)* and humidity (*h*) :

$$\frac{d\kappa}{dx} = \left(\frac{d\kappa}{dT}\right)_{\phi} \frac{dT}{dx} + \left(\frac{d\kappa}{dh}\right)_{T} \left(\frac{dh}{d\phi}\right)_{T} \frac{d\phi}{dx} \tag{2-19}$$

D_μ can be expressed in terms of D_M as a function of moisture content,

$$D_{\mu} = D_M \left(\frac{dM}{d\mu}\right)_T = D_M \left(\frac{dM}{dh}\right)_T \left(\frac{dh}{d\kappa}\right)_T \tag{2-20}$$

where D_μ : diffusivity coefficient, based on the chemical potential of water vapor

κ_v : chemical potential

D_M : diffusivity coefficient, based on the moisture content M.

Equations 2-18 and 2-20 are combined and simplified as,

$$\frac{\partial M}{\partial t} = \frac{\partial}{\partial x}\left[-D_M\left[\left(\frac{dM}{dh}\right)_T \left(\frac{dh}{d\kappa}\right)_T \left(\frac{d\kappa}{dT}\right)_M \frac{dT}{dx} + \left(\frac{dM}{dx}\right)\right]\right] \tag{2-21}$$

The chemical potential of water vapor is defined as,

$$\kappa_v = \kappa_{vo} + RT \ln\left(\frac{h}{100}\right) \tag{2-22}$$

This definition is then used to evaluate the corresponding derivatives:

$$\left(\frac{dh}{d\kappa}\right)_T = \frac{h}{RT} \tag{2-23}$$

$$\left(\frac{d\kappa_v}{dT}\right)_M = \left(\frac{d\kappa_{vo}}{dT}\right) + RT\ln\left(\frac{d\left(\ln h/100\right)}{dT}\right) + R\ln\left(\frac{h}{100}\right) \tag{2-24}$$

The second term of right side in equation (2-24) was replaced by E_l/T where E_l is the difference between the molar heat of vaporization of bound water and that of free water. Then equation (2-24) is expressed in the form:

$$\frac{\partial M}{\partial t} = \frac{\partial}{\partial x}\left[-D_M\left(\frac{h}{RT}\left(\frac{\partial M}{\partial h}\right)_T\left(\frac{d\kappa_O}{dT} + \frac{E_L}{T} + R\ln\left(\frac{h}{100}\right)\right)\frac{dT}{dx} + \frac{dM}{dx}\right)\right] \tag{2-25}$$

Models Based on Water Potential

Following Luikov's approach **[14]**, Fortin used the water potential concept to characterize water in wood in terms of free energy as explained by Tremblay and Benrabah **[23, 24]**. A model of isothermal wood drying using the gradient of water potential as the driving force was proposed.

Water potential can be defined as follows:

$$\psi = \overline{G} - \overline{G}_O \tag{2-26}$$

where ψ : water potential

G : specific Gibbs free energy of water in the state under consideration

G_O : specific Gibbs free energy of water in the standard reference state

The total water potential was given as:

$$\psi = \psi_m + \psi_o + \psi_p + \psi_g + \psi_{e.f} + \ldots \quad (2\text{-}27)$$

where ψ_g : gravitational potential

ψ_M : matric potential due to the combined effect of the capillary and sorptive forces

ψ_o : osmotic potential due to the presence of solutes in the water

ψ_p : pressure potential describing the effect of a system bulk pressure

$\psi_{e.f}$: component potential representing the integrated sum of the effects of all external force fields excluding of gravity

Additions of other component potentials are theoretically possible to the right hand side of equation (2-27).

Water potential is derived from the combination of the first and second laws of thermodynamics using the Gibbs free energy function. The basic relation for the derivation of the ψ components is given as:

$$dG=VdP-SdT-dW \tag{2-28}$$

Fortin [24] modeled the isothermal wood drying at atmospheric pressure and assumed that the only significant components of water potential are matric potential and osmotic potential. The matric potential ψ_m is defined as,

$$\psi_m = -P_M / \rho \tag{2-29}$$

A combined expression for ψ_m and ψ_o can be obtained by evaluating the Gibbs specific free energy of water vapor in equilibrium with water in wood as:

$$\psi_{m+o} = \frac{RT}{M_{M,W}} \ln \frac{P_w}{P_s} \tag{2-30}$$

where $M_{M,W}$: Molecular weight of water

P_w : partial pressure of water in equilibrium with water in wood

P_s : partial pressure of water vapor in equilibrium with pure free water

Mass transfer equation is given as:

$$\frac{\partial C}{\partial t} + \vec{\nabla} \bullet \vec{q}_m = 0 \tag{2-31}$$

The moisture concentration is:

$$MC = G_{SG}\rho_w \frac{M}{100} \tag{2-32}$$

where q_m : moisture flux vector

G_{SG} : specific gravity of wood

Specific gravity of wood is given as:

$$G_{SG} = \frac{w_0}{V_{moist}\rho_w} \tag{2-33}$$

where w_0 : the oven dry mass

V_{moist} : moist volume

Substituting equation (2-32) and (2-33) into (2-31) gives:

$$\frac{\partial M}{\partial t} + \left(\frac{100}{G_{SG}\rho_w}\right)\vec{\nabla} \bullet \vec{q}_m = 0 \tag{2-34}$$

Fortin assumed that temperature gradients are negligible and thermodynamic equilibrium exists between liquid water, water vapor, and bound water. It is assumed that

the gradient of water potential is the driving force for moisture movement in wood during drying.

The moisture flux vector is described by the following equation:

$$\vec{q}_m = -K(M,T) \bullet \vec{\nabla} \psi \tag{2-35}$$

where $K(M,T)$: effective water conductivity tensor

Thus, substituting Equation (2-35) into Equation (2-34), the mass transfer equation takes the following form:

$$\frac{\partial M}{\partial t} = \left(\frac{100}{G_{SG} \rho_w} \right) \vec{\nabla} \bullet \left[K(M,T) \bullet \vec{\nabla} \psi \right] \tag{2-36}$$

Using the water potential approach, Fortin developed a two dimensional finite element model to simulate the moisture distribution and compared the results with those obtained experimentally for isothermal convective drying of aspen at 20, 35, and 50°C.

b) Multi-Component Models

Whitaker [25] performed a detailed analysis of the Fick and Fourier laws applied to porous medium and developed a set of macroscopic equations where the fluxes of the different components are described using different transport coefficients and driving forces. Whitaker approach can be qualified as a multi-component approach since mass and energy conservations are written for liquid water, water vapor and for the gaseous mixture (water vapor + air).

Turner *et al.* applied the multi component model to describe heat and mass transfer in wood drying [26]. They summarized conservations laws as follows:

Energy conservation equation is:

$$\frac{\partial}{\partial t}\left(\gamma_w\rho_w H_w+\gamma_g(\rho_v h_v+\rho_a H_a)+\rho_b H_b+\rho_o h_s-\gamma_g P_g\right)+\nabla\cdot(\rho_w H_w\bar{v}_w+ (\rho_v H_v+\rho_a H_a)\bar{v}_g+H_b\overline{\rho_b v_b})=\nabla(\rho_g D_{eff}(H_v\nabla\omega_v+H_a\nabla\omega_a)+k_{eff}\nabla T) \quad (2\text{-}37)$$

Mass conservation equation for liquid is:

$$\frac{\partial}{\partial t}\left(\gamma_w\rho_w+\gamma_g\rho_v+\rho_b\right)+\nabla\cdot(\rho_w\bar{v}_w+\rho_v\bar{v}_g+\overline{\rho_b v_b})=\nabla(\rho_g D_{eff}\nabla\omega_v) \quad (2\text{-}38)$$

Mass conservation equation for air is:

$$\frac{\partial}{\partial t}\left(\gamma_g \rho_a\right) + \nabla \cdot (\rho_a \bar{v}_g) = \nabla(\rho_g D_{eff} \nabla \omega_a) \tag{2-39}$$

where γ : volume fraction

H : enthalpy

v : velocity

D_{eff} : effective diffusivity

ω : mass fraction

k_{eff} : effective thermal conductivity

The gas and liquid phase velocities are given by the generalized Darcy law as,

$$\bar{v}_l = -\frac{\theta_{relativve}\theta_{absolute}}{\mu_l}\nabla\varphi_l \ , \quad \nabla\varphi_l = \nabla P_l - \rho_l g \nabla\chi \tag{2-40}$$

where θ: permeability

φ : phase potential

χ : depth scalar

In order to close this system, the following constraints and constitutive relations are used by authors:

$$\gamma_g = \varphi S_g \quad \gamma_w = \varphi S_w \quad S_g + S_w = 1$$

$$P_g = P_v + P_a \quad P_v = \frac{\rho_v RT}{M_{M,v}} \quad P_a = \frac{\rho_a RT}{M_{M,a}}$$

$$P_w = P_g - P_c(S_w, T) \tag{2-41}$$

where S : volume saturation

The enthalpy–temperature relations are given by the following definitions:

$$h_s = C_{ps}(T - T_R) \qquad h_a = C_{pa}(T - T_R)$$

$$h_c = h_{vap} + C_{pv}(T - T_R) \qquad h_w = C_{pw}(T - T_R)$$

$$\overline{h}_b = h_w - \frac{1}{\overline{\rho}_b}\int_0^{\overline{\rho}_b} \Delta h_w d\rho \qquad h_b = h_w - \nabla h_w \tag{2-42}$$

The mass fractions of vapor and air in the gaseous phase are given, respectively, by:

$$\omega_v = \frac{\rho_v}{\rho_g} \quad \text{and} \quad \omega_a = \frac{\rho_a}{\rho_g} \tag{2-43}$$

The driving potential for the bound liquid migration is assumed to be proportional to a gradient in the chemical potential μ_b and can be written in terms of gradients in the vapor pressure and temperature as:

$$\overline{\rho_b v_b} = -\overline{\overline{D}}_b \nabla \mu_b = -\overline{\overline{D}}_b (1-\phi)\left(\frac{1}{\rho_v}\nabla P_v - \frac{S_v}{M_v}\nabla T\right) \qquad (2\text{-}44)$$

where S_v : the molar entropy

2.3.1.2 Comparison of Wood Drying Models

The multi-component approach gives a comprehensive description of the mechanisms involved during drying but it results in large sets of equations and requires the knowledge of properties or other physical parameters which are not easily obtainable. If separate treatment for each phase is to be avoided in order to simplify the problem, the utilization of models based on the potential energy term allows the development of a representative mathematical model. The chemical potential model proposed by Siau *et al.* [21] is rarely used in literature; further research is needed because of its complexity and dependence on material properties. The model based on water potential assumes isothermal drying. Thus, for transient application where the drying temperature is continuously increasing, the model is not applicable. Fortes and Okos [27] developed a model using the irreversible thermodynamics; it was observed that the cross effect terms were small compared to direct terms.

2.3.1.3 General Assumptions

Heat and mass transfer in porous media is complex. Several assumptions are often necessary to make the problem manageable. In this section, common assumptions used in the simplification of drying models are summarized:

- Since cross effects are generally considered small in comparison to gradients described by the Fick and Fourier laws, they can be neglected in some cases.
- In almost all multiphase porous media studies, solid, liquid, and gas (vapor + air) at any location are considered in thermal equilibrium. This assumption should be verified for rapid heating conditions.
- Gravity is ignored in most studies, because capillary forces are much stronger than gravity.
- Some properties can be considered isotropic if the information is not available.
- The enthalpies of the three phases are linear functions of temperature.
- The liquid water is incompressible.
- The viscosities of the liquid and gas phases are constant.
- To avoid the computational complexities, shrinkage is generally ignored except in studies where the goal is to compute the stress development and cracking. Therefore, the volume occupied by the solid does not change. Also it is assumed that no degradation of the solid occurs, consequently, the solid density remains constant.

CHAPTER 3

PRELIMINARY MODELS

3.1 Description of the Models

Before carrying out the furnace modeling, two preliminary models were developed in order to predict the flow and the temperature fields for different gas injection geometries and wood packing configurations.

In the first one, a three dimensional model of gas injection was represented. In the second one, the heat transfer in wood was modeled and the results were compared with the analytical solution.

3.2 Model Development

A commercial CFD program was used for gas flow and heat transfer calculations in gas phase. The fluid domain was discretized into small cells to form a grid and iterative methods were used to solve the Navier Stokes equations.

The k-ε model was used to represent the turbulence. The conservations equations were solved on discrete control volumes by integration. The solution of the set of Navier Stokes equations was carried out using CFX 4 commercial code.

3.3 Governing Equations

To model the system, the continuity equation, conservation equations for momentum, heat transfer and k-ε turbulence equations were solved simultaneously using the finite volume method.

Continuity equation is given as:

$$\frac{\partial \rho}{\partial t} + div\,(v.\rho) = 0 \tag{3-1}$$

General conservation equation in Cartesian coordinate system is:

$$\underbrace{\frac{\partial \rho\varphi}{\partial t}}_{\text{Transient Term}} + \underbrace{div\ (\rho v \varphi)}_{\text{Convective Term}} = \underbrace{div\ (\xi\ \ grad\ \ \varphi)}_{\text{Diffusion Term}} + \underbrace{S_{\varphi}}_{\text{Source Term}} \tag{3-2}$$

where φ general variable [velocity component (v_x, v_y, v_z), enthalpy or temperature (h, C_pT), mass fraction (m_A), turbulent kinetic energy (k) or turbulent dissipation (β)]

ξ exchange coefficient, viscosity, conductivity or diffusivity

S_φ Source term: body forces (gravity, centrifugal, electromagnetic forces), surface forces (pressure, viscous forces) acting on the system and any other additional terms

v velocity vector

ρ density

In the gas injection analysis part of this work, only the steady state momentum, turbulence, and the continuity equations were considered. The time dependent terms in the equations were taken as zero. In the heat transfer analysis, the unsteady-state heat transfer equation was solved in wood. In both cases, mass transfer was not modeled.

The physical properties which are available in PCP database of CFX-F3D material properties database interface were used **[29]**.

3.4 Gas Injection Analysis Results

3.4.1 Effect of Different Gas Injection Geometries on the Flow Distribution

In order to study the effect of gas behavior at the gas injection point and flow field created, only one inlet with a number of wood slabs were modeled for different gas inlet geometries.

The inlet gas injection geometries studied are a) square inlet, b) rectangular inlet and c) square inlet with a nozzle (see Figures 3.1 a, b, and c).

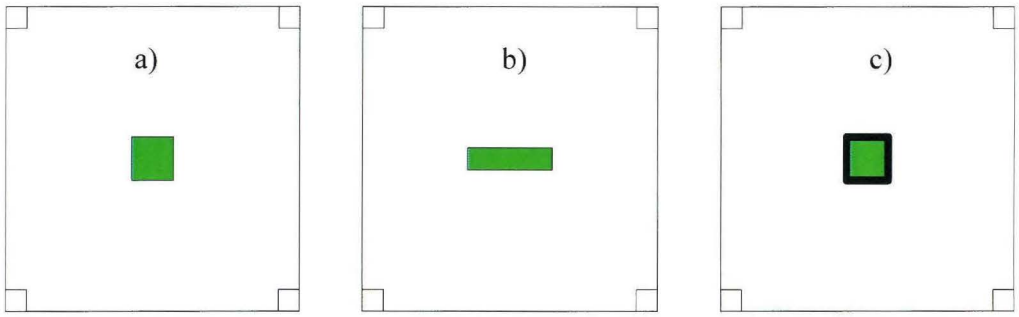

Figure 3.1 *Inlet Configurations: a) Square Inlet, b) Rectangular Inlet, c) Inlet with Nozzle*

Figure 3.2 shows the side view of the calculated flow field for square and rectangular inlets. (see Figure 3.1 a and b).

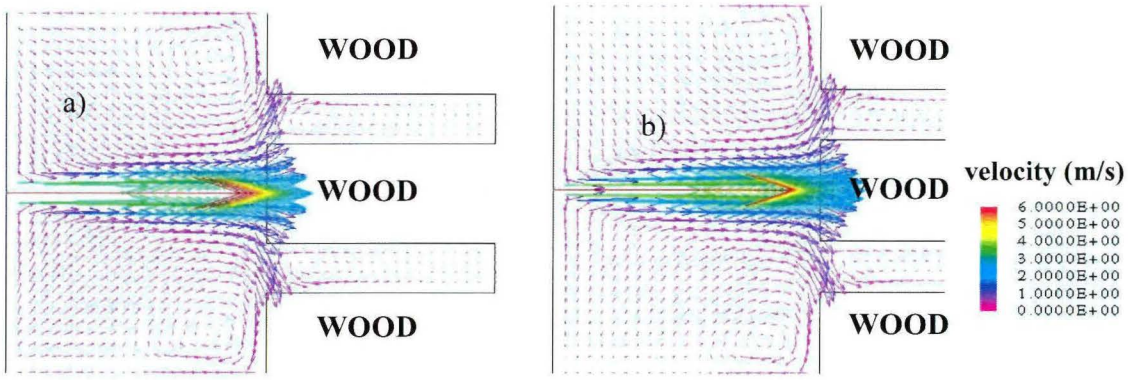

Figure 3.2 *Velocity Field of a) Square Inlet and b) Rectangular Inlet (Side View)*

Figure 3.3 shows the top view of the flow field for the same systems.

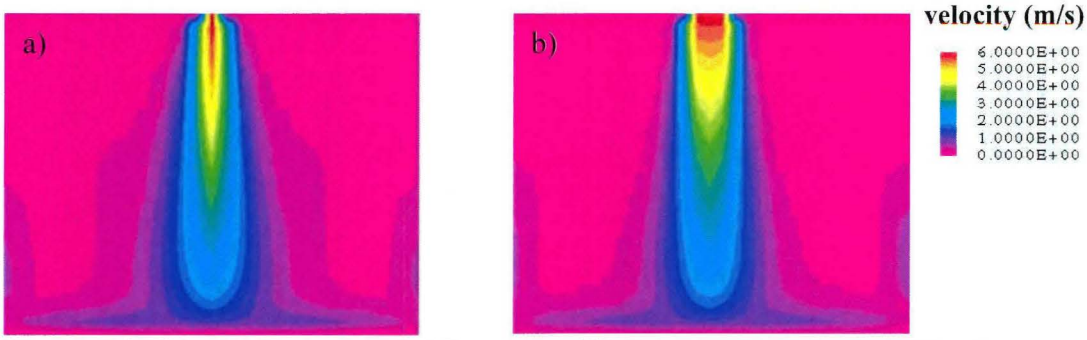

Figure 3.3 *Velocity Contours of a) Square and b) Rectangular Inlet (Top View)*

Similar results are presented for the inlets equipped with 6mm and 12 mm nozzles in Figure 3.4.

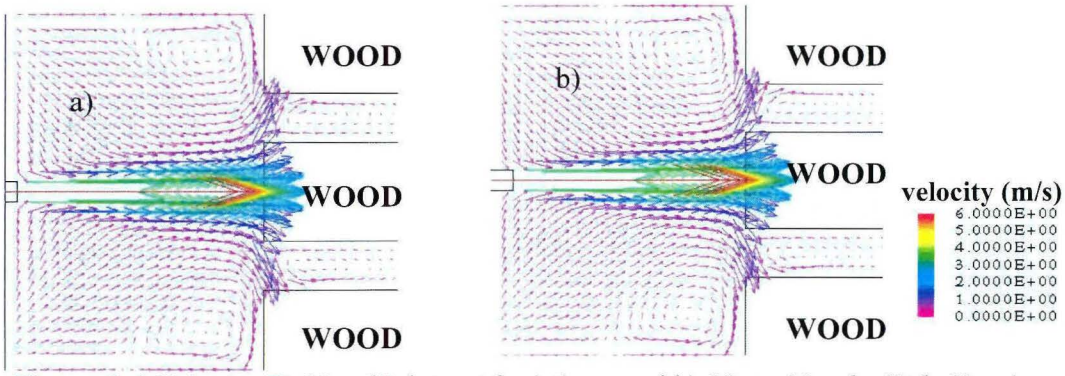

Figure 3.4 *Velocity Fields of Inlets with a) 6mm and b) 12mm Nozzle (Side View)*

As it can be seen from these figures, the geometry of the inlet doesn't affect the flow distribution significantly. The wood configuration relative to the inlet position has the major effect on the flow distribution.

3.4.2 Effect of Relative Positions of Wood and Gas Inlet on Flow Distribution

The effect of relative positions of wood slabs and gas inlet on the flow distribution was studied for two different configuration of the wood shown in Figure 3.5. These are:

a) Inlet placed in front of the flow channel (see Figure 3.5 a) and,

b) Inlet placed in front of the wood (see Figure 3.5 b).

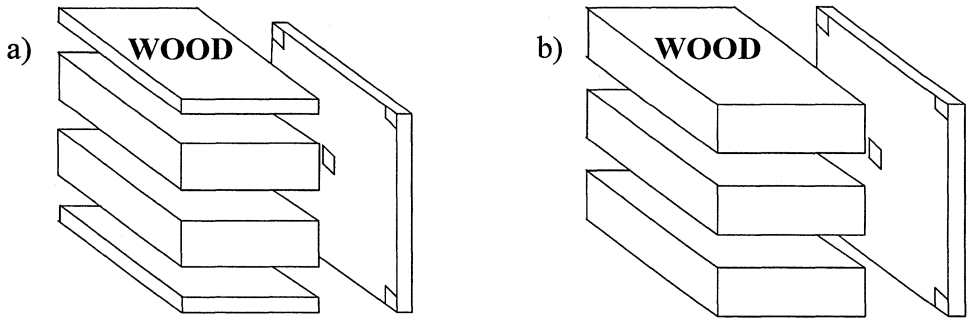

Figure 3.5 *Wood Configurations a) First Configuration, Inlet in Front of the Flow Channel; b) Second Configuration, Inlet in Front of the Wood*

The results of the calculations are presented in the following Figures. The Figures 3.6(a) and 3.6(b) show the side view of the flow distribution for two wood configurations.

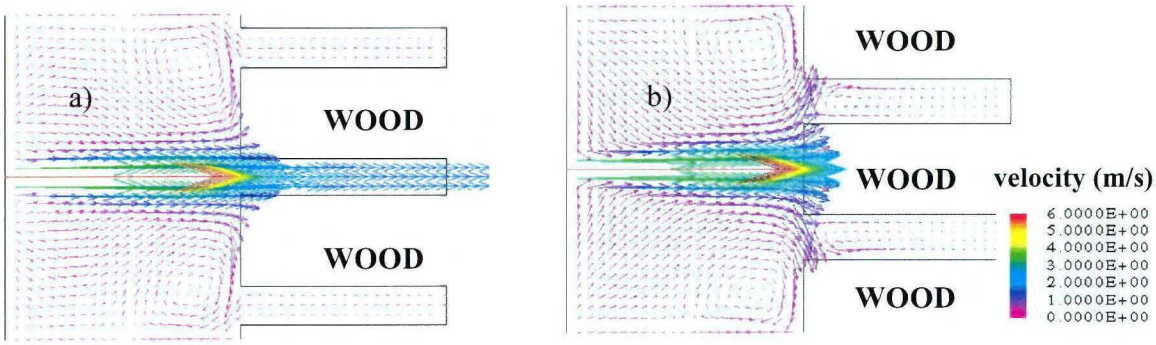

Figure 3.6 *Velocity Field at the Inlet with a) First and b) Second Configuration of the Wood (Side View)*

The effect of wood arrangement on the flow distribution between the wood layers can be easily seen from these figures. When the inlet is in front of the wood, the flow in the channel is very weak. If the inlet is in front of the channel, the gas flows though this channel. In these simulations inlets are represented as holes on the wall without any nozzle.

Figure 3.7 presents the top view of the flow field for the system shown in Figure 3.6 b.

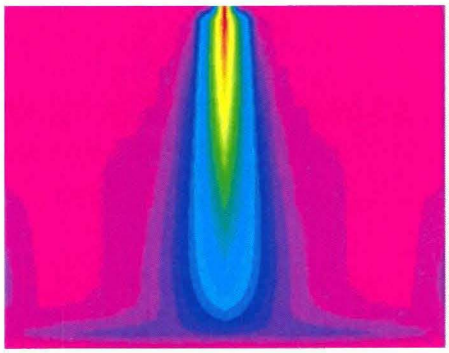

Figure 3.7 *Velocity Contours at Inlet (Top View)*

3.4.3 Prediction of the Gas Flow Though the Distribution Channel

In the plant at St.Ambroise, it was observed that the velocities are slightly different at various inlets depending on their location on the distribution channel. It was also seen that if the nozzle is removed from an inlet, the velocity slightly changes (around 5%). To explain this behavior observed in the plant, flow distribution in a horizontal gas distribution channel with ten inlets was modelled with and without nozzles. The results are presented in Figures 3.8 to 3.11. For all these cases, the gas inlet velocity to the channel is taken as 8m/s. Figures 3.8 to 3.11 have the same legend and it is presented in Figure 3.8.

Figure 3.8 shows the velocity distribution when the inlets are not equipped with nozzles. In the channel, the velocity decreases progressively through the channel as the gas flows, as expected. However, the velocities at the inlets close to the end of the channel are higher compared to those closer to the inlet side of the channel due to the pressure build up (7.5%). The velocity distribution in the channel is shown for ten inlets with nozzles in Figure 3.9.

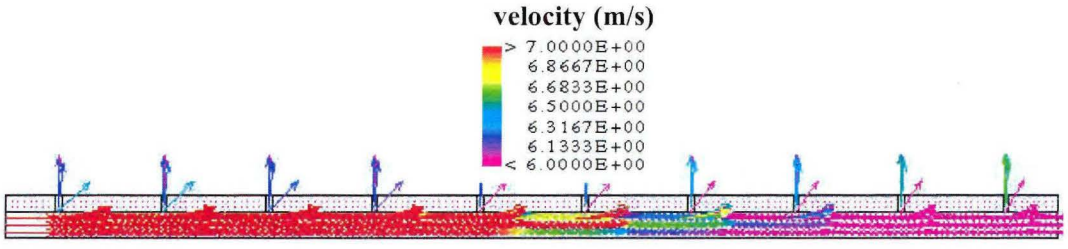

Figure 3.8 *Velocity Distribution of the Gas in the Channel for Inlets without Nozzle (Top View)*

Figure 3.9 *Velocity Distribution of the Gas in the Channel for Inlets with Nozzle (Top View)*

The trend is similar to the inlets without nozzles. However, the differences between the inlet velocities at various locations along the channel are less pronounced when nozzles are present compared to those without nozzles (5%).

The velocity profiles in the channel are also presented for the following cases:

a) when the nozzle is removed from the first inlet (Figure 3.10),

b) when the nozzle is removed from the last inlet (Figure 3.11).

In these cases, all the other nine inlets have nozzles. The velocity of the inlet increases when the nozzle is removed in both cases compared to the cases when all the inlets had nozzles (see Figure 3.9). This is due the elimination of additional friction in the nozzle.

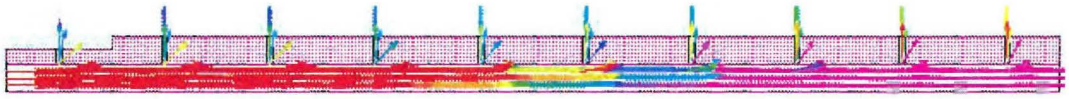

Figure 3.10 *Velocity Distribution of the Gas in the Channel for First Inlet without Nozzle and Nine Other Inlets with Nozzles (Top View)*

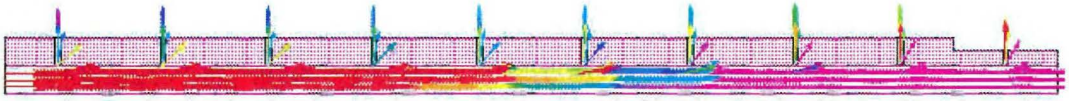

Figure 3.11 *Velocity Distribution of the Gas in the Channel for First Nine Inlets with Nozzles and Last Inlet without Nozzle (Top View)*

3.5 Numerical and Analytical Heat Transfer Analysis

Heat transfer and temperature distribution in a piece of wood was calculated numerically (section 3.5.1) and analytically (section3.5.2) in order to predict the temperature distribution. The results were compared in section 3.5.3.

3.5.1 Numerical Results

The wood at 298 K initial temperature was heated from two sides. The temperatures of the side faces was raised to 473 K and kept constant at this value. The distribution of the temperature in the wood for a period of 6,000s was calculated. In Figure 3.12, temperature distribution in the middle plane at 4,000s is shown with shaded contours.

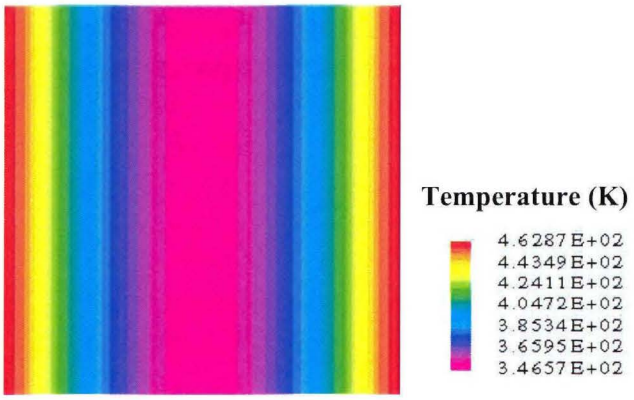

Figure 3.12 *Temperature Distribution in the Wood at t=4,000s.*

Temperature distribution in the same plane at 5,000s is given in Figure 3.13.

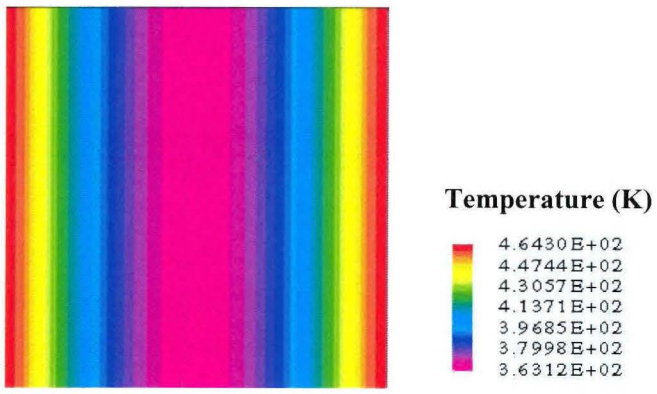

Figure 3.13 *Temperature Distribution in the Wood at t=5,000s.*

Final temperature distribution (t=6,000s) in the same plane is shown in Figure 3.14. The wood was not heated uniformly at the end of the heating period.

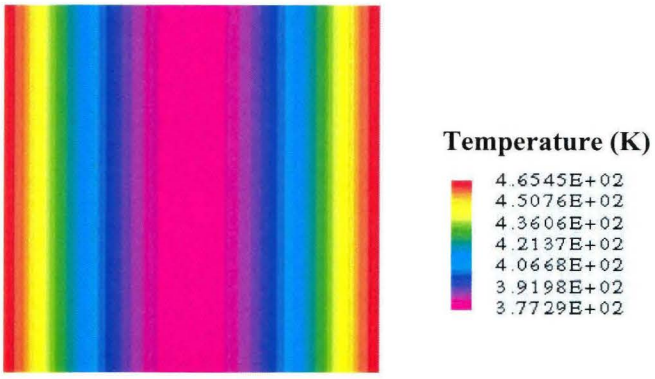

Figure 3.14 *Temperature Distribution in the wood at t=6,000s.*

Temperatures obtained for three different time intervals are tabulated in Table 3.1.

Table 3.1 *Temperature Distribution in the Wood (Predicted by the model)*

		Temperature (K)		
		t = 4,000 s	t = 5,000 s	t = 6,000 s
Distance from the (m) center	0	346	363	377
	0.1	352	368	382
	0.2	369	383	396
	0.3	398	408	416
	0.4	433	439	443
	0.5	463	464	465

3.5.2 Analytical Results

Temperature distribution in the wood was also calculated [28] analytically using Heisler charts, for one dimensional transient conduction in a plane wall for the same time periods. The calculated values are given in Table 3.2.

Table 3.2 *Temperature distribution in the Wood (Analytical)*

		Temperature (K)		
		t = 4,000 s	t = 5,000 s	t = 6,000 s
Distance from the center (m)	0	368	389	400
	0.1	373	393	403
	0.2	387	404	413
	0.3	410	423	429
	0.4	438	445	449
	0.5	447	452	455

The analytical calculations were done in two steps. First one is the calculation of the mid-plane temperature (T_p) from Biot and Fourier numbers. The second step is the calculation of the temperature at the other planes from T_p.

The main difference between the results presented in Table 3.1 and 3.2 is resulted from the determination of mid-plane temperature T_p, in other words from the first step of the analytical calculations. When the second step of analytical calculations were performed with mid-plane temperature found from the numerical method instead of the analytical one (first step), it is seen that the temperature distributions are similar. The results are compared in Table 3.3.

Table 3.3 *Comparison of Temperature Distribution in the Wood(Analytical and Numerical)*

t	x	T (Analytic Solution)	T(Model Prediction)	Difference
4,000	0	346	346	0
4,000	0.1	352	352	0
4,000	0.2	369	369	0
4,000	0.3	397	398	-1
4,000	0.4	431	433	-2
4,000	0.5	441	463	-22
5,000	0	363	363	0
5,000	0.1	369	368	1
5,000	0.2	383	383	0
5,000	0.3	407	408	-1
5,000	0.4	437	439	-2
5,000	0.5	446	464	-18
6,000	0	377	377	0
6,000	0.1	382	382	0
6,000	0.2	394	396	-2
6,000	0.3	415	416	-1
6,000	0.4	441	443	-2
6,000	0.5	449	465	-16

analytical calculations. When the second step of analytical calculations were performed with mid-plane temperature found from the numerical method instead of the analytical one (first step), it is seen that the temperature distributions are similar. In this case, the temperature distribution in the wood is almost the same for both methods; however, there is difference in the surface temperature. We can conclude that for both methods there are two critical planes; mid-plane and the surface of the wood. The error is mainly resulted from the inaccurate reading of the Heisler charts in the analytical calculations. Better solution can be obtained by solving analytical equations.

3.6 Conclusions

The gas inlet geometries and wood configurations were investigated to see the effects of these parameters on the velocity field. It is concluded that with current injection geometry it is difficult to obtain homogenous gas distribution in the furnace.

The modelling results showed that the stationary inlet geometries do not have much effect on gas distribution around the woods. However, it is observed that two different wood configurations resulted in significantly different gas distributions.

The temperature distribution calculated in a small block of wood was compared with the analytical results. The differences were observed between the model and analytical calculations are due to the error in Heisler chart readings at two critical planes; mid plane and surface plane.

CHAPTER 4

FLOW MODEL

4.1 Description of The Model

A 3D, steady-state, and isothermal flow model of the wood heat treatment furnace was developed in order to predict the flow field. The uniformity of the gas distribution is very important because the heat is transferred to wood from the hot gas. If the supply of hot gas is not similar to different parts of the charge, its treatment won't be uniform and this will result in a non-homogeneous product. The gas circulation is also important for the removal of the humidity released from the wood layers.

4.2 Model Development

The equations together with the boundary conditions were solved numerically by a commercial CFD program. The physical flow domain was discretized. The CFX4 commercial code was used to solve the equations.

4.3 Governing Equations

The continuity and conservation equations described in section 3.3 can be written, respectively, as follows:

$$\frac{\partial \rho}{\partial t} + div\,(U\,.\rho) = 0 \qquad (4\text{-}1)$$

$$\frac{\partial \rho v}{\partial t} + div\,(\rho v \otimes v) - div\,(\mu_{eff}\ gradv\ ) = B - divP\ + div\,(\mu_{eff}\ divv\,) \qquad (4\text{-}2)$$

where v: velocity

x, y, z : coordinate axis

μ_{eff} : effective viscosity including the turbulent viscosity: $\mu_{eff} = \mu + \mu_T$

B : body force

The transport equation for the turbulence kinetic energy k is:

$$\frac{\partial \rho k}{\partial t} + div\,(\rho v \otimes k) - div\,((\mu + \frac{\mu_T}{\sigma_k})\ gradk\ ) = P_{prod}\ + G_{BF}\ - \rho\beta \qquad (4\text{-}3)$$

where k : turbulence kinetic energy

σ : stress tensor

P_{prod} : shear production $P_{prod} = \mu_{eff} \nabla U \cdot (\nabla U + \nabla U) - \frac{2}{3} \nabla U (\mu eff \nabla U + \rho k)$

G_{BF} : production due to the body force

β : turbulence dissipation rate

The transport equation for the turbulence dissipation rate is:

$$\frac{\partial \rho \beta}{\partial t} + div(\rho v \otimes \beta) - div((\mu + \frac{\mu_T}{\sigma_k}) grad \beta) = C_1 \frac{\beta}{k} (P_{prod} + C_3 - C_2 \rho \frac{\beta^2}{k}) \qquad (4\text{-}4)$$

where C : constants

For the steady-state model, the terms representing the change of dependant variable with time (see equations 4.2, 4.3, and 4.4) are taken zero.

4.4 Boundary Conditions

- No slip condition (velocities are zero at the solid surfaces)
- Velocities are known at the gas injection inlets.
- Outlets are specified as mass flow boundaries. This insures that the mass balance is respected.
- Wood is represented as solid, 3D solid patch.

4.5 Assumptions

The assumptions used in the model development are:

- Steady state
- There is no heat transfer, mass transfer, or chemical changes.

4.6 Numerical Procedure

The Navier-Stokes equations are solved using the finite volume method and structured grid. The equations are discretized by applying the conservation laws to each of the control volumes. Each equation was integrated over each control volume to obtain a discrete equation which connects the variable at the centre of the control volume with its neighbors.

All the equations, which have the general formula given in equation (3-2), take the following form after the integration over the control volume:

$$\int \frac{\partial \rho \varphi}{\partial t} dV + \int \rho v \varphi \cdot n dA - \int \xi \ grad \ \varphi \cdot n dA = \int S \varphi dV \qquad (4\text{-}5)$$

The first term on the left hand side was taken as zero for the steady-state solution. All terms in all equation were discretized in space using second order centered differencing

apart from the advection terms, and the convection coefficients obtained using the Rhie-Chow interpolation formula [29].

On the discretized mesh, the Navier-Stokes equations were written as a large system of nonlinear equations. The differential equations were linearized and solved implicitly with SIMPLE algorithm using a 0.5 under-relaxation factor for all the dependant variables until convergence was achieved.

4.7 The Physical Domain

The furnace details were given in section 2.1.4 of Chapter 2. A two-dimensional view of the furnace and its charge, as seen from the door side, is shown in Figure 4.1.

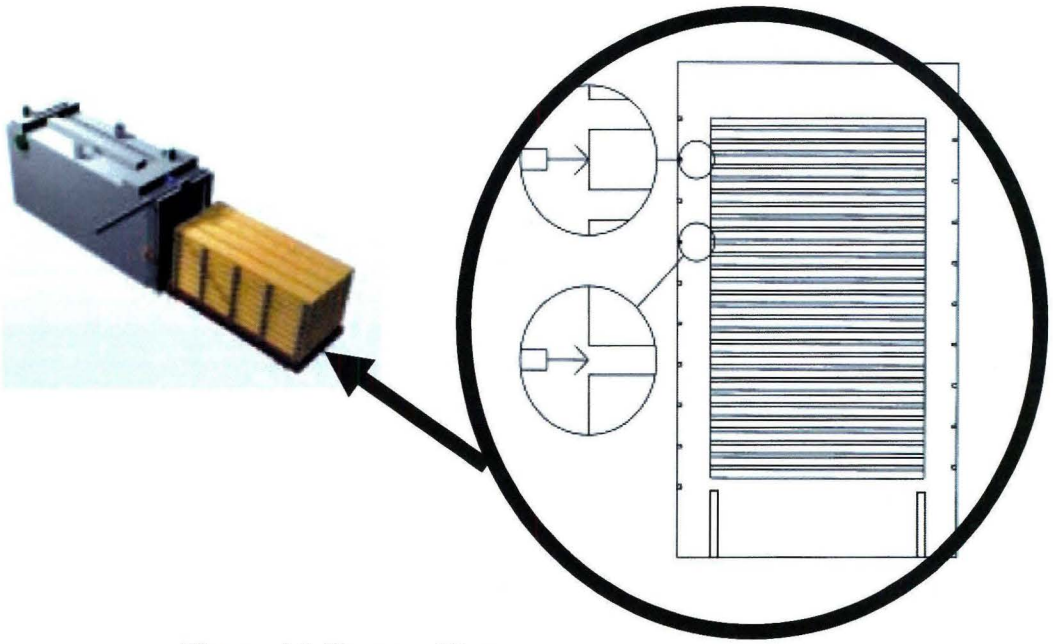

Figure 4.1 *Furnace View*

To represent the whole furnace, millions of cells are required. This is difficult due to the memory limitations of the computer. In the furnace, the inlets and outlets are placed at the side walls in staggered configuration. This configuration is repetitive except at the two ends of the furnace. Therefore, one representative section of the furnace was modelled. Preliminary simulations were carried out to find the minimum number of cells required to solve the flow correctly, and 204,000 cells were found to be appropriate. Since the section is repetitive the simulation is valid at all parts of the furnace except at the ends.

There are 26 rows of wood and 25 channels between the wood layers (channel no 2-26). First channel is the volume under the trolley supporting the wood pile and last channel (channel no 27) is the volume above the wood pile. The modelled section, the arrangement of wood layers and channel numbers can be seen in Figure 4.2. The details of the geometry are given in Appendix 2 (see Figures A2.1, A2.2, A2.3, and A2.4). The walls on both sides of the wood are equipped with inlets and outlets. At inlets, the gas is injected whereas, at the outlets it is suctioned out. The inlets and outlets are staggered.

The geometry created for the model has the dimensions:

$h_1 = 2.552$ m

$h_2 = 5.104$ cm

$h_3 = 7.656$ cm

w= 1.549 m

Total number of wood slabs is 26.

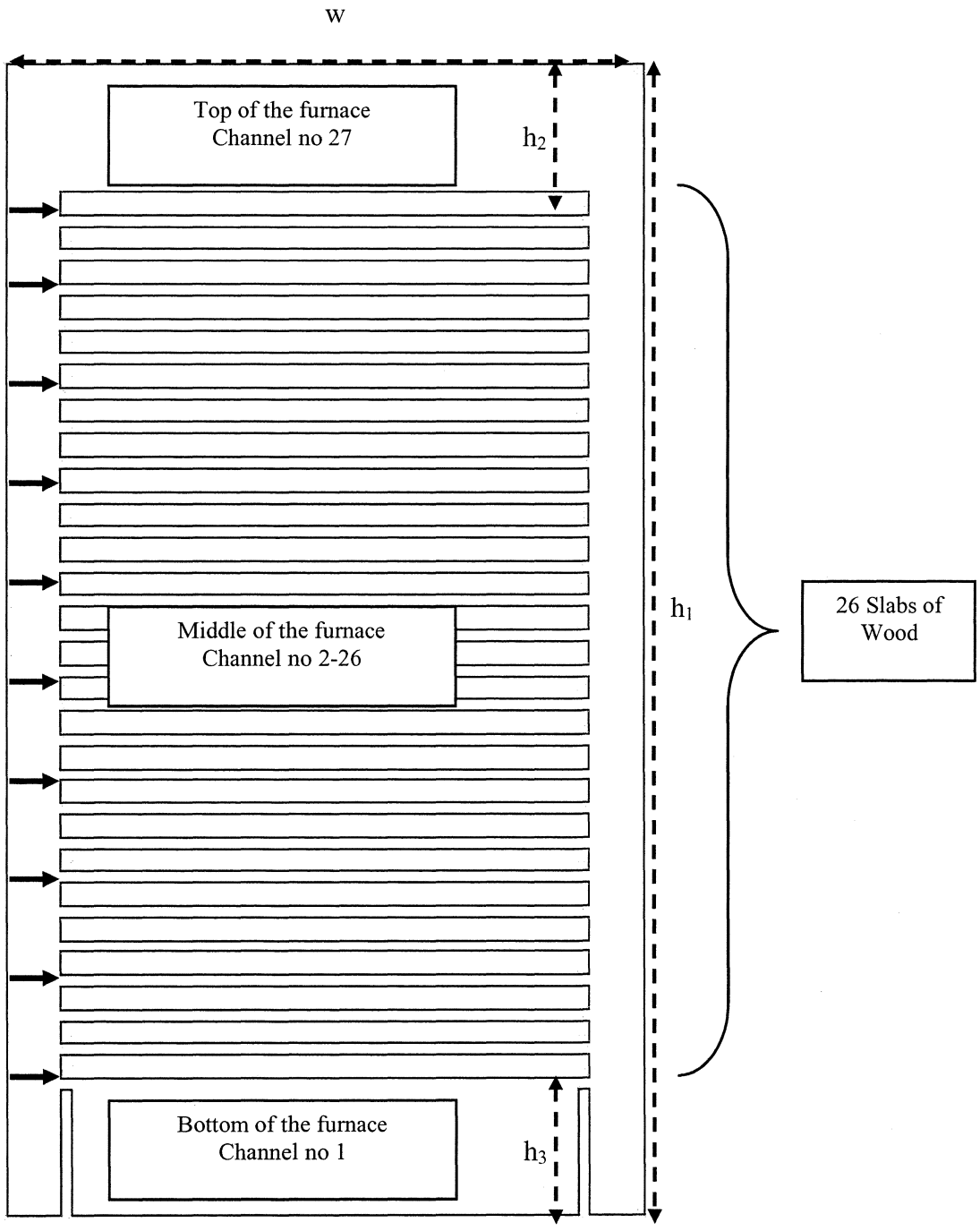

Figure 4.2 *Wood Arrangement and Channel Numbers in the 2D View of the Furnace*

4.8 Model Inputs and Parameters

In the model, there is no heat and mass transfer; only the steady-state flow field was calculated for different gas injection velocities which are summarized for each case in Section 4.10.

The physical properties for air and water which are available in PCP database in CFX-F3D material properties database interface were used.

4.9 Methodology

In the command file, the physical domain was created, and the grid was generated. To represent the whole furnace, many of cells are required. Simulations were carried out to find the minimum number of cells required to solve the flow, and 204,000 cells were found to be appropriate. When the cell sizes are chosen, the following factors should be taken into account:

- A side of cell can not be more than twice the side of the adjacent cell, if they are on the same axis,
- A minimum of two cells is required between solid surfaces to calculate the flow.

Initial values, physical constants, and turbulence parameters were set in the command file. The flow field was computed using CFX. The objective was to find the conditions leading to uniform flow distribution.

4.10 Results and Discussion

The predicted flow field for the St. Ambroise furnace is given in Figure 4.3. The maximum velocity (5m/s) is shown with red on the figures. This corresponds to the injection velocity.

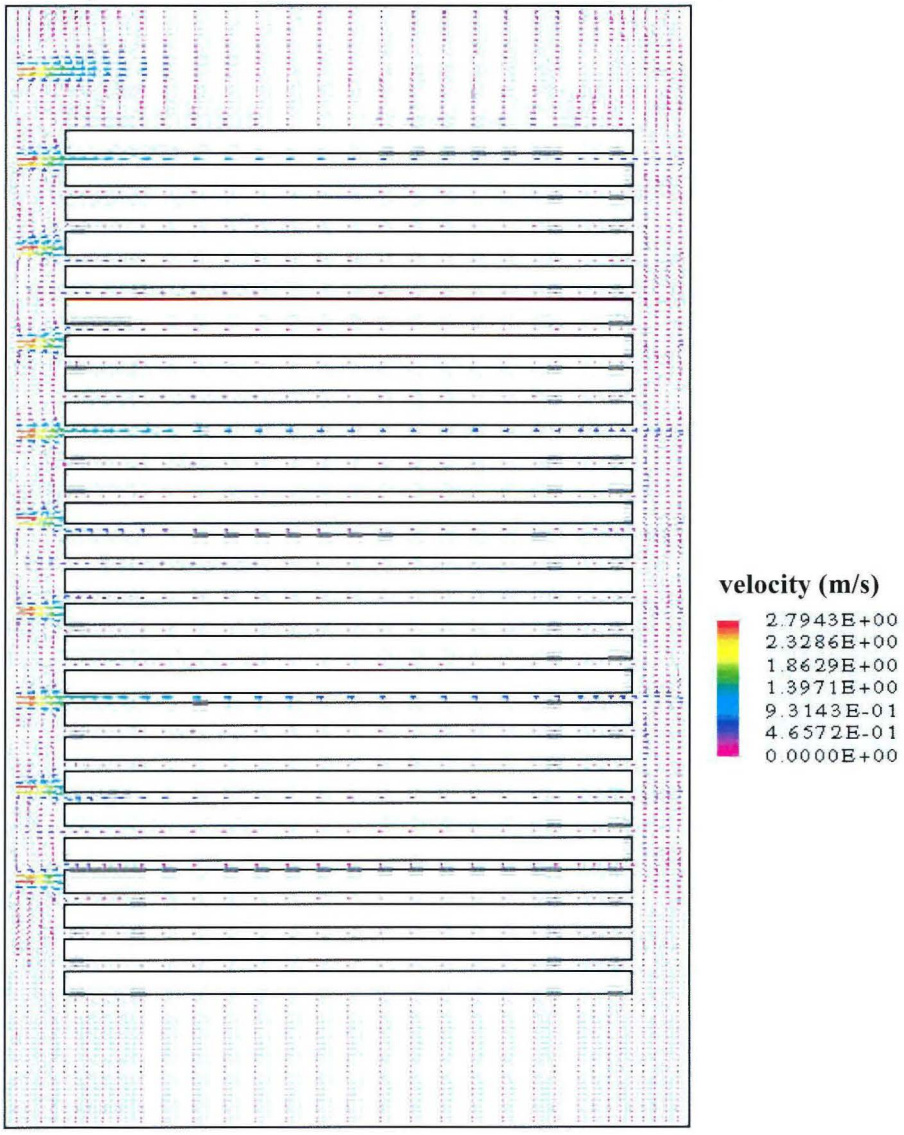

Figure 4.3 *One section of the Furnace at St.Ambroise*

The results showed that the flow distribution is not uniform in the furnace. When the inlet is in the front of the channel between the wood layers, the gas can flow through; but when the inlet is in front of wood, the gas hits to the wood and dissipates. If the gas is not distributed uniformly, the wood will not be treated uniformly. Therefore, the inlet geometry was studied in more detail.

4.11 Parameter Analysis and Results

A number of parameters were varied in order to identify the conditions leading to a more uniform flow distribution compared to the actual distribution calculated in the furnace. The cases simulated are:

- Case 1: change in injection velocities
- Case 2: change in injection angles
- Case 3: blocking the regions above and below the wood pile
- Case 4: change in injection geometry

For all cases, the wood dimensions and distance between the wood layers as well as the furnace dimensions are kept constant. The gas mass flow rate between the wood layers was calculated in the middle of the channels and compared.

4.11.1 Effect of Injection Velocity

This part of the work is aimed at studying the effects of different injection velocities on the flow. Simulations were carried out for three different injection velocities (6m/s, 3m/s and 1m/s). For these three cases, the injection velocities were identical for each nozzle. Another case was simulated for varying injection velocities (3.2-6.3 m/s, see Table 4.1) along the vertical direction.

Table 4.1 *Injection Velocities*

Injection number		**Injection Velocity (m/s)** Left wall	Right Wall
Bottom	1-2-3	6.3	6.3
	4-5-6	4.3	4.3
	7	4.3	6.2
	8	6.2	6.2
	9	6.2	3.2
Top	10	3.2	-

The gas velocity was higher at the channels that are directly in front of the injection nozzle and lower in the others. Therefore, this last simulation was carried out to see if imposing varying velocities at different levels of the furnace could compensate for this effect. Figure 4.4 compares the mass flow rates calculated at the mid-point of all the

channels for different injection velocities. It is desired to obtain equal mass flow rates in all channels.

However, it can be seen from the Figure 4.4 that in some channels (channel no 5-7-10-13-15-18-21-23-26), which are placed directly in front of the nozzle, gas mass flow rate is much higher than the mass flow rate in others which are positioned between nozzles.

Increasing the injection velocity increases the gas mass flow rate in the channels which are in front of the inlets (such as in channels no10 and 26); however, increase in mass flow rate in the other channels is not significant (such as in channels no 9 and 25). Therefore, increasing the velocity does not solve the problem of non-uniform flow distribution.

Instead of using the same injection velocity along the vertical plane, varying injection velocities can be imposed at different inlets. Velocities at the channels which are directly in front of the inlets can be decreased and the others can be increased. However, this is not a practical solution because the dimensions of the wood pile can differ slightly from one charge to another as expected during an industrial operation. Even 1-2 mm change can affect the gas flow because the injection nozzle has only a diameter of 12 mm.

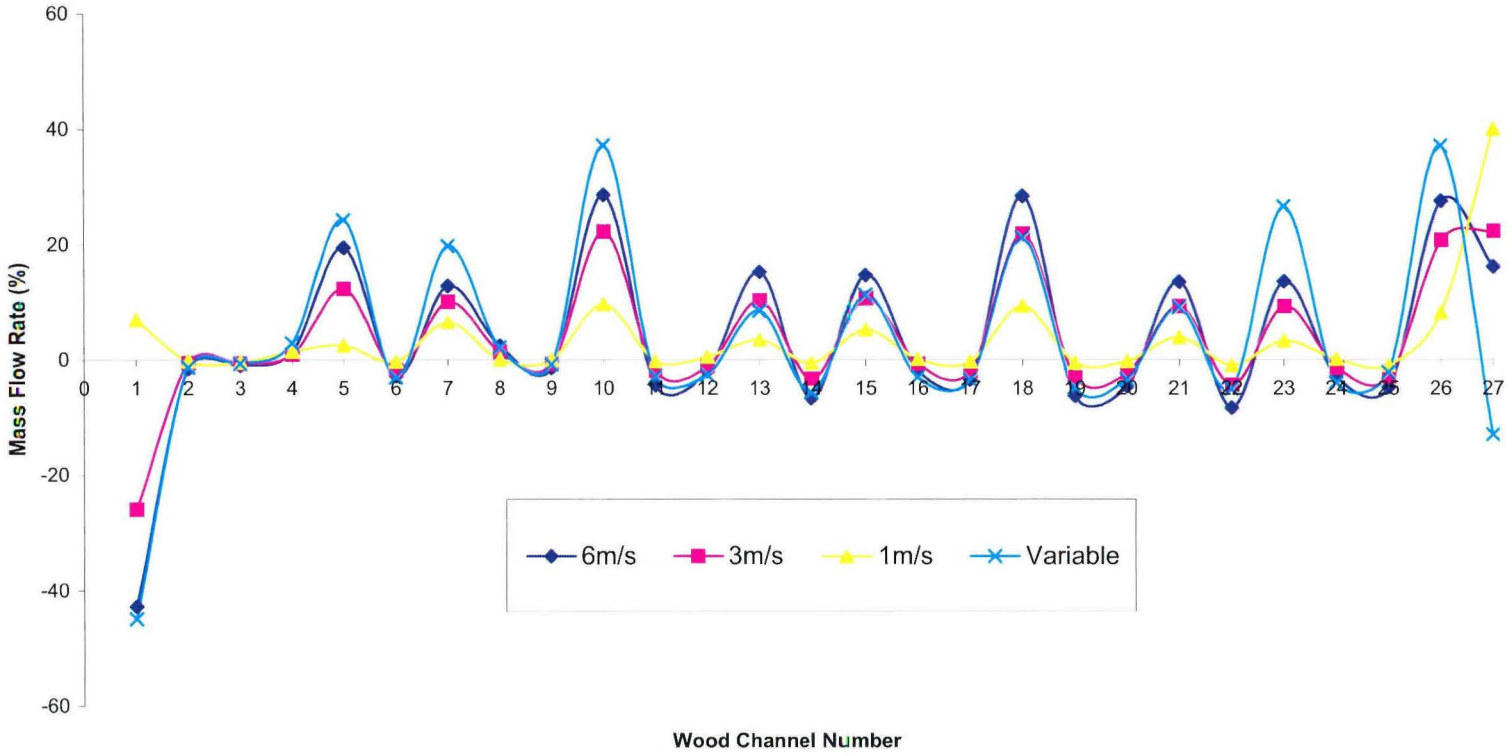

Figure 4.4 *Effect of Injection Velocity on the Mass Flow Rate in Different Channels*

4.11.2 Effect of Injection Angles

This part's objective is to study the effects of different injection angles on the flow distribution.

The gas is injected horizontally without any angle in the actual furnace. The simulations were carried out using three different injection angles (15°-30°-45°). The results of these cases are compared with the flow predicted for the actual angle used (0°-Original) in Figure 4.5. The same results are also presented in Figure 4.6 without the bottom and top channels in order to see the mass flow rate fluctuations between the channels better.

As the angle increases mass flow rate fluctuations between the channels are reduced; however, there is more gas circulating at the top and bottom of the wood layers compared to the case representing the actual situation. This gas does not enter between the wood layers. In the simulations, the nozzles were positioned towards the furnace bottom. Therefore there is more gas entering to the lower channels compared to the upper ones.

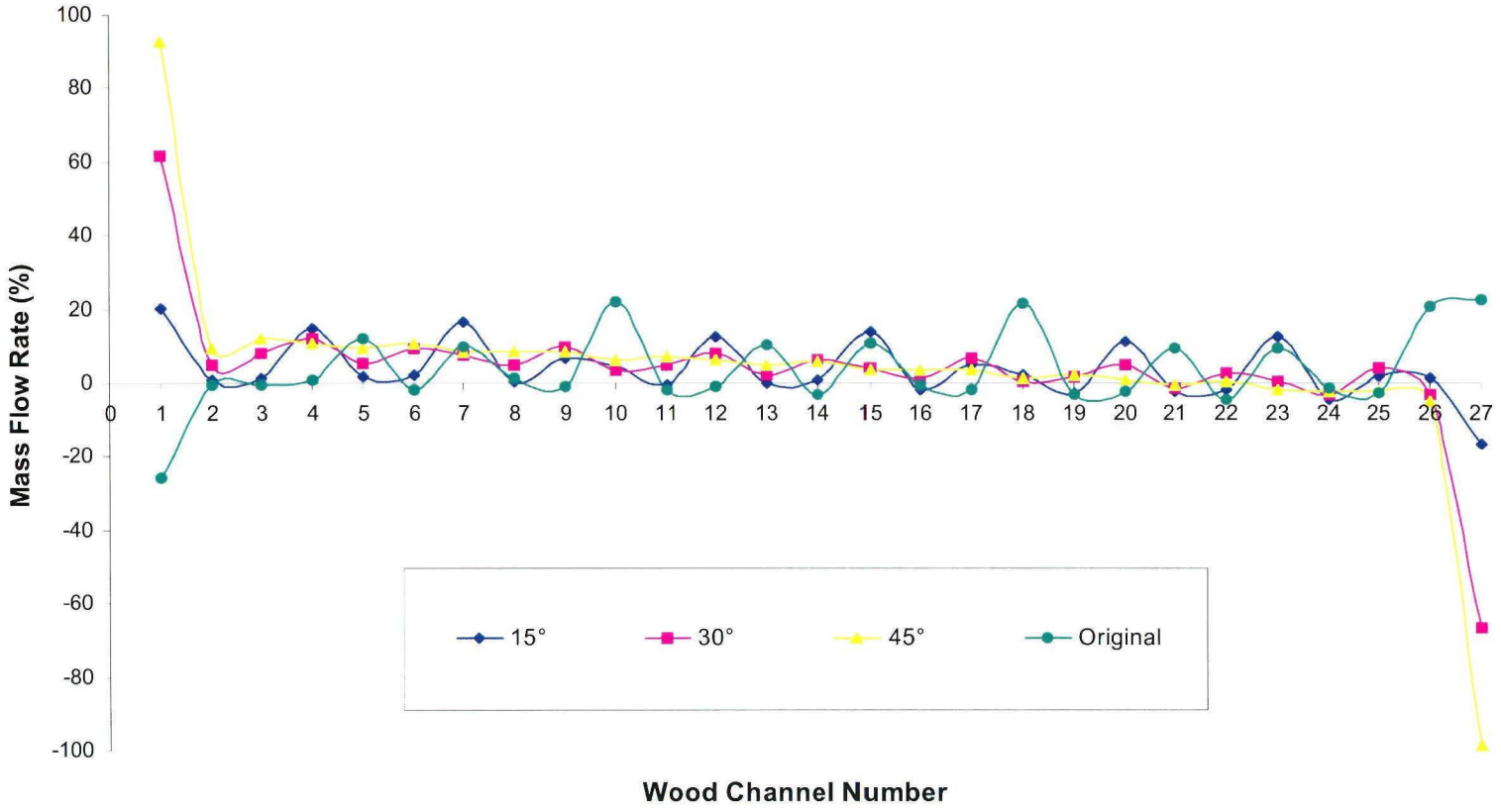

Figure 4.5 *Effect of Injection Angle on the Mass Flow Rate in Different Channels*

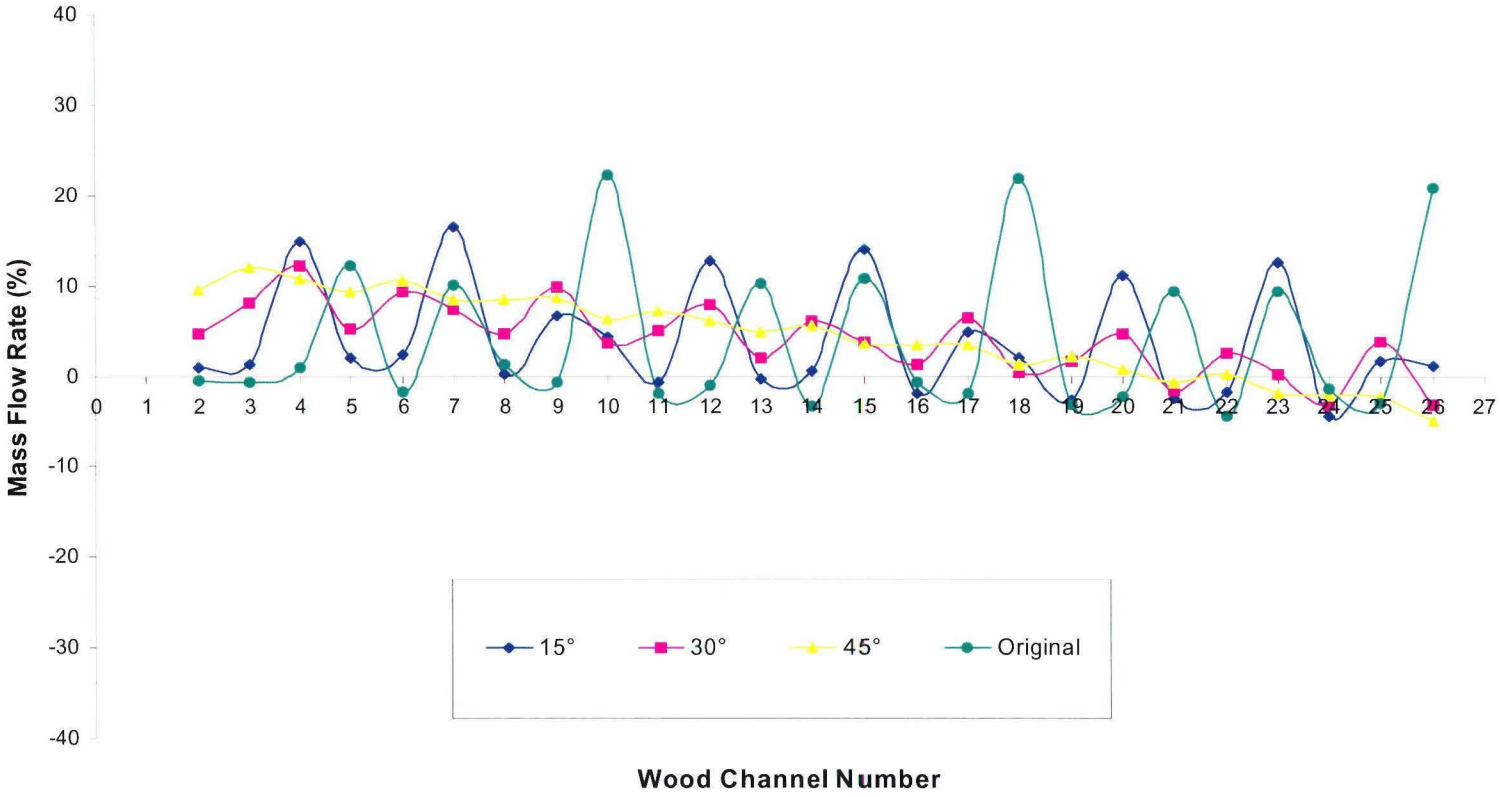

Figure 4.6 *Effect of Injection Angle on the Mass Flow Rate in Different Channels without Top and Bottom Channels*

4.11.3 Blocking the Regions Above and Below the Wood Pile

This part's objective is to decrease gas flow at the top and bottom of the furnace and force the gas to pass between the wood layers. For this purpose, the following four simulations were carried out:

a. The upper and lower regions of the wood pile were blocked using the actual furnace geometry. In practice, it is possible to close the sides of the trolley and this can also help prevent the resin accumulation and facilitate the operation of the trolley. Blocking the upper part can be more difficult because of the chimney.
b. Top injection nozzle was taken out of operation in order to decrease the flow circulation at the top without blocking the upper and lower regions of the wood pile
c. Top injection nozzle was taken out of operation and the upper and lower regions of the wood pile were blocked

The mass flow rate passing through the channels were compared for the conditions given above in Figure 4.7. When upper and lower parts of the wood pile were blocked the gas mass flow rate decreases in the first and last channels compared to the cases without blockage. As can be seen from the figure, gas flow rate increases in channels where it was low previously (channels 2-3-6-14-16-17-22-24-25) and decreases slightly in channels where it was high (channels 5-10-13-18-26). The resulting gas distribution is slightly more uniform than the original case; however, the flow direction is different in different channels (shown as positive and negative mass flow rates on the figure).

Blocking the upper injection nozzle did not result in a significant change in flow distribution.

As a summary, it can be said that blocking the upper and lower regions can help flow to become more uniform but other alternatives should be searched to improve the overall performance of the furnace and quality of the product.

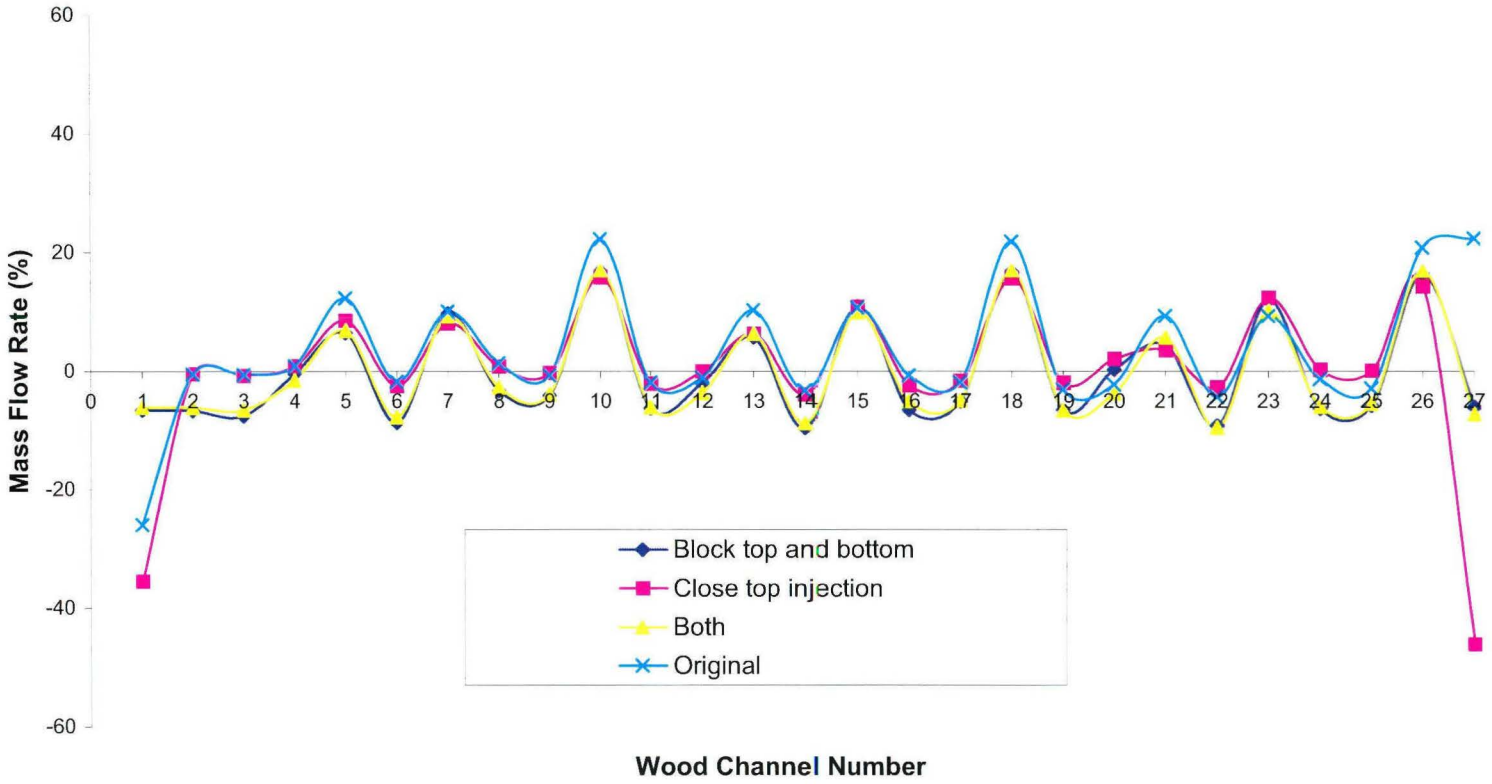

Figure 4.7 *Effect of Blocking Top and Bottom Channels and/or Top Injection Nozzle on the Mass Flow Rate in Different Channels*

4.11.4 Effect of Injection Geometry

This part's objective is to test the applicability of new injection geometry which has a greater surface area compared to that of the nozzle used currently.

The injection design considered consists of two co-centric rectangular prisms with truncated tops. The gas is injected from the truncated side. The angles of the sidewalls of the inner and outer prisms are different. The center of the prisms was blocked to prevent jet behavior. Figure 4.8 shows the new injection design. The total inlet mass flow rate was calculated using the inlet velocity of 3 m/s for the original nozzle design and this is kept constant during the simulations using the new design in order to be able to compare different cases.

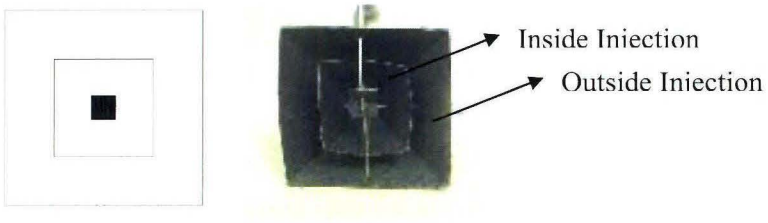

Figure 4.8 *New design: Co-centric Rectangular Prisms*

Following combinations of angles were used in simulations:

-Inside angle: 15° outside angle: 25°

-Inside angle: 15° outside angle: 30°

-Inside angle: 20° outside angle: 30°

-Inside angle: 20° outside angle: 35°

In most of the simulations with the new injection design, only the lower part of the wood pile (under the trolley) was blocked. The upper side of it was not blocked because this is more difficult to apply to the actual furnace due to the presence of the chimney. However, this condition can always be incorporated to the model. The results of the simulations carried out with new injection design using different angles are compared in Figure 4.9. The same results are compared with the simulation results obtained using the current nozzle in Figure 4.10.

It can clearly be seen from the Figures 4.9 and 4.10 that the new injection design eliminates the fluctuation significantly in the flow distribution in the channels resulting in more uniform gas distribution between wood layers. Consequently, this design will probably give more homogenous product. Blocking under the trolley increases the mass flow rate between the wood layers. Changing the angles of the new injection design did not seem to affect the mass flow rate significantly. In the actual furnace, the mass flow rate is very high in the channels which are in front of the injection nozzles and lower or negative in the others showing that the flow is in the other direction. This is the result of the re-circulation created in the furnace with jet like gas injection. When the new injection design is used, although the mass flow rate is not very high, the flow distribution is uniform and back re-circulation of gas is eliminated (no negative mass flow rate). It is believed that a very high mass flow rate is not necessary between the layers during heat treatment. The important factor is to have steady flow to supply heat to wood and remove the humidity released from the wood. This will be shown in the model results when heat and mass transfer in wood is incorporated into the model.

The results of the all the simulations presented in this chapter are compared in Figure 4.11 to see the effect of different injection configurations on the mass flow rate, consequently, on the flow distribution between the wood layers as well as around the wood pile. The proposed injection design seems to give the most uniform distribution.

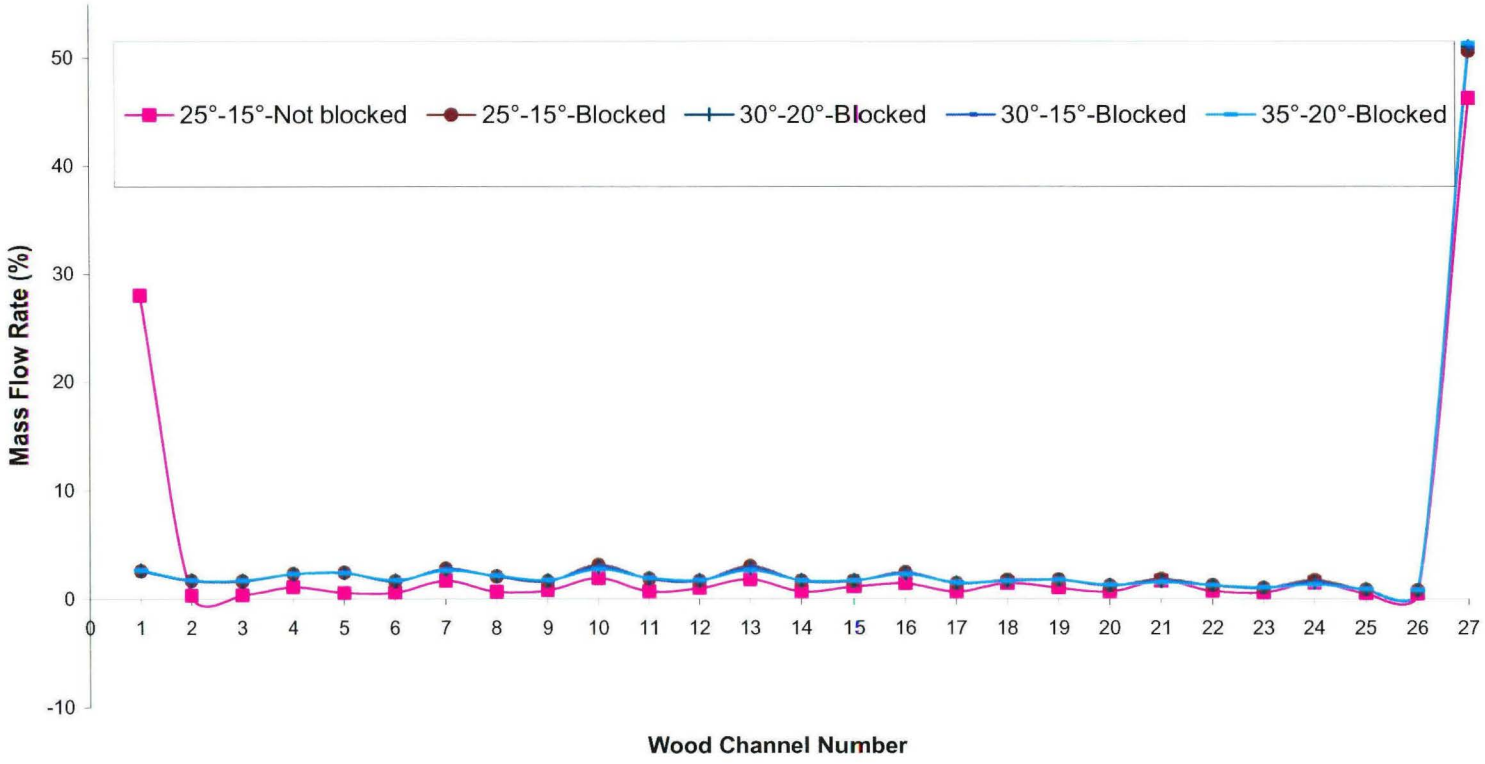

Figure 4.9 *Effect of New Injection Design on the Mass Flow Rate in Different Channels*

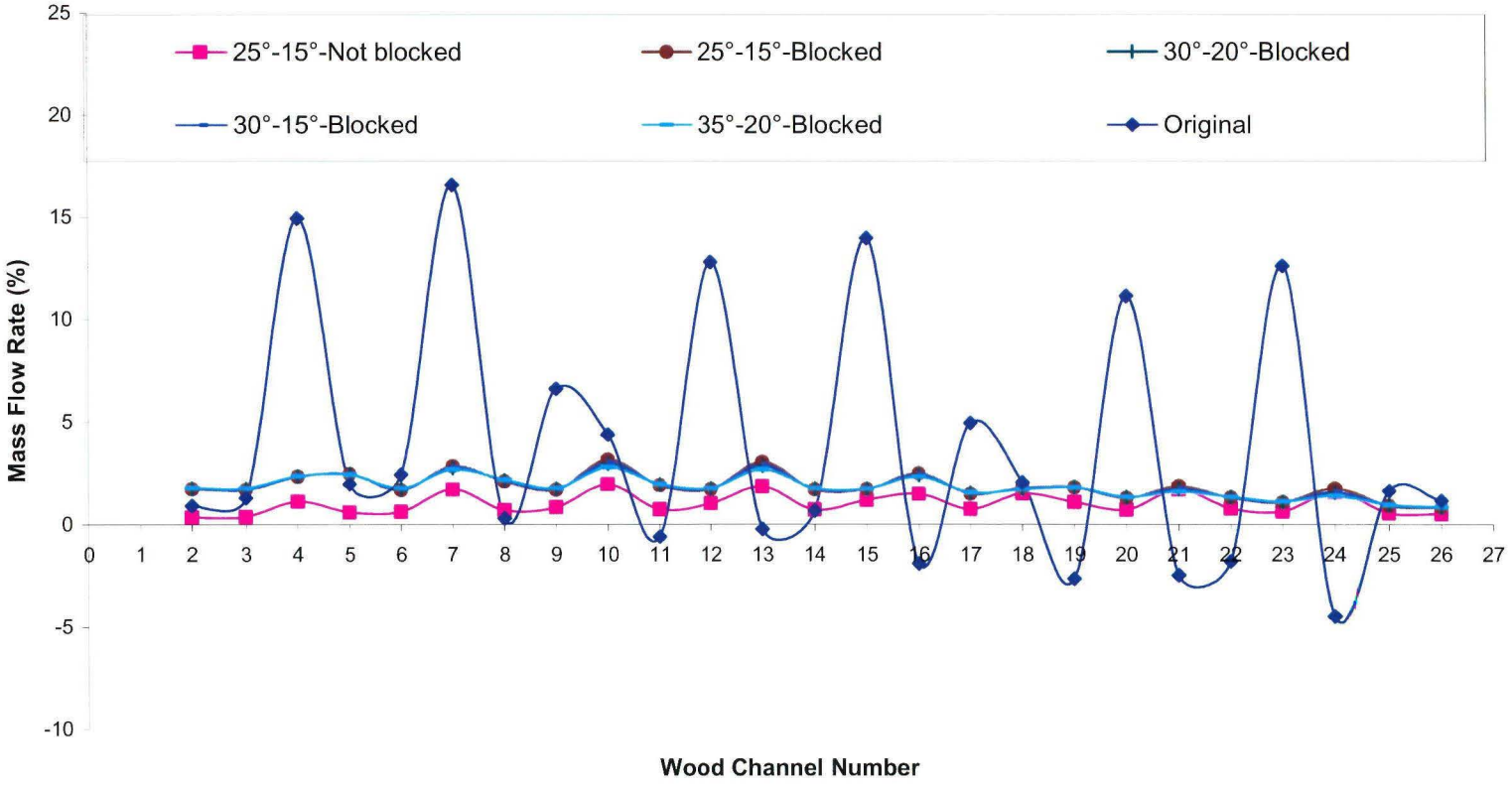

Figure 4.10 *Effect of New Injection Design on the Mass Flow Rate in Different Channels without Top and Bottom Channels*

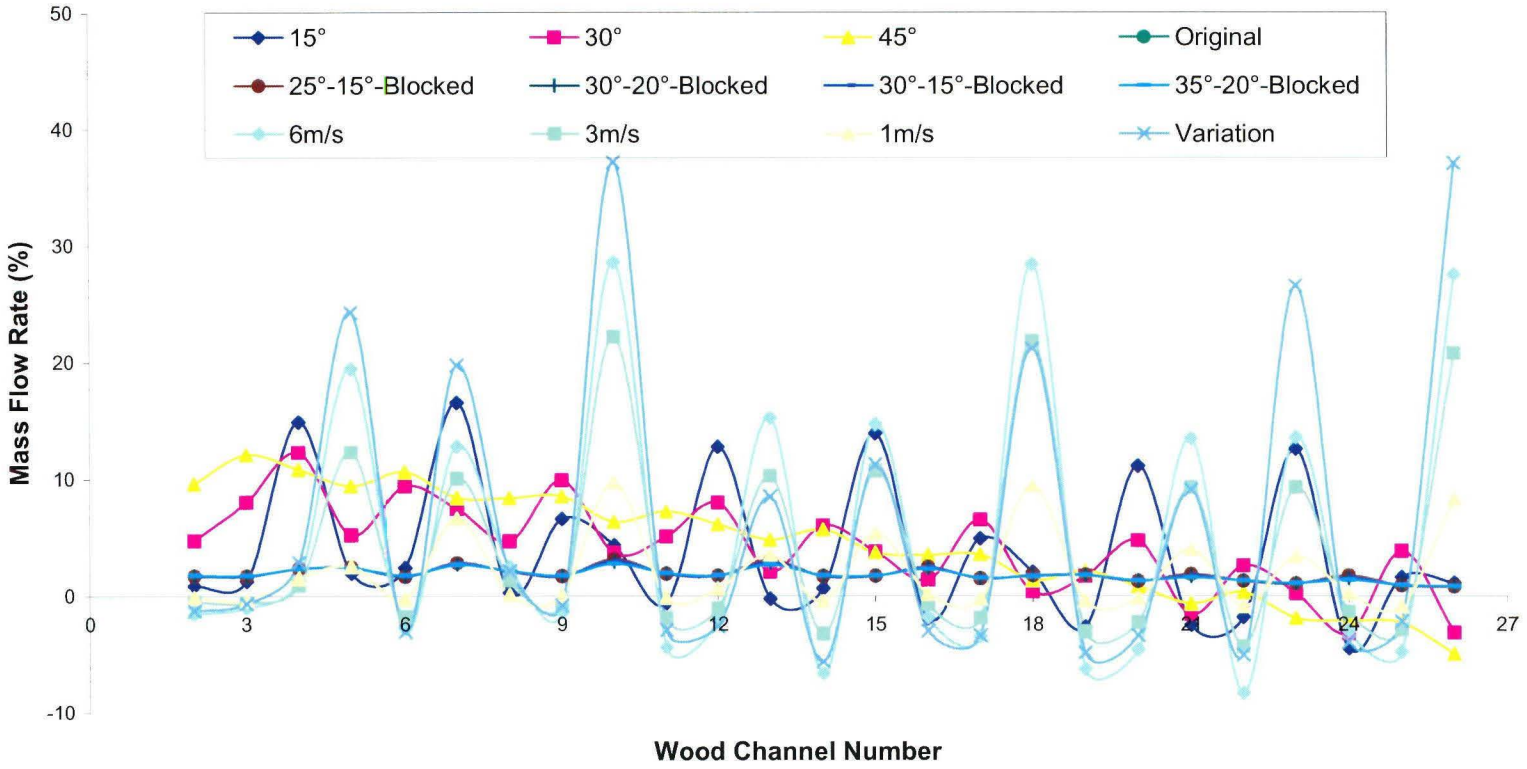

Figure 4.11 *Overview of Simulation Results*

4.12 Conclusions

This model only predicts the gas flow distribution in the furnace. The heat and mass transfer are not solved in this model. However, the model shows very clearly that the gas flow distribution is not uniform in the furnace. A parametric study was carried out using:

a) the current gas injection nozzle,

b) different injection parameters such as injection velocity and injection angle,

c) blocking the empty regions around the wood pile and forcing the gas through the channels between wood layers,

d) different injection design using two co-centric truncated rectangular prisms.

The above parametric study showed that:

- Changing injection velocity has a minor effect on the gas distribution.
- Changing injection angle does not prevent mass flow rate fluctuations in the channels between the wood layers.
- Blocking the upper and lower sides of the wood pile seems to help the gas distribution. With this configuration, gas is forced to go through the channels between the wood layers. This can also prevent the accumulation of resins on the trolley.
- New injection design improves significantly the distribution of gas in the channels. This design combined with the blockage of the empty regions below the wood pile gives the best result among the injections configurations presented in this chapter.

CHAPTER 5

HEAT TRANSFER MODEL

5.1 Description of Model

In the previous chapter, a 3D steady-state mathematical flow model, which was developed to calculate the gas distribution in the wood heat treatment furnace, was presented. This model is modified to solve the unsteady-state flow and temperature field in the gas. Then an 1D sub-model which solves the heat transfer in the wood was incorporated into the 3D model. The overall model gives the temperature profile in wood layers in addition to gas temperature and velocity profile in the furnace.

The model was validated by comparing the temperatures measured in plant with the predictions of the model.

5.2 Model Development

The heat transfer takes place by conduction within the wood and by convection between the wood layers and gas. Temperature distribution in the wood was calculated from the heat

balance using the Fourier's Law. The wood properties such as thermal conductivity, heat capacity, and density were taken constant. In this model, the mass transfer equations were not solved separately. An apparent thermal conductivity and a heat transfer coefficient were used to represent all the phenomena taking place. This approach is also used by other researchers [32]. Implicit form of finite-difference technique was used to solve the transient conduction with no internal heat generation. The linear, algebraic equation system was solved by using LU factorization.

5.3 Governing Equations

The heat balance in the wood is given as:

$$\rho c_q \frac{\partial T}{\partial t} = div\ (k_{app}\ \nabla T) \tag{5-1}$$

At the surface, the boundary condition is:

$$div\ (k_{app}\ \nabla T) + \alpha_q\ (T_a - T_s) = 0 \tag{5-2}$$

where k_{app} : apparent conductivity (see Appendix 3)

α_q : heat transfer coefficient

T_a : ambient temperature

The initial condition is:

$$T(x,0) = T_0$$

For the gas temperature the equation used with the gas properties is given below;

$$\rho_G c_{q_G} \frac{\partial T}{\partial t} = -div(v\rho_G c_{q_G} T) + div(k_G \nabla T) \qquad (5\text{-}3)$$

5.4 Assumptions

- Phase change is not considered.
- Mass transfer is not solved separately; however, the apparent conductivity and the heat transfer coefficient were introduced in the formulations to represent all the phenomena.
- The effect of the wood porosity is also assumed to be accounted for by the apparent conductivity.
- Anisotropy of the wood is not considered; and the heat transfer in the shortest dimension is assumed to be dominant leading to a one-dimensional analysis.
- Wood properties are taken constant.
- Deformation of wood is neglected.

5.5 Numerical Procedure

The heat balance equation (5-1) can be written in one-dimensional form as:

$$\frac{\partial T}{\partial t} = a_q \frac{\partial^2 T}{\partial x^2} \tag{5-4}$$

where a_q : thermal diffusivity $\left(\frac{k_{app}}{\rho c_q}\right)$

Implicit form of the finite-difference solution for the transient conduction problem was considered. The volume of wood was divided into a number of equal finite slices. The problem was discretized in space and time.

$$\Delta x = L_x / n_n$$

$$\Delta t = \tau / n_t \tag{5-5}$$

where Δx : mesh length,

L_x : total control volume thickness,

n_n : total number of nodes,

Δt : time length,

τ : total operation time,

n_t : total number of time steps.

The discretized form of the equation (5-4) takes the following form:

$$(1+2Fo)T_n^{p+1} - Fo(T_{n+1}^{p+1} + T_{n-1}^{p+1}) = T_n^p \quad n=2,\ ...,\ n_n\text{-}1 \tag{5-6}$$

where Fo : Fourrier number $\left(\frac{a_q \Delta t}{\Delta x}\right)$

The superscript p is used to denote the time dependence of T. The time derivative is expressed in terms of the temperature difference associated with the *new (p+1)* and *previous (p)* times. **[28]**

The discrete form of the boundary condition (Eq 5-2) takes the following form:

$$(1+2Fo+2FoBi)T_n^{p+1} - 2FoT_{n\pm1}^{p+1} = 2FoBiT_a - T_n^p \qquad n=1 \text{ and } n=n_n \tag{5-7}$$

where Bi : Biot number $\left(\frac{\alpha_q \Delta t}{k_{app}}\right)$

Equations (5-6) and (5-7) can be combined and written as;

$$[M]_s [T]_n^{p+1} = [M]_I \qquad n=1,\ldots,n_n \tag{5-8}$$

where $[T]$: the temperature solution matrix (at time $p+1$, an at node m)

$[M_s]$: the system matrix, which reflects the thermo physical properties of the medium

$[M_l]$: the limiting matrix, which reflects the initial, boundary, and previously calculated solution matrix (T_m^p)

Algebraic matrix equations were computed by LU factorization algorithm.

5.6 The Physical Domain

The model was applied to the St.Ambroise furnace. A vertical section equipped with inlets and outlets was modelled and given in Figure 4.2 of Chapter 4.

5.7 Initial Conditions and Parameters

The initial wood conditions are:

Wood temperature: 23 °C

The initial gas conditions are as follows:

Gas temperature: 23°C

The injection gas temperature is increasing gradually depending on the wood temperature. Generally, the aim is to have a 20°C difference between the wood and the gas temperatures. However, since the temperature distribution in the wood is not uniform, the average thermocouple readings were used to calculate injection temperature in the plant. The injection gas temperature obtained from the plant for one representative run is given in Figure 5.1.

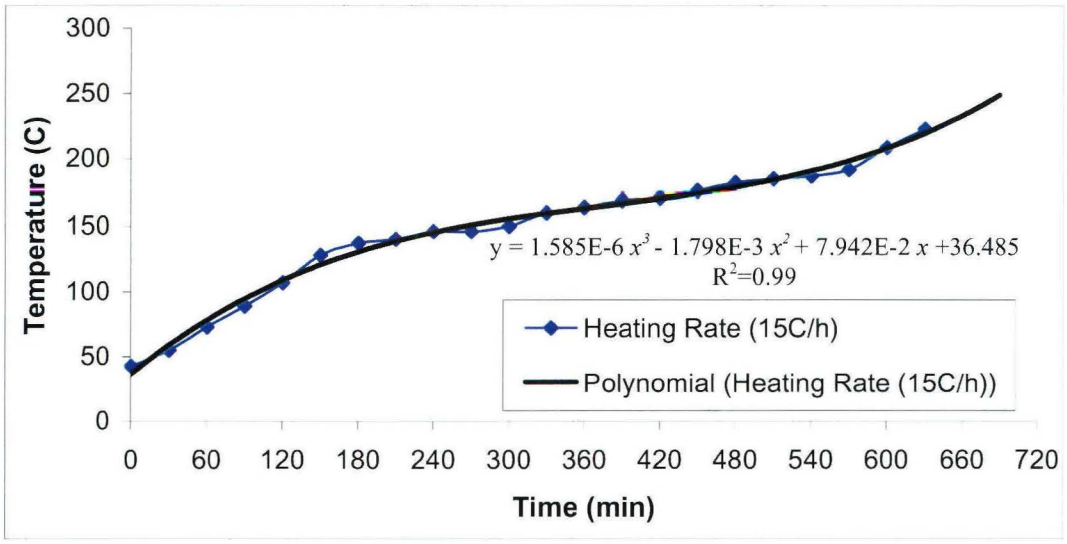

Figure 5.1 *Injection Gas Temperatures for a 15°C/hr Heating Rate*

The inlet gas temperature given in Figure 5.1 represents a global heating rate of 15°C/h. However, the heating rate for the first period (0-180min) is around 28°C/h whereas, for the second period (180-660min), it is around 10°C/h, and for the last period (660-720min), the heating rate is 14°C/h.

The physical properties for air and water which are available in PCP database in CFX-F3D material properties database interface were used. For the wood, parameters given in Table 5.1 were used.

Table 5.1 *Numerical Values of Parameters used in Model*

Property	Value	Source
k_{app}	0.12 W/mK	Preliminary Estimations See Appendix 3
α_q	9 W/m^2 K	

5.8 Methodology

The gas flow in the furnace was calculated using the CFD code CFX as explained before (Chapter 4). A FORTRAN code (USRBCS) was written to add the gas injection conditions to the model. Another FORTRAN (USRSRC) code was written in which the temperature of the surrounding gas was read, and the distribution of the temperature in the wood was calculated in one dimension (implicitly with finite-difference technique). To solve the linear, algebraic equation system, a subroutine was added to this code in order to compute LU factorization. Finally, heat transfer between the gas and the wood was calculated and expressed in the heat balance equation of surrounding gas.

The heat transfer is solved in y-direction in each slab of wood since this is the main direction of heat transfer between the wood and the gas (see Figure 5.2). The time step is

taken as five minutes. Each slab is divided into three cells in this direction. The hot gas enters the channels between the layers in x-direction. As the heat is transferred from gas to wood, the gas cools down. The 3D model solves for the gas temperatures and the velocities. The 1D sub-model solves for the wood temperatures. There is a transfer of mass and heat between the gas and the wood. However, the 3D model (gas side) has more cells than the 1D model (wood side). Therefore, the channels are divided into three sections. The average gas temperature for each section is calculated and used as the boundary condition. Although the main transfer in wood is in y-direction, the effect of gas cooling in x-direction is also reflected in the temperature profile of wood.

Temperatures in the middle and at the surface of each wood layer (in a total of 26 layers) at three different positions are calculated (see Figure 5.2). The middle temperatures are compared with the plant data since there is no plant data on the surface temperatures.

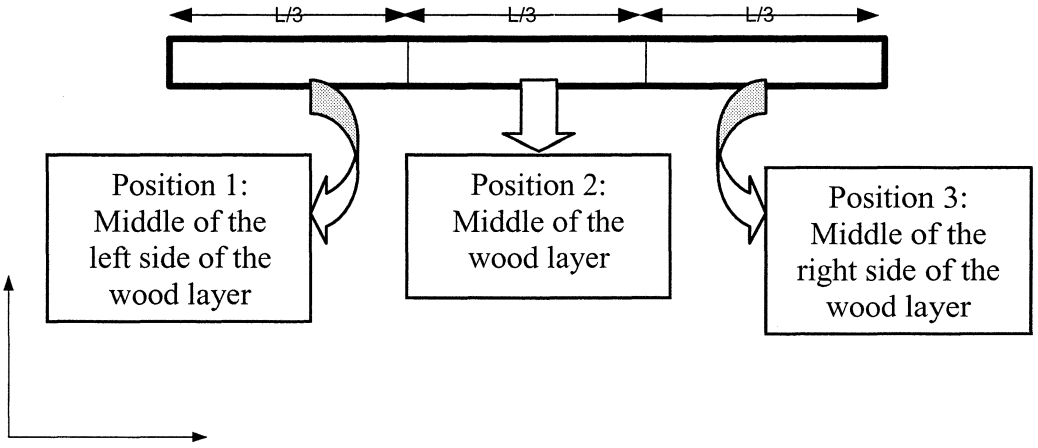

Figure 5.2 *Temperature Comparison Points in a Wood Layer*

5.9 Results and Discussion

5.9.1 Comparison of Model Prediction with the Plant Data

The temperatures of bottom, middle and top wood layers predicted by the model at position 2 are shown in Figure 5.3.

Predicted temperatures were compared with the plant data in the following figures for bottom wood layer (Figure 5.4), middle wood layer (Figure 5.5), and top wood layer (Figure 5.6).

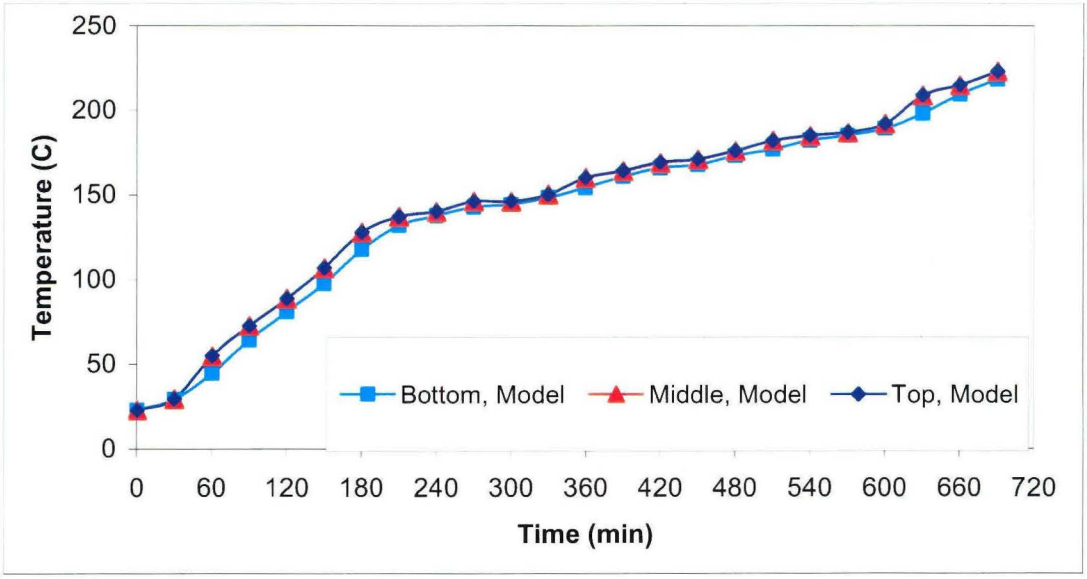

Figure 5.3 *Predicted Temperatures for Bottom, Middle and Top Wood Layers (Position 2)*

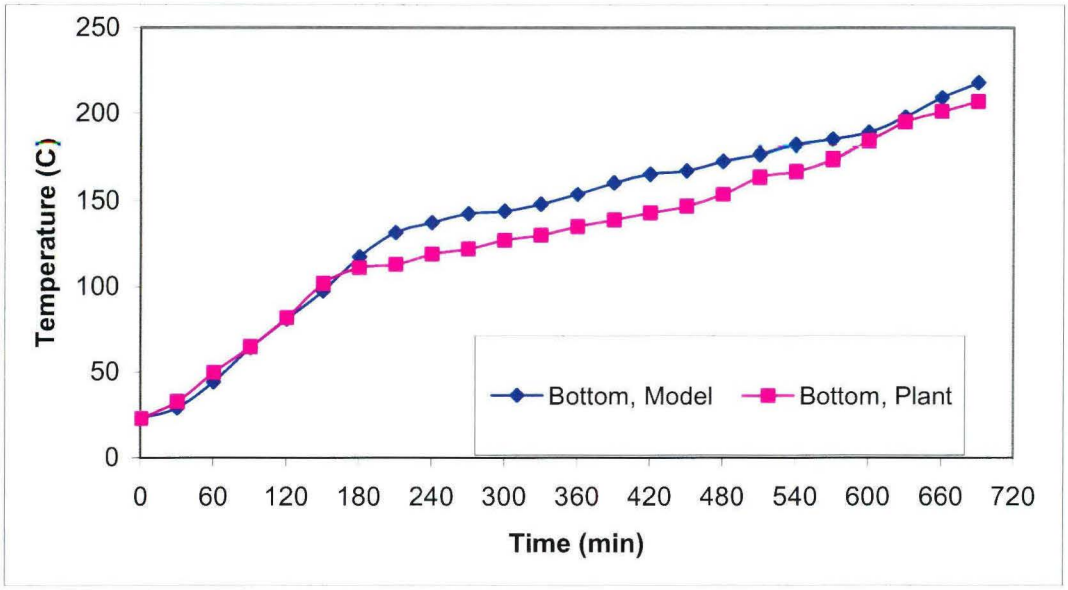

Figure 5.4 *Comparison of Predicted Temperatures with the Plant Data for Bottom Wood Layers (Position 2)*

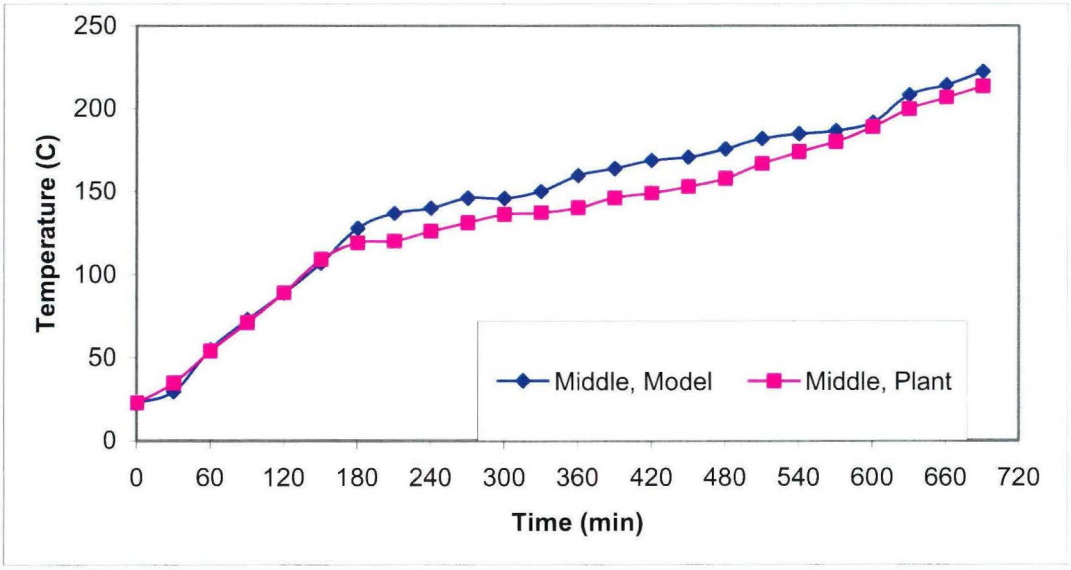

Figure 5.5 *Comparison of Predicted Temperatures with the Plant Data for Middle Wood Layers (Position 2)*

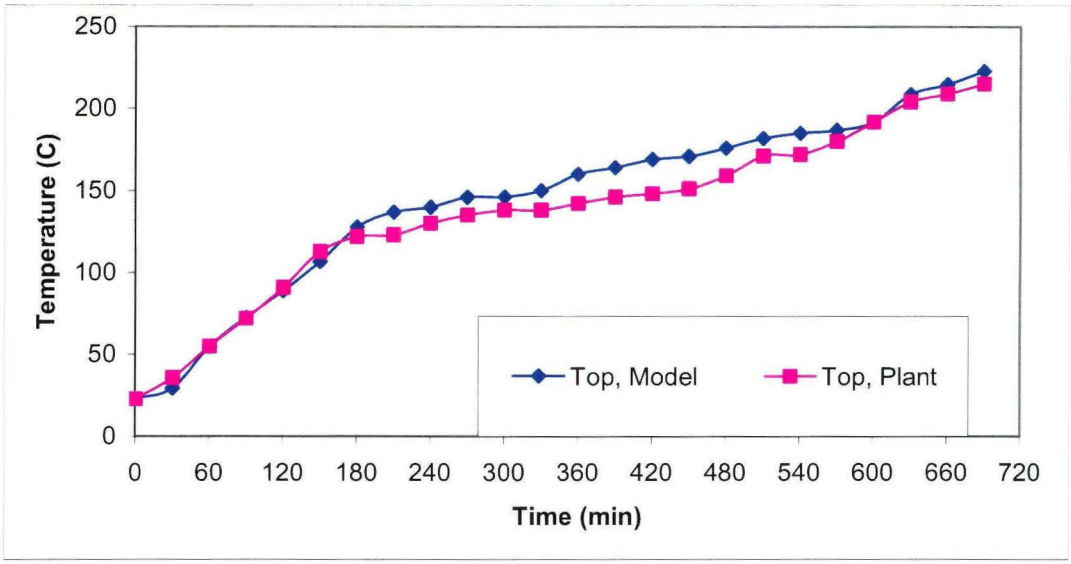

Figure 5.6 *Comparison of Predicted Temperatures with the Plant Data for Top Wood Layers (Position 2)*

5.9.2 Furnace Modifications and Results

It is desired to increase the wood production by using a larger furnace. However, it is important to know what would be the effect of this change on the quality of the product. A mathematical model is a very useful tool for predicting the behavior of the furnace for such modifications. This saves industry a considerable amount of time and money because it predicts the usefulness of the suggested changes and reduces the number of industrial trials. A number of simulations were carried out using the heat transfer model (no mass transfer) to study the effects of different furnace geometry modifications on the gas and wood temperatures.

Figure 4.2 shows the original dimensions of the furnace which were modified in this part of the study. There are 26 layers of wood in the furnace. The conditions of the simulations are presented in Table 5.1 and in Figure 5.7. Case 1 represents the St.Ambroise industrial furnace as is. In Case 2, the furnace dimensions were kept constant, but the wood charge was increased by decreasing the free distance between the wood pile and the top and bottom of the furnace (h_2 and h_3). The furnace height (h_1) is increased in Case3 whereas the furnace width (w) is increased in Case 4. In these cases the reduced values of h_2 and h_3 were used (same as those of Case 2). In Case 3, one row of inlet (at one side) and outlet (at the other side) were added to the top and the number of wood layers is increased to 38. In all cases, the distance between the wood pile and the side walls with gas inlet and outlets was kept constant.

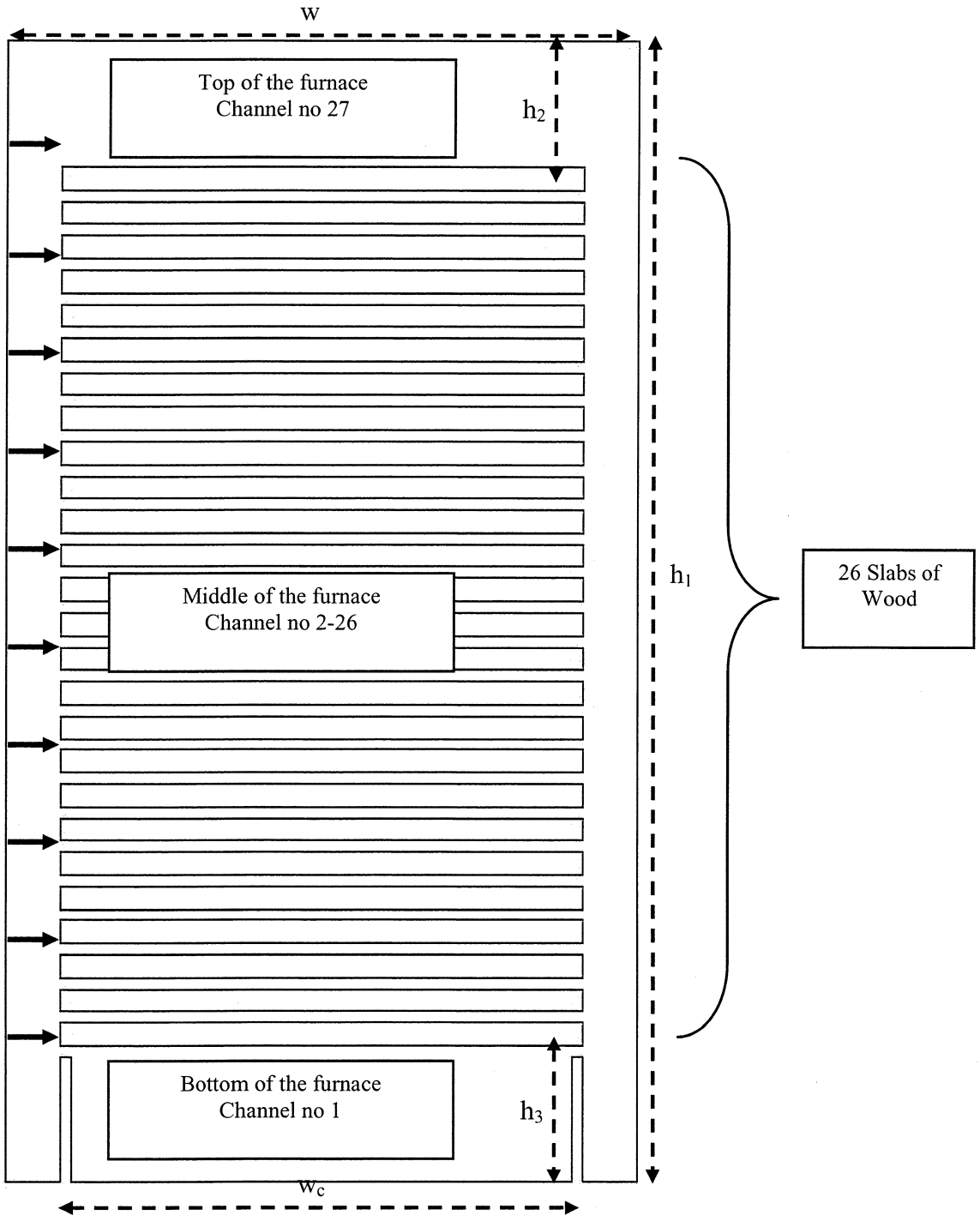

Figure 5.7 *Wood Arrangement and Channel Numbers in the 2D View of the Furnace*

Table 5.1 *Simulation Conditions*

Case	h_1 (m)	h_2 (cm)	h_3(cm)	w (m)	Comments
1	2.552	28.070	30.62	1.549	Actual dimensions
2	2.552	7.656	5.104	1.549	h_2 and h_3 are decreased, charge is increased.
3	3.164	7.656	5.104	1.549	h_1 (height) is increased by 0.612m, h_2 and h_3 are kept constant
4	2.552	7.656	5.104	2.057	w (width) and w_c (width of the charge) are increased by 0.508m

The change of wood temperature with time predicted for the modified furnace geometries was compared in Figure 5.8, 5.9, and 5.10 for bottom, middle, and top wood layers at the position 2, respectively. In general, it seems that the modifications do not have a significant effect on the temperature of middle and top layers of wood. However, the bottom layer of wood seems to be affected more by the modifications especially at earlier times.

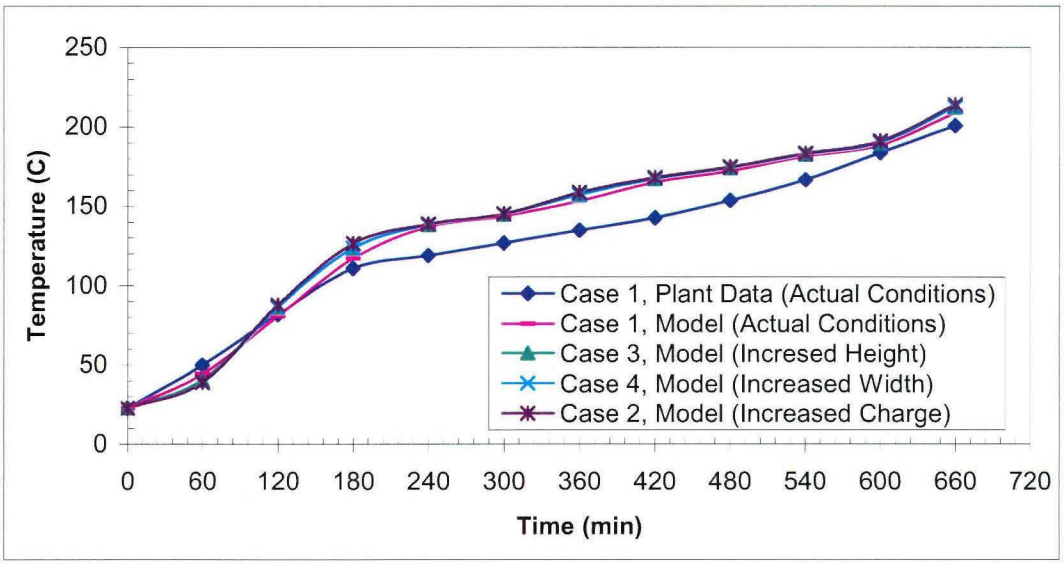

Figure 5.8 *Comparison of Temperatures Predicted by the Model for Different Furnace Geometries at the Bottom Wood Layer (Position 2)*

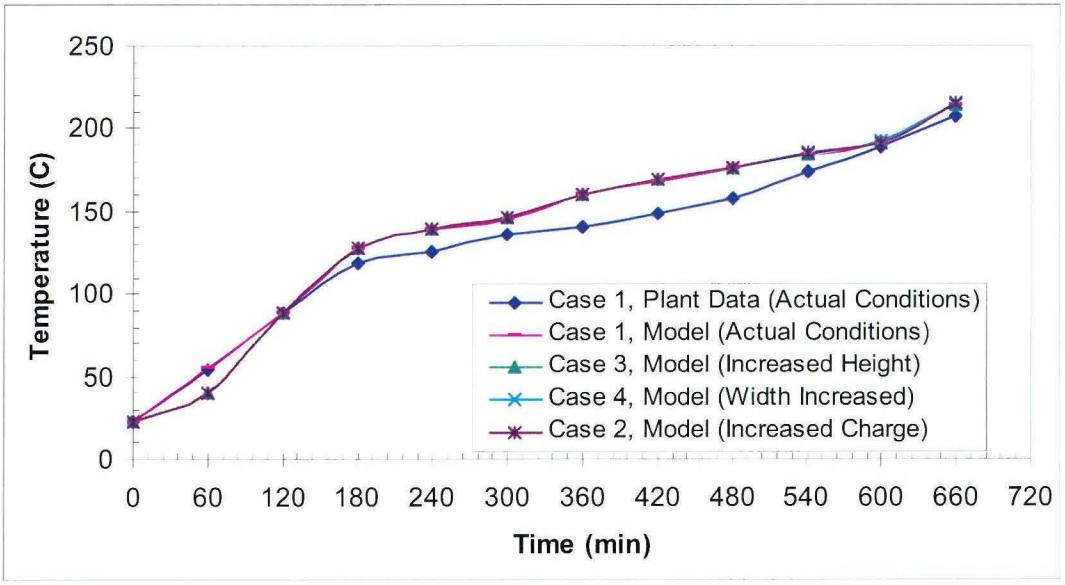

Figure 5.9 *Comparison of Temperatures Predicted by the Model for Different Furnace Geometries at the Middle Wood Layer (Position 2)*

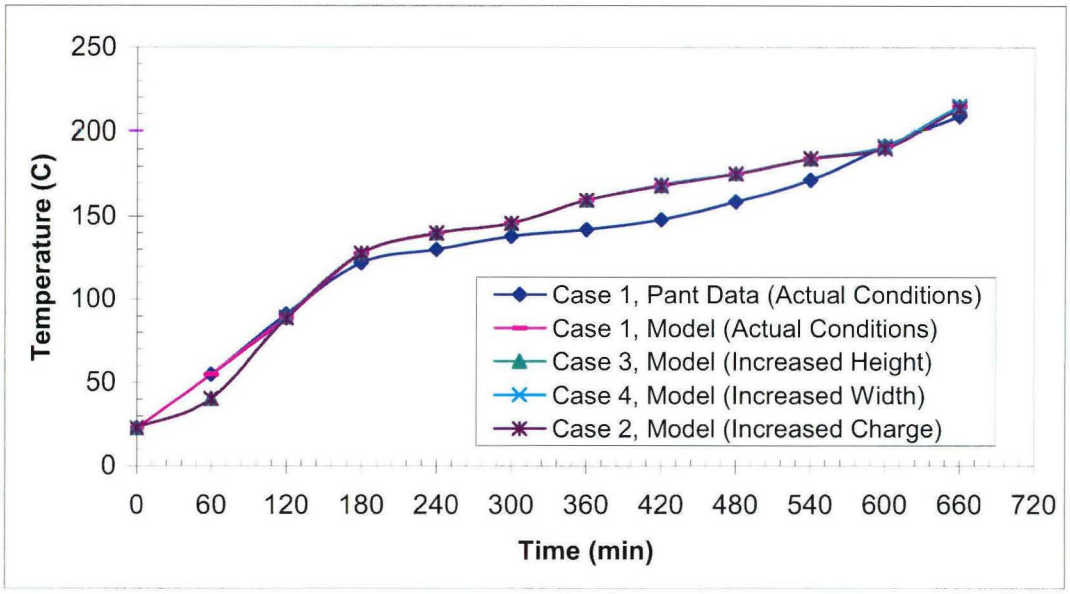

Figure 5.10 *Comparison of Temperatures Predicted by the Model for Different Furnace Geometries at the Top Wood Layer (Position 2)*

Figures 5.11, 5.12 and 5.13 compare the temperatures of different wood layers predicted by the model for increased charge, width and height, respectively, at different times for position 2.

Again, it can be seen from these figures that the model results differ only slightly at earlier times for bottom layers. The modifications do not seem to have a significant effect on the temperature, consequently, the quality of wood for the other layers.

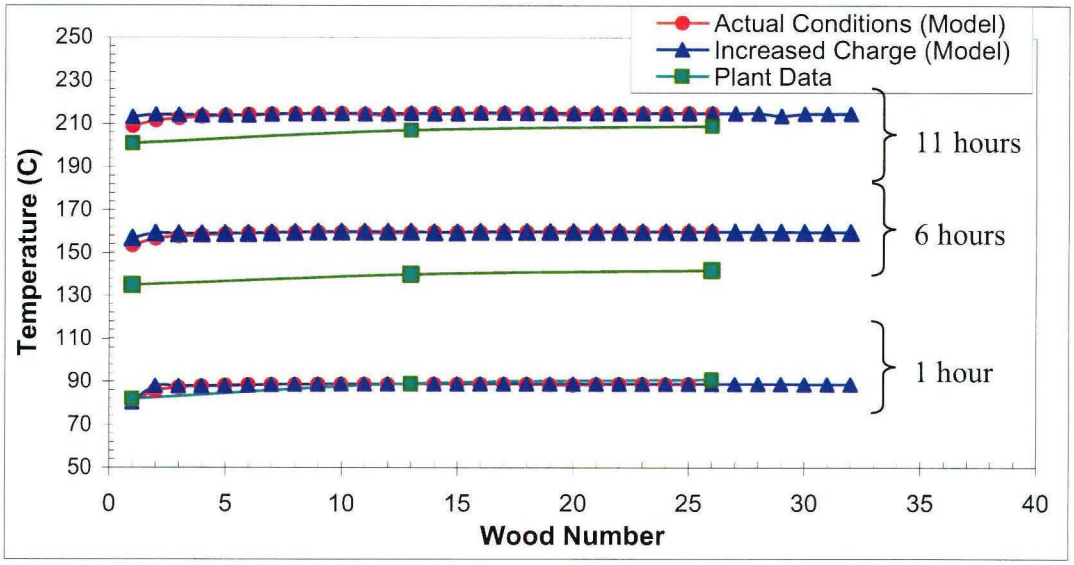

Figure 5.11 *Comparison of Temperatures of Different Wood Layers Predicted by the Model for Increased Charge at Different Times (Position 2)*

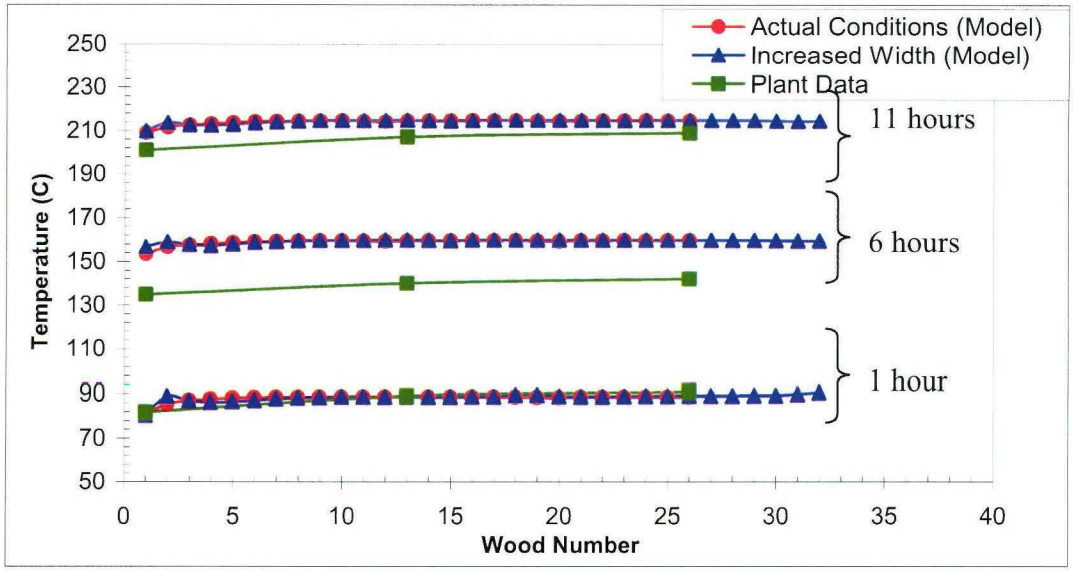

Figure 5.12 *Comparison of Temperatures of Different Wood Layers Predicted by the Model for Increased Width at Different Times (Position 2).*

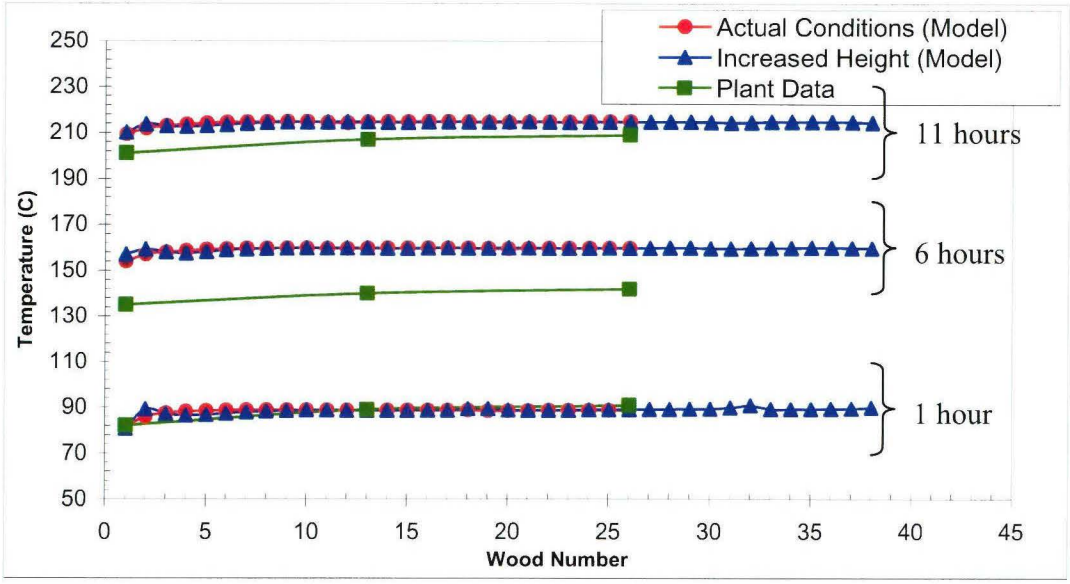

Figure 5.13 *Comparison of Temperatures of Different Wood Layers Predicted by the Model for Increased Height at Different Times (Position 2)*

The temperatures of different wood layers are presented in Figures 5.14 and 5.15 after 6 and 11 hours of operation, respectively. These figures show that the differences between different modifications are observed in bottom 6-7 layers. However, the differences are a few degrees and probably due to flow patterns created at the bottom of the furnace.

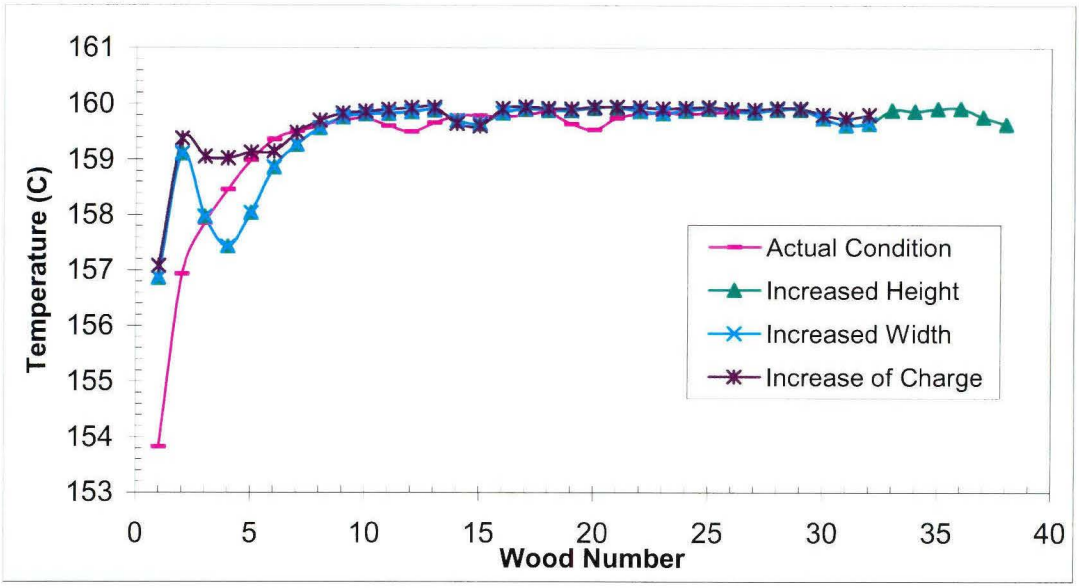

Figure 5.14 *Comparison of Predicted Wood Temperatures in Different Wood Layers after Six Hours of Operation (Position2)*

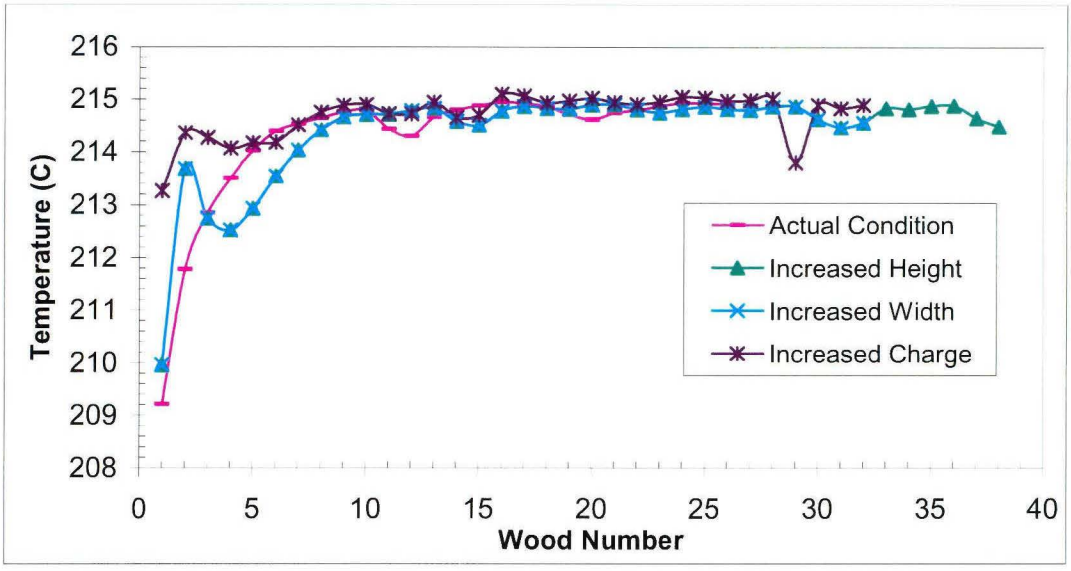

Figure 5.15 *Comparison of Predicted Wood Temperatures in Different Wood Layers after Eleven Hours of Operation (Position 2)*

The temperatures in positions 1, 2, and 3 (see Figure 5.2) for bottom and top wood layers after six and eleven hours of operations are presented in Figures 5.16 to 5.17. The differences between the wood temperatures of different modifications are greatest for the bottom layer for earlier times (see Figure 5.16). This difference decreases with increasing time (see Figure 5.17). At the top layer, the geometrical modifications do not affect the wood temperature as shown in Figures 5.18 and 5.19.

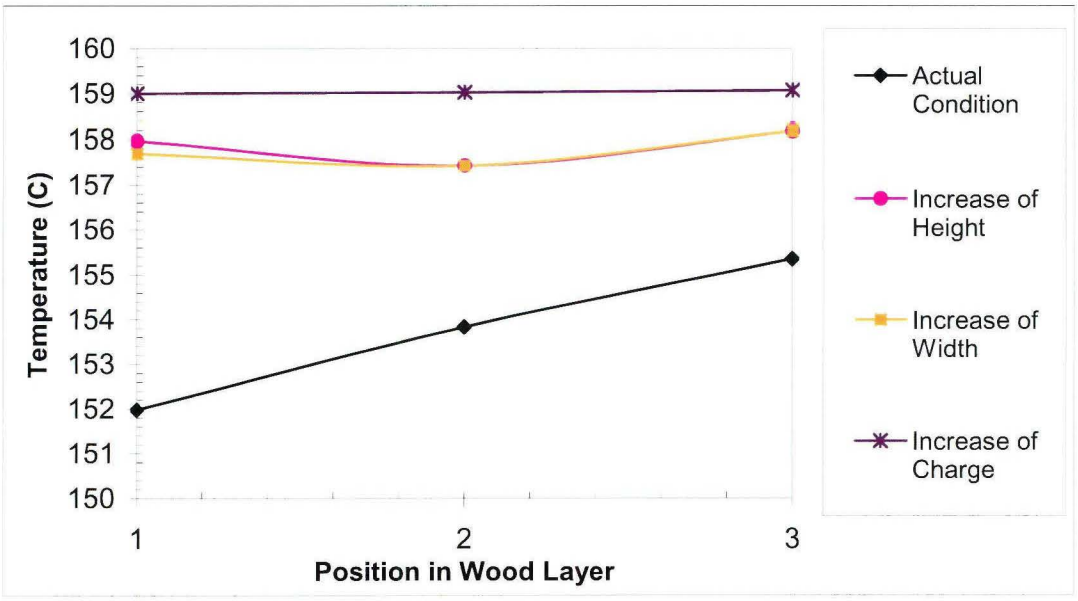

Figure 5.16 *Comparison of Predicted Wood Temperature in the Bottom Wood Layer after Six Hours of Operation*

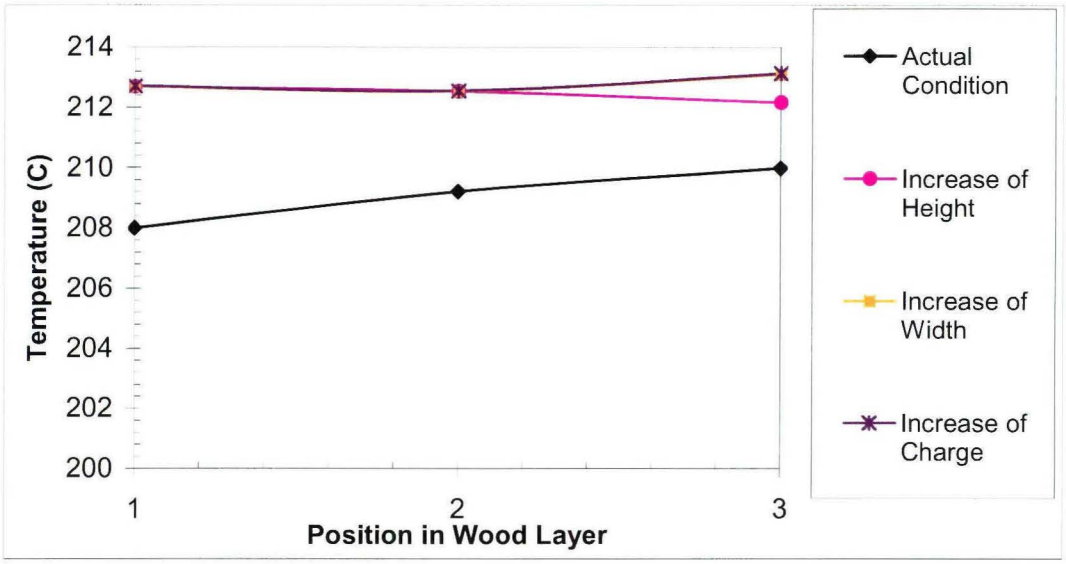

Figure 5.17 *Comparison of Predicted Wood Temperature in the Bottom Wood Layer after Eleven Hours of Operation*

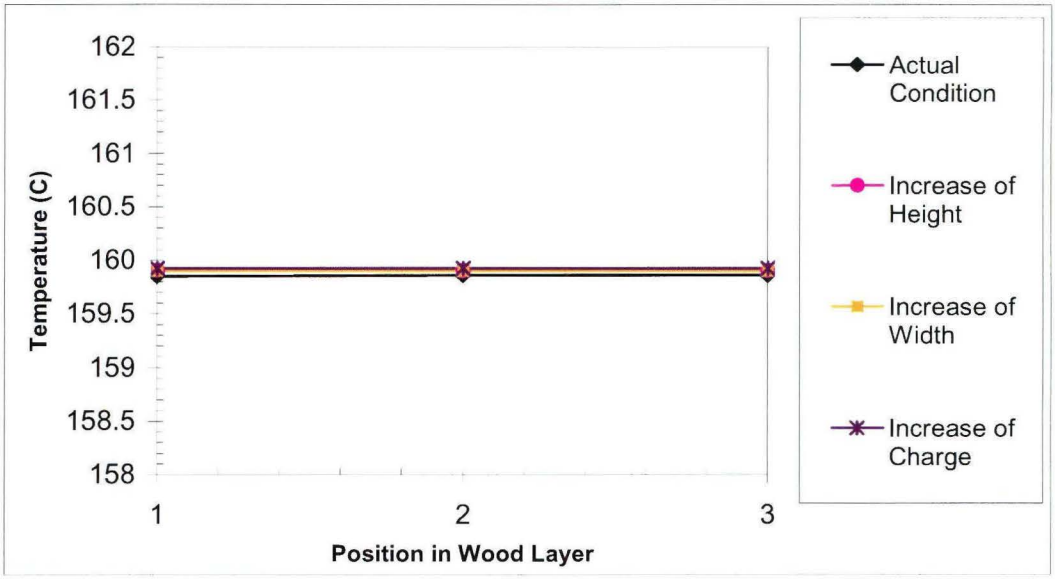

Figure 5.18 *Comparison of Predicted Wood Temperature in the Top Wood Layer after Six Hours of Operation*

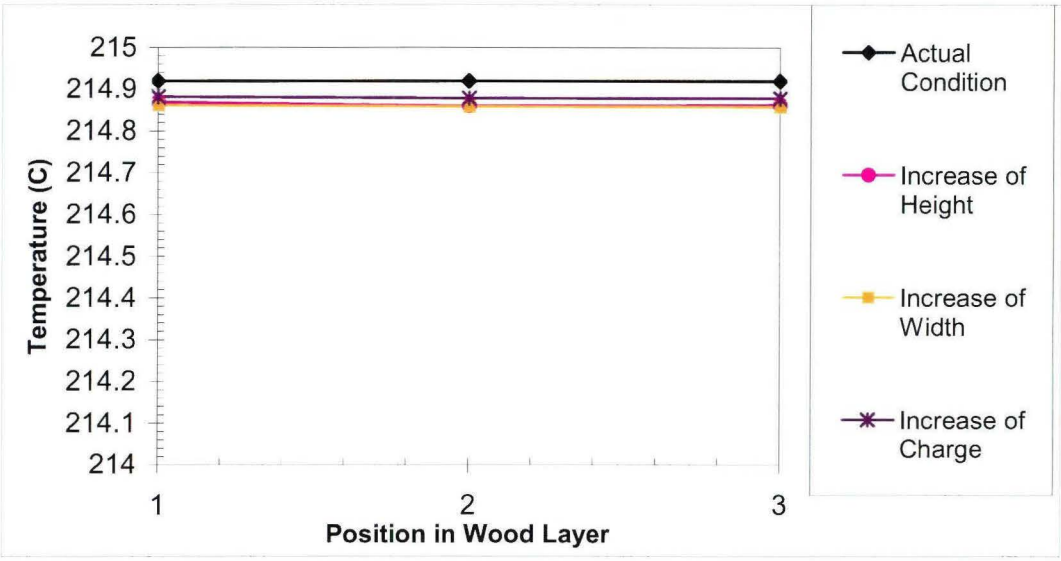

Figure 5.19 *Comparison of Predicted Wood Temperature in the Top Wood Layer after Eleven Hours of Operation*

5.10 Conclusions

Heat transfer model was introduced into previously developed flow model for the furnace at St. Ambroise in order to predict the temperature distribution both for gas and the wood layers during the furnace operation. The mass transfer is not taken into account in this model. However, the heat transfer model gave a good agreement with the plant data.

The furnace geometry was modified and the effect of this modification on the wood temperature distribution was studied. The furnace modifications carried out are:

a) increase in charge

b) increase in furnace height

c) increase in furnace width

The above studies show that the furnace dimensions can be increased without changing the quality of the product significantly within the range investigated. It is observed that the wood temperatures at the bottom of the furnace are lower than the middle and top layer temperatures during the operation. The temperatures along the bottom layer (in flow direction) differ at the early stages of the operation; however, they are uniform at the top layer during the same stages. As the time passes, the temperature difference between the layers decreases giving a uniform temperature along the layers.

The production can be increased by about 23% if the charge is increased, 24.5% if the furnace width is increased, and 42% if the furnace height is increased. However, these modifications do not have an effect on the product uniformity. As discussed previously, the modification of injection geometry is more effective in increasing the flow uniformity. However, these modifications do not have an effect on the product uniformity. Modifications which are previously discussed (see Chapter 4) are more effective in improving the uniformity of the product.

CHAPTER 6

MASS TRANSFER MODEL

6.1 Description of Model

The determination of heat and mass transfer in porous capillary bodies is of great practical importance in many technologies. For quality evaluation, knowledge of temperature and humidity in wood products is crucial.

A one-dimensional unsteady-state model was developed to describe the heat and mass transport process in drying of wood. The model is based on the conservation of mass and energy and uses constant parameter values from literature [16,21,28]. This model was coupled with a 3D unsteady-state model solving flow, heat, and mass transfer in gas.

The modelling results for temperature and humidity profiles during the operation are compared with the plant data. A reasonable agreement is obtained.

6.2 Model Development

The interrelation between heat and mass transfer in porous media can be described by Luikov's coupled system of partial differential equations by applying the methods of irreversible thermodynamics.

The implicit finite difference method was used for the solution of coupled heat and mass transfer problems in capillary porous media. The solution of the system of linear, algebraic equations was achieved by using LU factorization.

6.3 Governing Equations

To model the coupled heat and mass transfer in a porous media, the basic equations given by Luikov were studied by several researchers [16], [14], [15] and simplified into a set of governing differential equations for transient flow in drying.

6.3.1 Mass Balance Equation of Wood

Mass balance equation can be written for each of the components as:

$$\frac{\partial(\rho_0 M_i)}{\partial t} = -divj_{m_i} + I_i \qquad i=1,2,3,4 \qquad (6\text{-}1)$$

where j_m : mass flux

I : mass sources or sinks due to phase transition. For the overall balance $\Sigma_i I_i=0 \quad i=1,2,3,4$

Subscripts are referred to the following material components:

0 porous body

1 vapor

2 liquid

3 solid

4 inert gas

In the inert gas (dry gas) there is no chemical conversion or phase change ($I_4 = 0$). At drying temperature, phase change corresponds to the transition of liquid into vapor ($I_2 = -I_1$). The mass content of the liquid equals the total mass content;

$$M = \sum_i M_i = M_2 \qquad i=1,2 \tag{6-2}$$

Mass flux is related to the gradient of moisture concentration (Fick Law) and also to the gradient of temperature (Soret effect).

$$j_m = -a_m \rho_0 (\nabla M + \delta' \nabla T) \tag{6-3}$$

where a_m : mass diffusion coefficient

δ' : thermal gradient coefficient

As a result, the mass balance equation for the *i*th component (6-1) takes the following form;

$$\frac{\partial(\rho_0 M)}{\partial t} = div\left[a_m \rho_0 (\nabla M + \delta' \nabla T)\right] \tag{6-4}$$

Luikov expresses moisture content in terms of moisture potential provided that c_m is constant.

$$M = c_m U \tag{6-5}$$

The concept of mass transfer potential (moisture potential) is analogous to temperature in heat flow, while moisture content is analogous to heat content.

Final form of the mass balance equation is:

$$\rho_0 c_m \frac{\partial U}{\partial t} = div\left[\underbrace{k_m \nabla U}_{\text{Fick law}} + \underbrace{(k_m \delta)\nabla T}_{\text{Soret effect}}\right] \tag{6-6}$$

6.3.2 Energy Balance Equation of Wood

The energy balance equation is as follows:

$$\frac{\partial(\rho_0 c_q T)}{\partial t} = -divj_q - \sum_{i=1}^{2} h_i I_i \qquad (6\text{-}7)$$

where j_q : heat flux,

$\sum_{i=1}^{2} h_i I_i$: source (or sink) of heat.

Heat flux is related to the gradient of temperature (Fourrier Law) and also to the gradient of moisture content (Dufour effect). However, this is considered insignificant for porous capillary bodies. So, the heat flux equation is:

$$j_q = -k_q \nabla T \qquad (6\text{-}8)$$

The source or sink of heat due to the phase change of water is:

$$\sum_{i=1}^{2} h_i I_i = -\lambda div\left[a_m \rho_0 \varepsilon(\nabla M + \delta' \nabla T)\right] \qquad (6\text{-}9)$$

The final energy balance equation takes the following form:

$$\rho c_q \frac{\partial T}{\partial t} = div\underbrace{\left[k_q \nabla T\right]}_{\text{Fourier law}} + \underbrace{\varepsilon\lambda k_m \left[\nabla U + \delta \nabla T\right]}_{\text{Non-isothermal diffusion law}} \tag{6-10}$$

At the surface, the boundary conditions associated with these equations are:

$$j_m + \alpha_m (U - U_a) = 0 \tag{6-11}$$

$$j_q + \alpha_q (T - T_a) + (1-\varepsilon)\lambda\alpha_m (U - U_a) = 0 \tag{6-12}$$

The first term of equation (6-11) is the diffusive mass transfer term and the last term is the convective mass transfer term.

For the equation (6-12) the first term is the conductive heat transfer term. The second term of the same equation is the convective heat transfer term, while the last term is the amount of heat required for the phase change of liquid.

The initial conditions were assumed to be constant and represented by:

$T(x,0) = T_0$ and $U(x,0) = U_0$

6.3.3 Heat and Mass Balance Equations for Gas

For the gas temperature and gas humidity the governing equations used with the gas properties are given in equation (6-13) and (6-14), respectively:

$$\rho_G c_{q_G} \frac{\partial T}{\partial t} = -div(v\rho_G c_{q_G} T) + div(k_G \nabla T) \tag{6-13}$$

$$\rho_G \frac{\partial U}{\partial t} = -div(\rho_G v U) + \rho_G div(D \nabla U) \tag{6-14}$$

6.4 Assumptions

Heat and mass transfer in porous media is complex. Several assumptions are often necessary to make the problem manageable. In this section, assumptions used in the simplification of the heat treatment model are summarized:

- No filtrational mass transfer occurs. The gradient of total pressure inside the body is zero.
- In almost all multiphase porous media studies, liquid, and gas (vapor + air) at any location are considered in thermal equilibrium [14].
- Gravity is ignored, because capillary forces are much stronger than gravity.

- Properties are independent of the coordinates, time, temperature, and humidity due to the lack of detailed information.
- The viscosities of the liquid and gas phases are constant.
- The water is present only as liquid.
- Dufour effect is ignored.
- Chemical reactions associated with water loss are not taken into account.
- Heat and mass transfer in longitudinal direction are negligible.
- The liquid water is incompressible.
- To avoid the computational complexities, shrinkage is ignored. It was assumed that the initial volume occupied by the solid does not change. The effect of the water evaporation on the density is not taken into account. Also it was assumed that no degradation of the solid occurs and the solid density remains constant.

6.5 Numerical Procedure

The balance equations are written as:

$$\frac{\partial T}{\partial t} = a_{11}\nabla^2 T + a_{12}\nabla^2 U \tag{6-15}$$

$$\frac{\partial U}{\partial t} = a_{21}\nabla^2 T + a_{22}\nabla^2 U \tag{6-16}$$

where

$$a_{11} = \frac{k_q + \varepsilon\lambda k_m \delta}{\rho c_q}$$

$$a_{12} = \frac{\varepsilon\lambda k_m}{\rho c_q}$$

$$a_{21} = \frac{k_m \delta}{\rho c_m}$$

$$a_{22} = \frac{k_m}{\rho c_m} \tag{6-15}$$

Introducing matrix notation:

$$[B] = \begin{pmatrix} T - T_a \\ U - U_a \end{pmatrix} \quad [A] = \begin{bmatrix} a_{11}\ a_{12} \\ a_{21}\ a_{22} \end{bmatrix} \tag{6-16}$$

Thus, Equations (6-13) and (6-14) are expressed in matrix forms,

$$\frac{\partial [B]}{\partial t} = [A]\nabla^2[B] \tag{6-17}$$

In the same matrix form, boundary equations are expressed as follows:

$$[C]\nabla[B] + [D]\cdot[B] = 0 \tag{6-18}$$

where $$[C]=\begin{bmatrix} k_q & 0 \\ k_m\delta & k_m \end{bmatrix}$$

$$[D]=\begin{bmatrix} \alpha_q(1-\varepsilon)\lambda\alpha_m \\ 0 \qquad \alpha_m \end{bmatrix} \tag{6-19}$$

Finally the initial condition is:

$$[B](x,0)=[B]^0 \tag{6-20}$$

where $$[B]^0=\begin{pmatrix} T_0-T_a \\ U_0-U_a \end{pmatrix} \tag{6-21}$$

An implicit numerical scheme based on the finite difference approach is used. The volume of the piece of wood is divided into a number of equal finite slices. The problem is discretized in space and time.

$$\Delta x = L_x / n_n \qquad \Delta t = \tau / n_t \tag{6-22}$$

where Δx : mesh length,

L_x : total control volume length,

n_n : total number of nodes,

Δt : time length,

τ : total operation time,

n_t : total number of time steps.

Implicit finite difference method yields:

$$(1+2r[A])[B]_m^{p+1} - r[A][B]_{m+1}^{p+1} - r[A][B]_{m-1}^{p+1} = [B]_m^p \qquad m=2,\ldots,n_n\text{-}1 \qquad (6\text{-}23)$$

where $$r = \frac{\Delta t}{\Delta x^2} \qquad (6\text{-}24)$$

The superscript p is used to denote the time dependence of T and U. The time derivative is expressed in terms of the temperature difference associated with the *new (p+1)* and *previous (p)* times **[28]**.

Discrete form of boundary condition is:

$$(1+[D][C]^{-1}\Delta x)[B]_m^{p+1} - [B]_{m\pm1}^{p+1} = [D][C]^{-1}\Delta x[B]_m^p \qquad m=1 \text{ and } m=n_n \qquad (6\text{-}25)$$

The final form of the discretization equation takes the following form:

$$[\overline{A}][X]_m^{p+1} = [\overline{B}]_m \qquad m=1,\ldots,n_n \qquad (6\text{-}26)$$

where $[\overline{A}]$: the system matrix (combination of [A],[C],[D]), whose elements reflect the thermo physical properties of the medium,

$[X]_m^{p+1}$: the solution matrix (temperature and humidity at time *p+1* at node *m*),

$[\overline{B}]_m$: the limiting matrix, which describes the initial and boundary conditions and previously calculated solution matrix ($[X]_m^p$).

Algebraic matrix equations were computed by LU factorization algorithm.

6.6 The Physical Domain

The model was applied to St.Ambroise furnace. A vertical section equipped with one set of inlet and outlet was modelled and shown in Figure 4.2 in Chapter 4.

6.7 Initial Conditions

The initial wood temperature is 23 °C and wood humidity is13%.

The initial gas temperature is 23°C, gas humidity is 2.6% and gas injection velocity is 15 m/s

The injection gas temperature profile is given in Figure 5.1 in Chapter 5.

6.8 Parameters Used in The Model

A detailed literature search was carried out to find the necessary parameters used in the model. However, it was found that all the models were developed for drying process at low temperature. In addition, the physical properties are different for different types of woods. A research which is aimed at characterizing the heat transfer properties is being carried out at the university, so in the future the developed model will give better solution for each type of wood with the known properties. Currently, the properties shown in Table 6.1 are used in the model.

Table 6.1 *Numerical Values of Parameters used in Model*

Property	Value	Source
a_m	10^{-9} m^2/s	[16]
c_q	1284 J/kgK	[16]
λ	$2.5*10^6$J/kg	[16]
ε	0.3	[16]
ρ	500 kg/m^3	[16]
α_m	$1.67*10^{-6}kg/m^2s°M$	[21]
k_q	0.13 W/mK	[21]
δ	2°M/K	[21]
c_m	$0.01kg_{moisture}/kg_{dry\ body}$ °M	[21]
α_q	10 W/m^2 °K	[28]

6.9 Methodology

The same methodology, as explained previously in Chapter 5, was followed in order to predict temperature and humidity distributions.

6.10 Results and Discussion

Temperatures in the each wood slab at three positions were calculated with the model every 15 min for 12 hours of operation. For the simplicity, only the bottom, middle, and top wood layer temperatures at position 2* (the middle of the slab, see Figure 5.2) were compared at every 30 min in Figure 6.1.

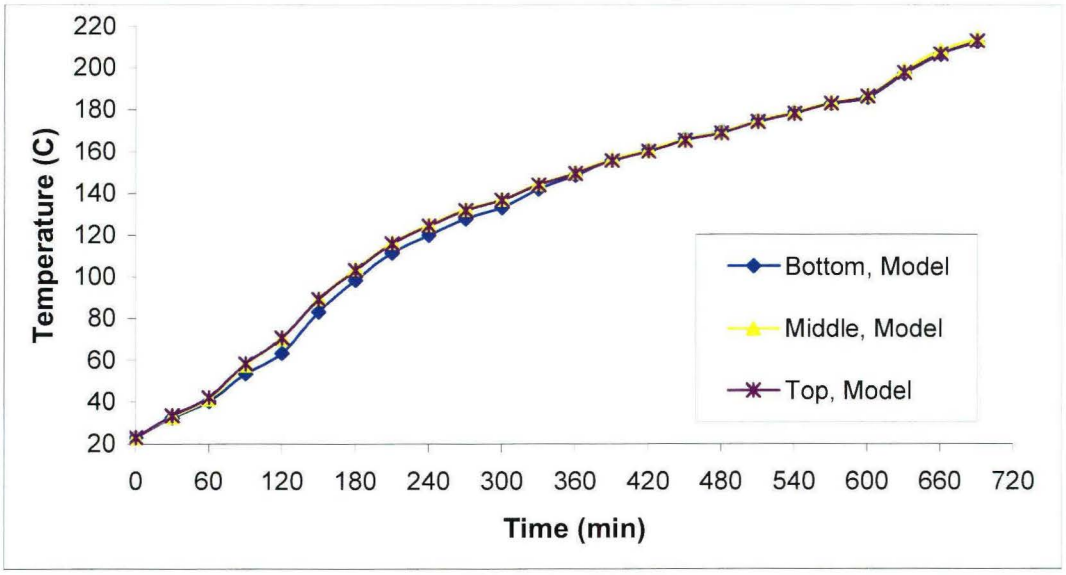

Figure 6.1 *Temperature Distributions at the Bottom, Middle, and Top Wood Layers for Whole Operation*

* All the Figures representing wood properties from 6.1 to 6.5 and from 6.16 to 6.23 are given for the wood position 2.

When the mass transfer model is added to the previous flow model, it is seen that that the gas temperature distribution is much more uniform. The middle and top gas temperatures are very similar; that is why, the wood temperatures are close at these regions. However, it is still possible to observe slightly lower temperatures at the bottom of the furnace.

Figure 6.2 compares the temperatures of the bottom, middle, and top wood layers predicted by the model with the plant data taken from St.Ambroise furnace at position 2. The agreement between the predictions and the data is good.

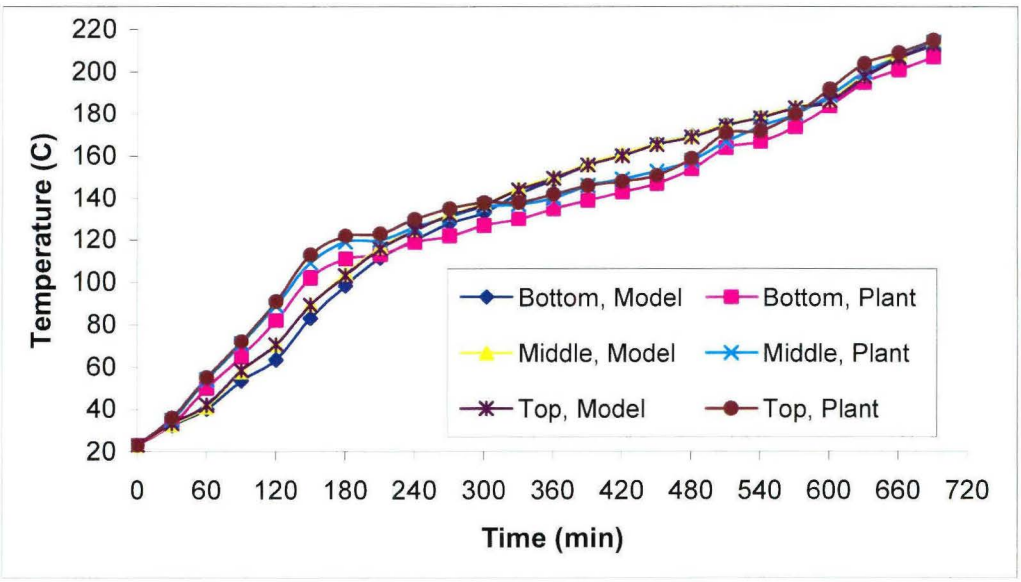

Figure 6.2 *Comparison of Predicted Temperatures with the Plant Data for Bottom, Middle and Top Wood Layers at Position 2*

In Figures 6.3, 6.4, and 6.5, the bottom, middle, and top wood layer temperatures are compared respectively. The model predicts well the temperature profiles in the wood. The

temperature differences between the bottom, middle, and top of the wood layers present in the plant data were also predicted by model. There is some difference between the plant and model data especially for the first period. The main difference can be due to the lack of detailed information on material properties and the non-uniform character of the wood. The furnace operation and geometry are the same for the model and for the plant; however, in the plant, the initial humidity of the wood may vary significantly (6-8%), whereas in the model, the wood has constant initial moisture content. Also the transfer phenomena in the wood change according to the structure of the wood. Heartwood and sapwood do not have the same transfer rate. The structural irregularities in the wood, which are not predictable with the model, result in different products.

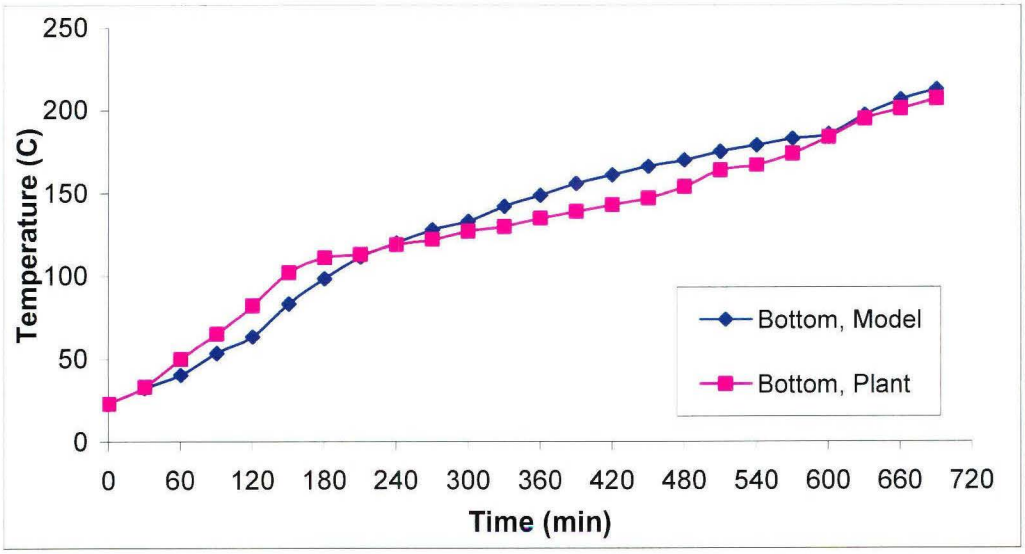

Figure 6.3 *Comparison of Predicted Temperatures with the Plant Data for Bottom Wood Layers*

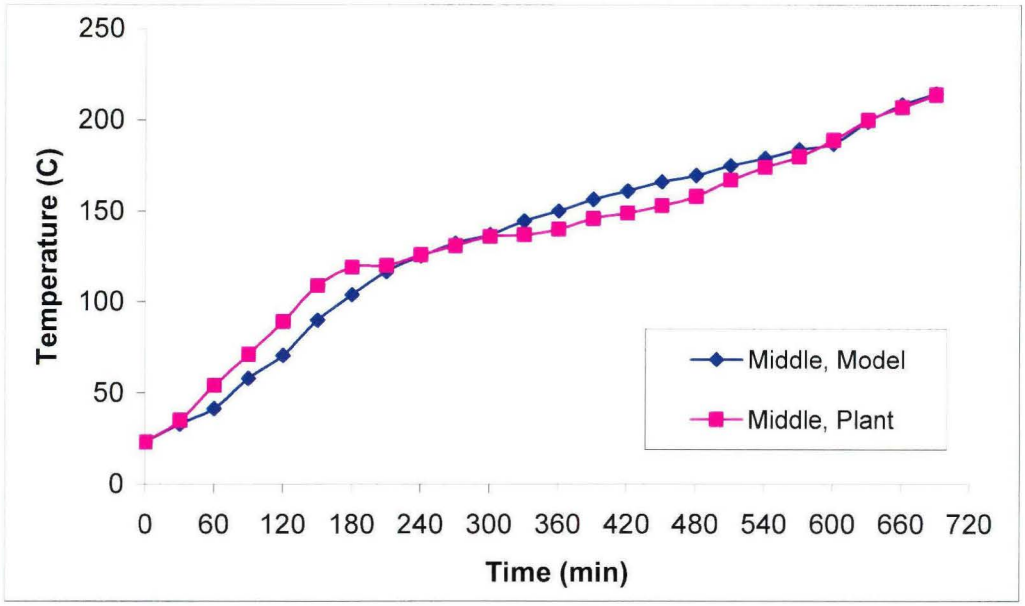

Figure 6.4 *Comparison of Predicted Temperatures with the Plant Data for Middle Wood Layers*

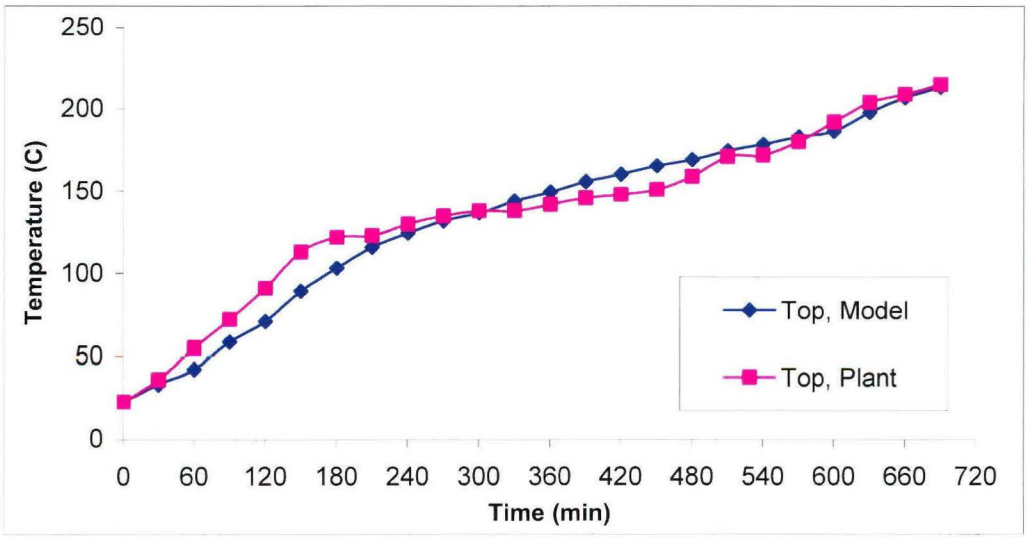

Figure 6.5 *Comparison of Predicted Temperatures with the Plant Data for Top Wood Layers*

The temperatures of different wood layers are presented in Figures 6.6 and 6.7 after two and six hours of operation, respectively. These figures show that the differences between different wood layers are few degrees and due to flow patterns created at the furnace, this difference tends to increase with time.

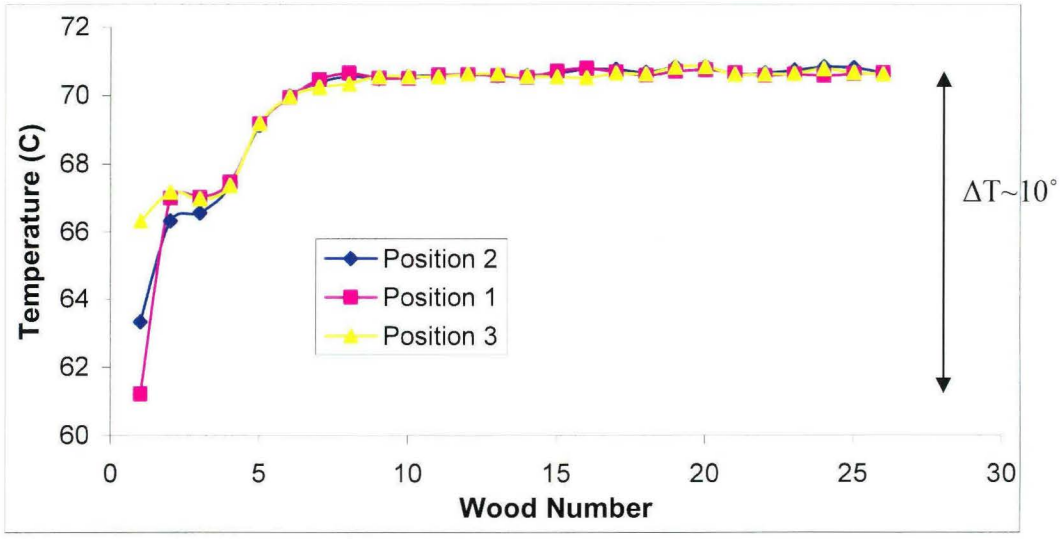

Figure 6.6 *Comparison of Predicted Wood Temperature in Different Wood Layers after Two Hours of Operation*

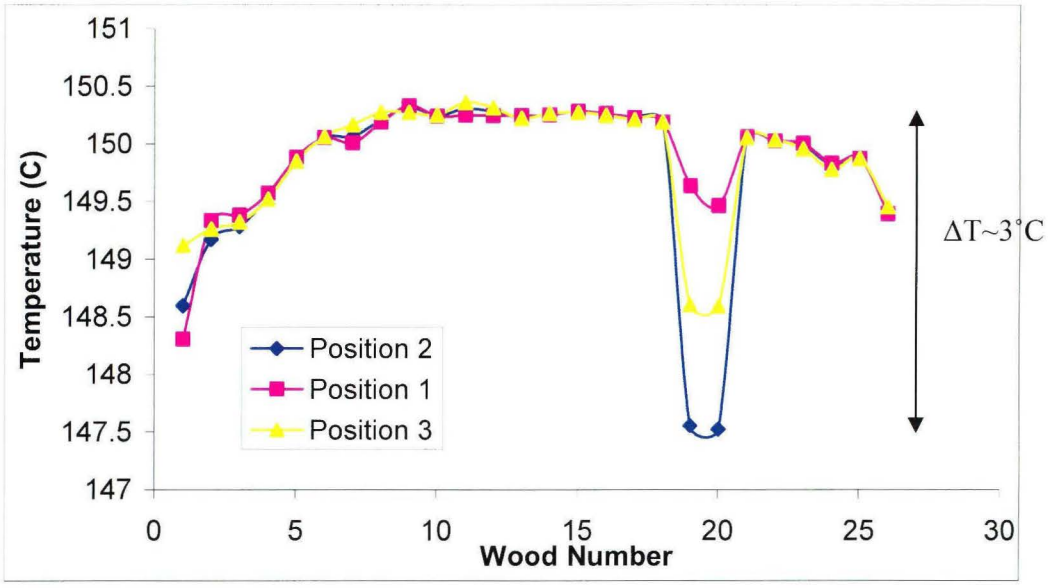

Figure 6.7 *Comparison of Predicted Wood Temperature in Different Wood Layers after Six Hours of Operation*

It is observed that, at the bottom wood slabs, the wood temperature is lower than that of the upper part during the first six hours of operation. Since the gas flow is not equal in each channel and the gas temperatures vary, the wood temperatures also differ. A weak gas flow is also observed in the 20^{th} channel; as a result, the temperatures of 19^{th} and 20^{th} wood layers are lower than the temperatures of the others.

In Figure 6.8, the distribution of gas flow after six hours of operation is presented. The gas velocity is lower in the 20^{th} channel. The distributions of temperature and water vapor mass fraction in the gas at the same time are shown in Figures 6.9 and 6.10, respectively. The keys are given with the figures. This figure also shows that the gas flow is weak at the bottom of the furnace and also at 8^{th}, 9^{th}, 16^{th}, 17^{th}, in addition to 20^{th} channel.

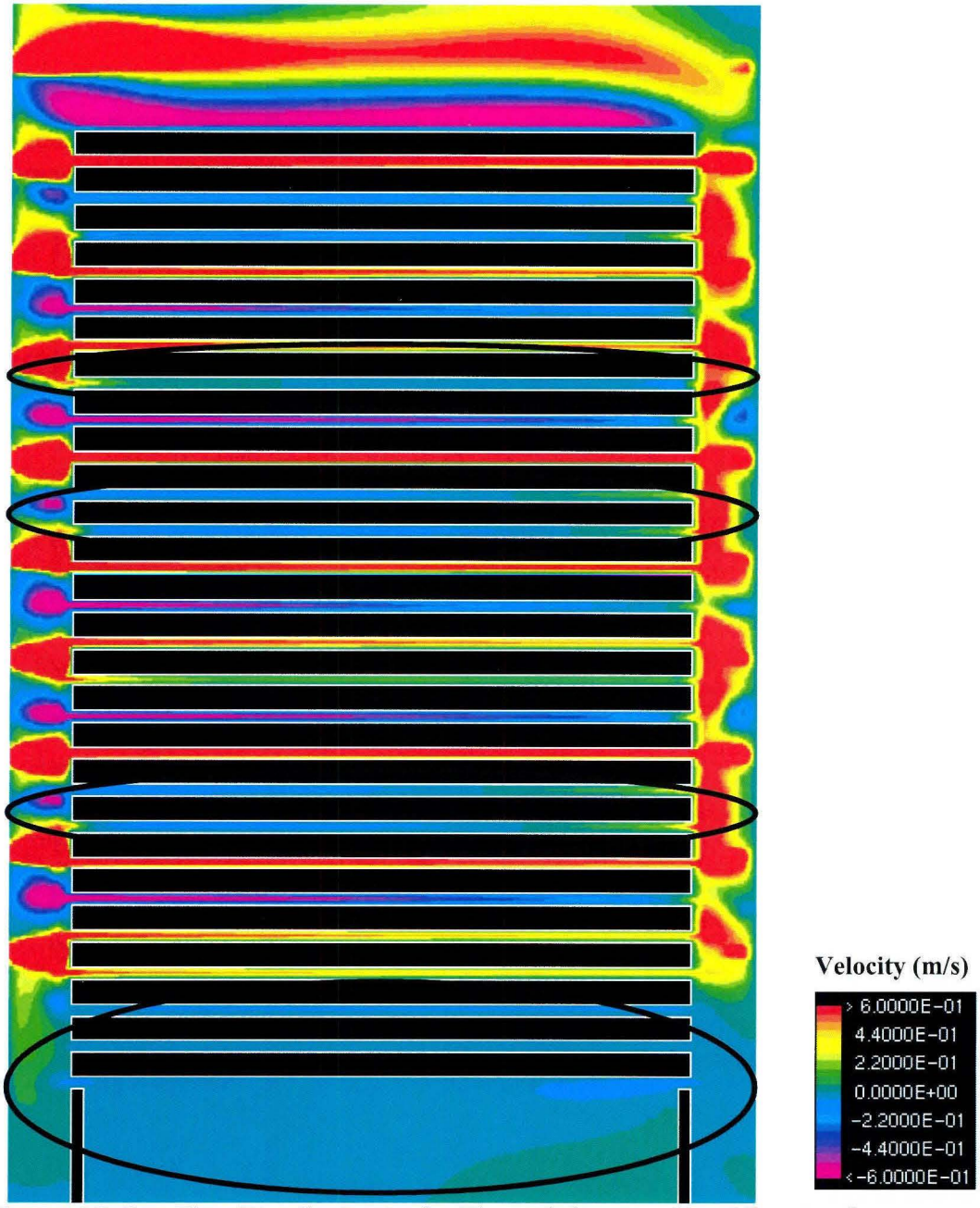

Figure 6.8 *Gas Flow Distribution in the Channels between Wood Layers after Six Hours of Operation*

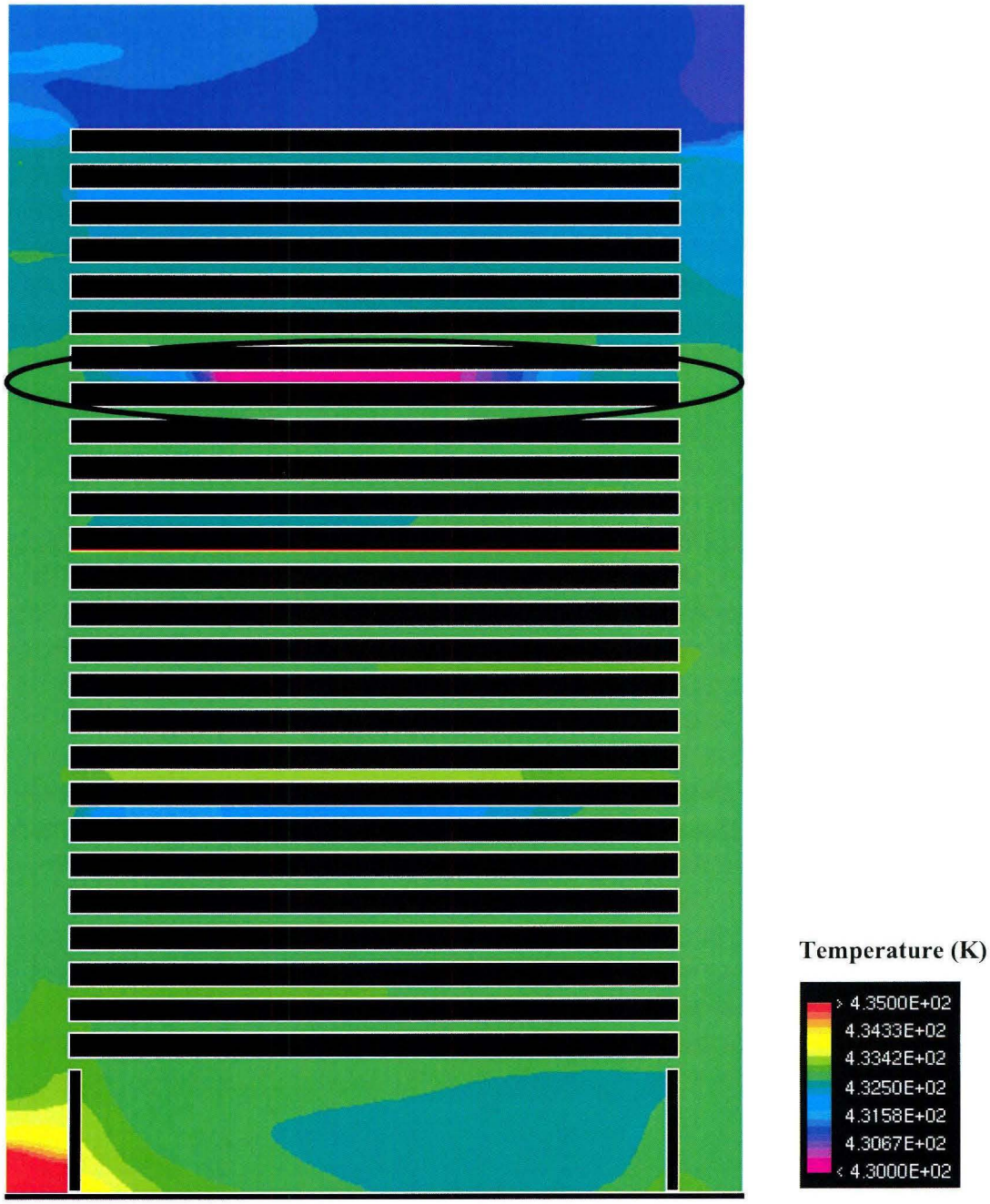

Figure 6.9 *Gas Temperature Distribution in the Channels between Wood Layer after Six Hours of Operation*

Figure 6.9 shows the temperature distributions of the gas and the wood layers. The low temperatures observed for 19th and 20th wood slabs caused by the weak gas flow present in 20th channel (see Figure 6.8).

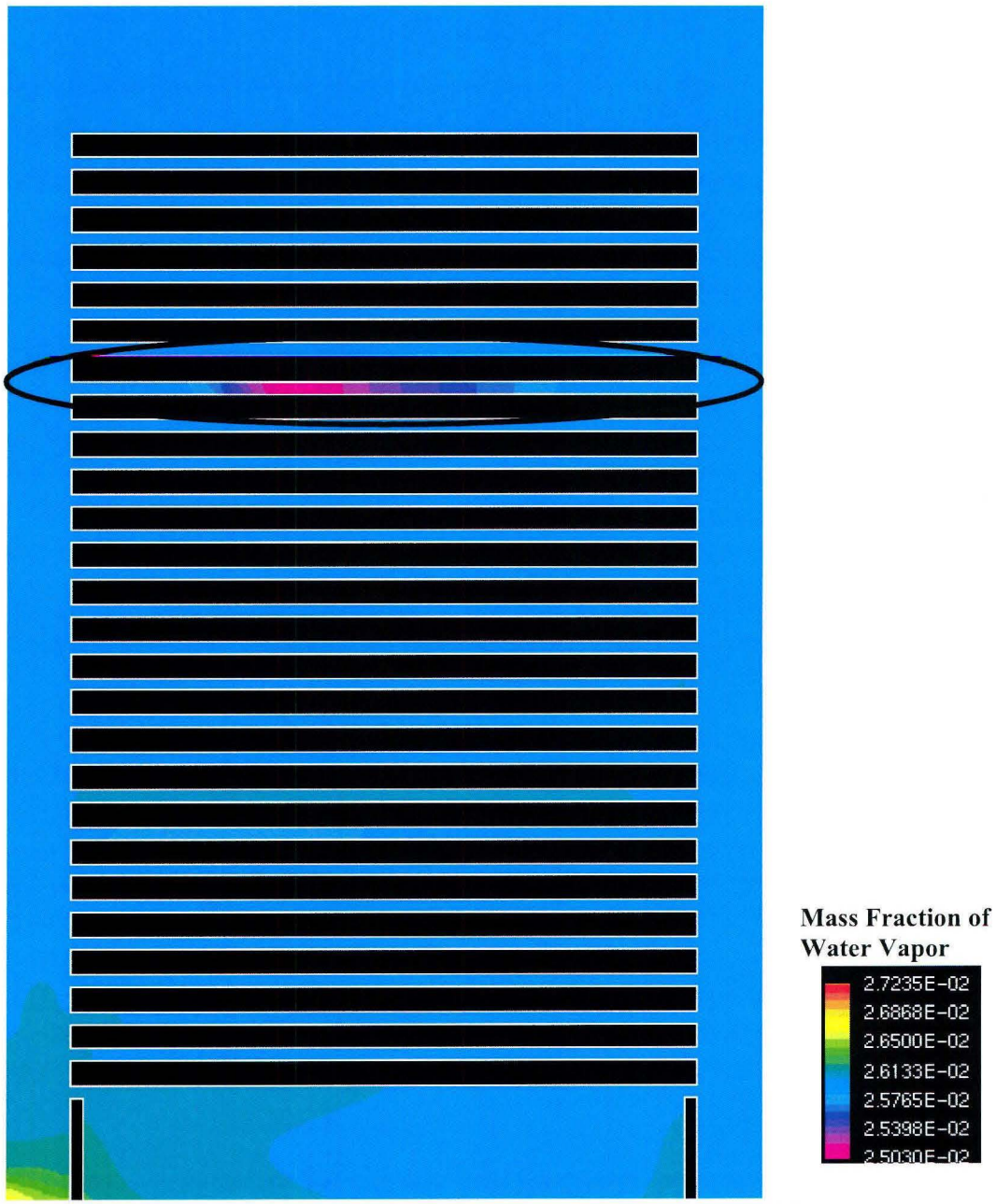

Figure 6.10 *Distribution of Water Vapor Fraction in the Channels between Wood Layers*

The mass fraction of water vapor in gas is shown in Figure 6.10. The mass fraction of water vapor in the gas is uniform in the furnace except in the 20th channel which has low gas flow. In the coupled heat and mass transfer, the transport phenomenon is a function of flow, temperature and mass fraction profiles of the environment.

In Figures 6.11 and 6.12, the predicted wood temperatures after ten and twelve hours of operation can be seen. At this time, the transfer rate is increased in the 20th channel.

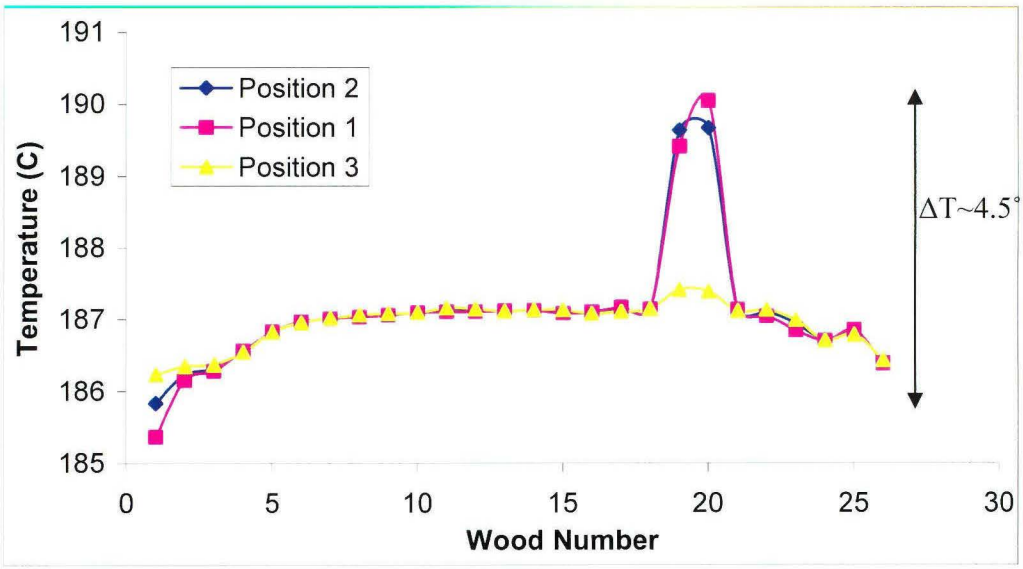

Figure 6.11 *Comparison of Predicted Wood Temperature in Different Wood Layers after Ten Hours of Operation*

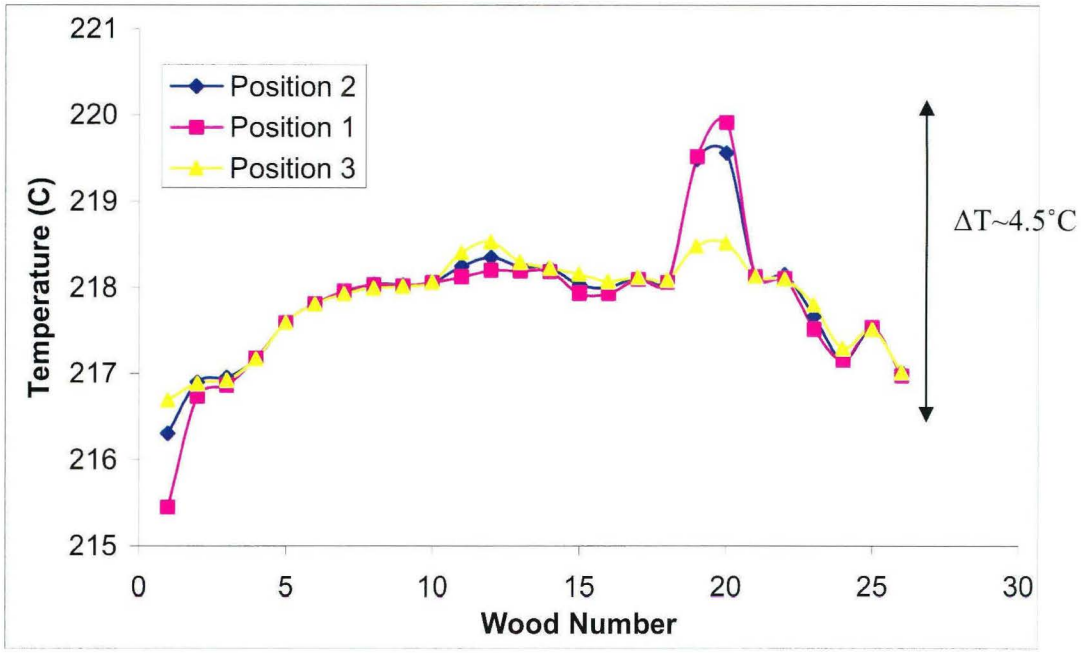

Figure 6.12 *Comparison of Predicted Wood Temperature in Different Wood Layers after Twelve Hours of Operation*

In Figure 6.13, the distribution of gas flow at the final time step can be seen. The key is given with the figure. A similar flow pattern to that shown in Figure 6.8 can be seen in this figure.

The distributions of the temperature and water vapor fraction in the gas are represented in Figures 6.14 and 6.15, respectively. The bottom of the furnace has low temperatures and mass fraction distribution, which explains the temperature difference in the furnace showed in Figures 6.11 and 6.12. The mass fraction of water vapor is increasing slightly with time. In Figure 6.10 it is about $2.57*10^{-2}$%; in Figure 6.15, it is about $2.62*10^{-2}$%, except at the bottom of the furnace.

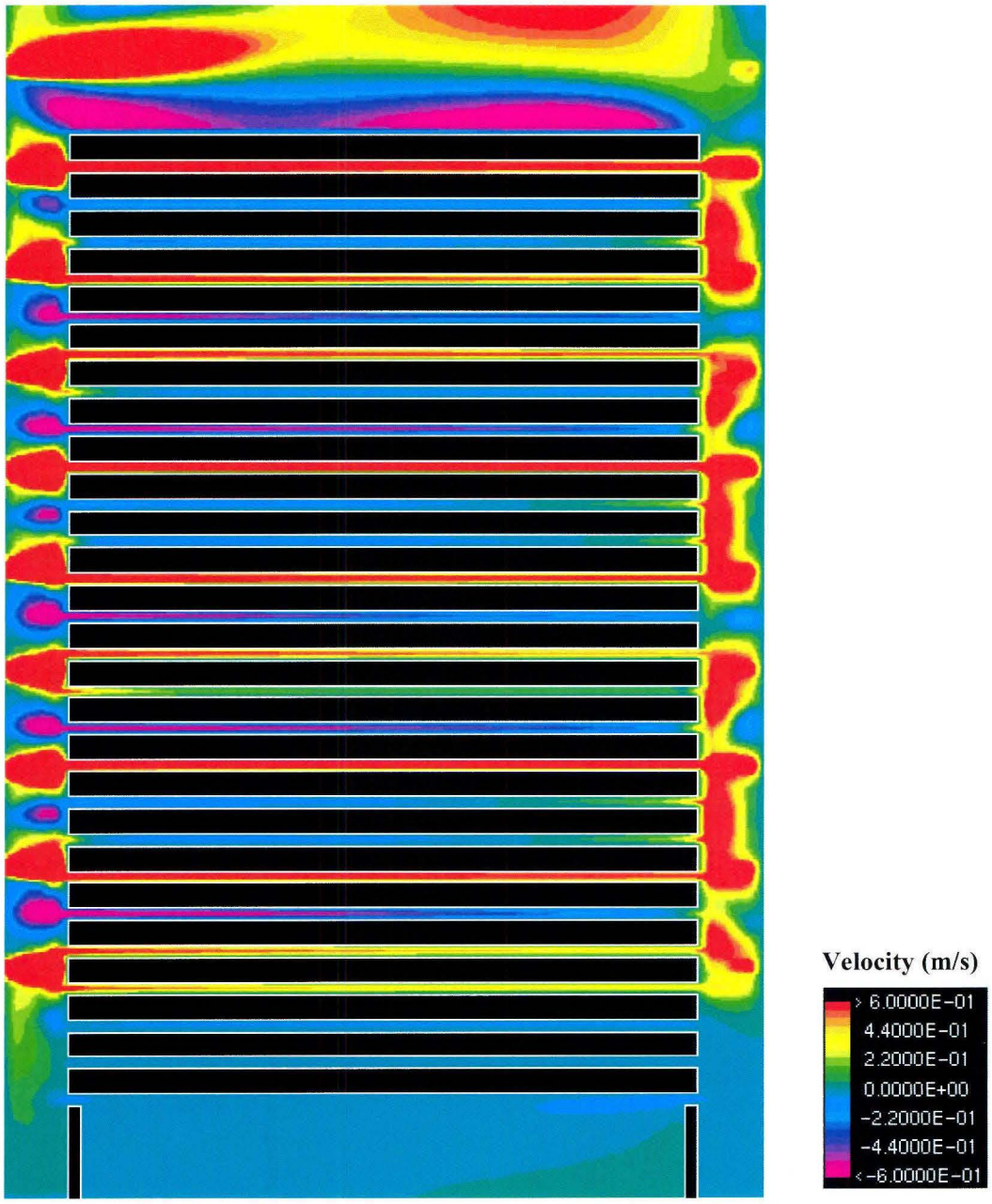

Figure 6.13 *Gas Flow Distribution in the Channels Between Wood Layers at Final Time Step*

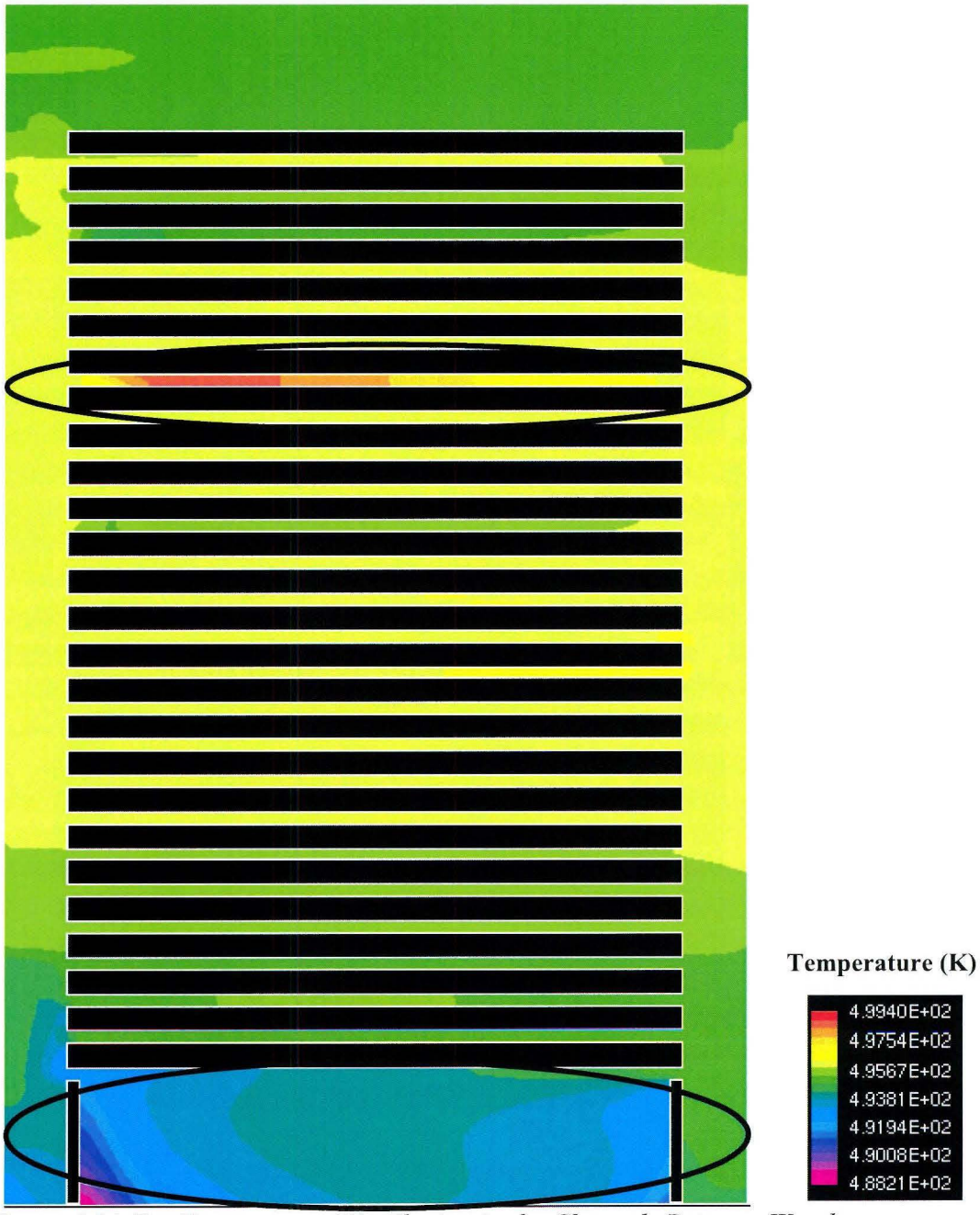

Figure 6.14 *Gas Temperature Distribution in the Channels Between Wood Layers at Final Time Step*

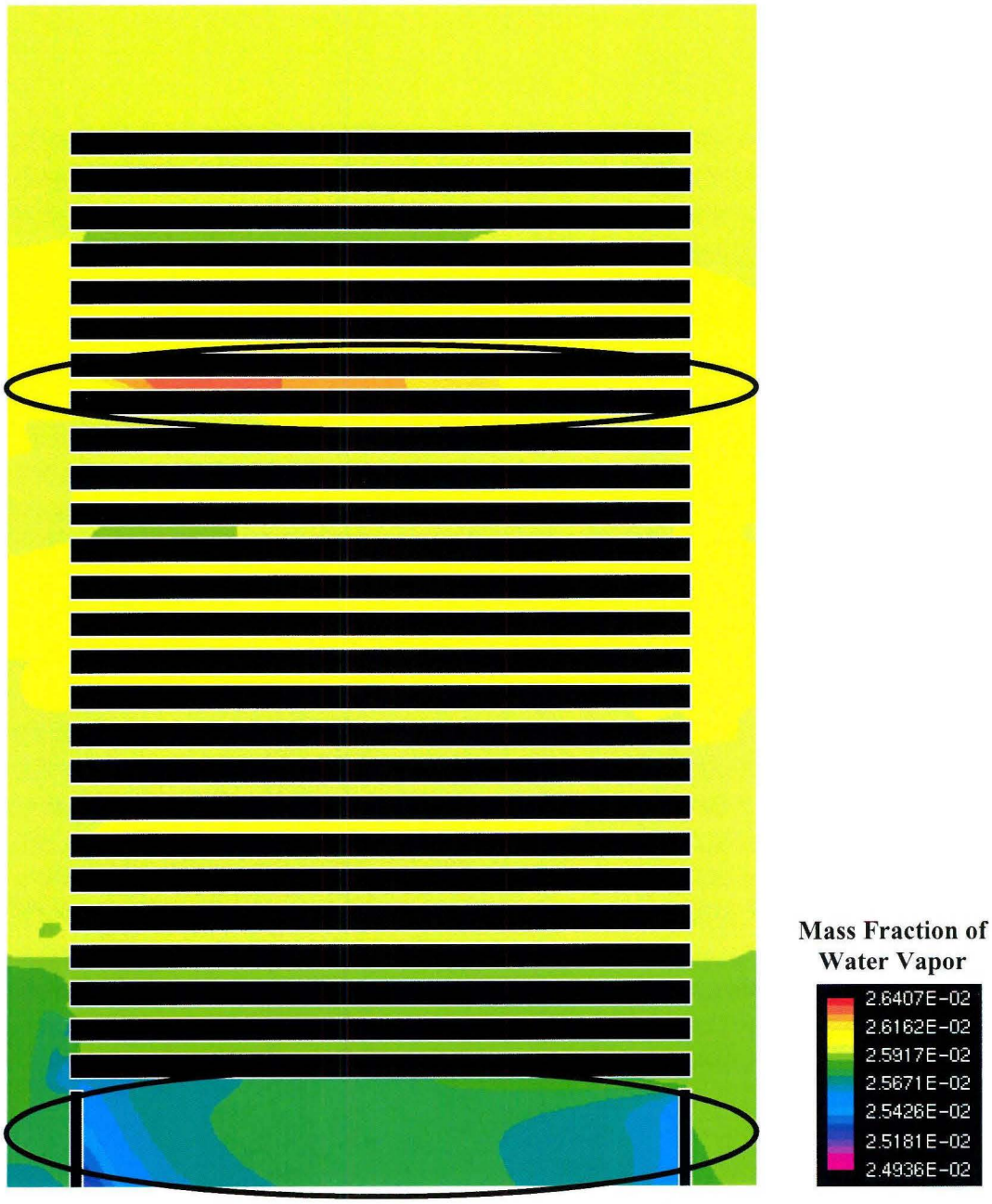

Figure 6.15 *Distribution of Water Vapor Fraction in the Channels between Wood Layers at Final Time Step*

There is no data for the moisture content of the wood during operation. For the time being, it is not possible to compare the moisture contents predicted by the model with the data during the operation. The initial moisture content of the wood is generally around 13% because it is pretreated. However, the initial moisture content varies significantly in different parts of wood. A 6-8% difference in the moisture content is expectable. Final moisture content of the wood is around 3-4 %.

The moisture content obtained from the model is given in the Figure 6.16

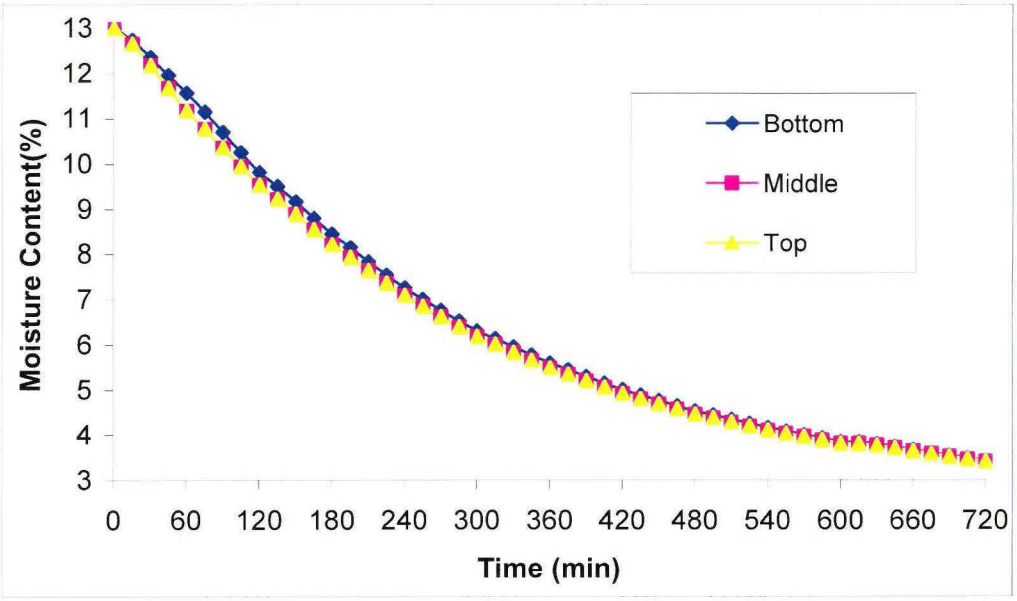

Figure 6.16 *Wood Moisture Content at the Bottom, Middle, and Top Wood Layers*

In Figures 6.17, 6.18, and 6.19, the moisture content of the bottom, middle, and top wood layers are presented. Since the temperature at the bottom is lower, the humidity is higher. Mass transfer in this region occurs much more slowly than in the other parts of the furnace.

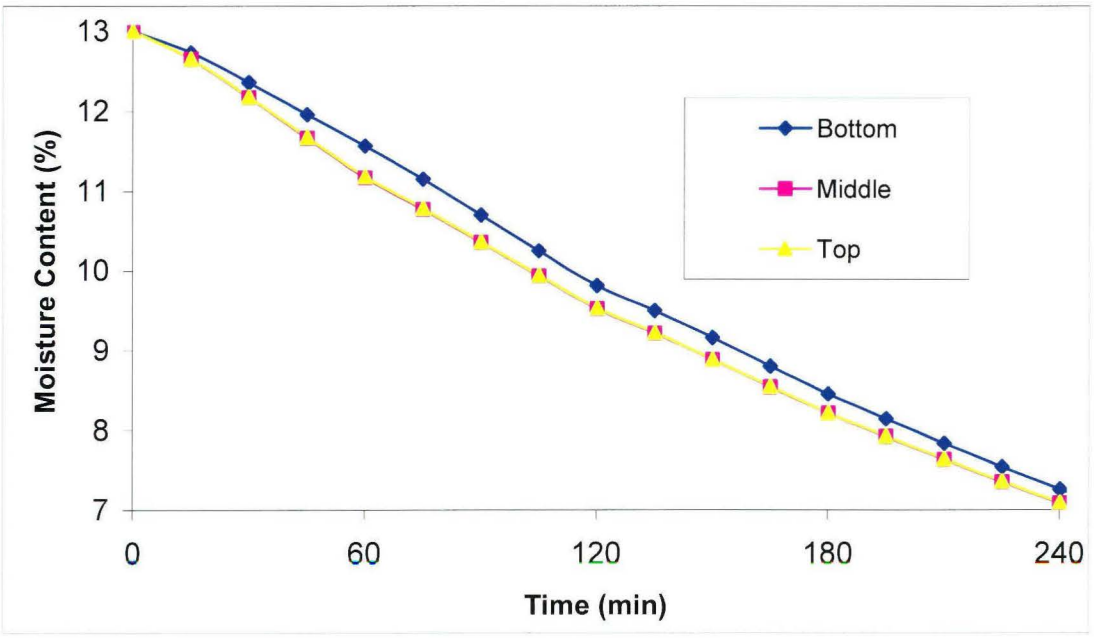

Figure 6.17 *Wood Moisture Content at the Bottom, Middle, and Top Wood for The First Period of Operation (0-4 hours)*

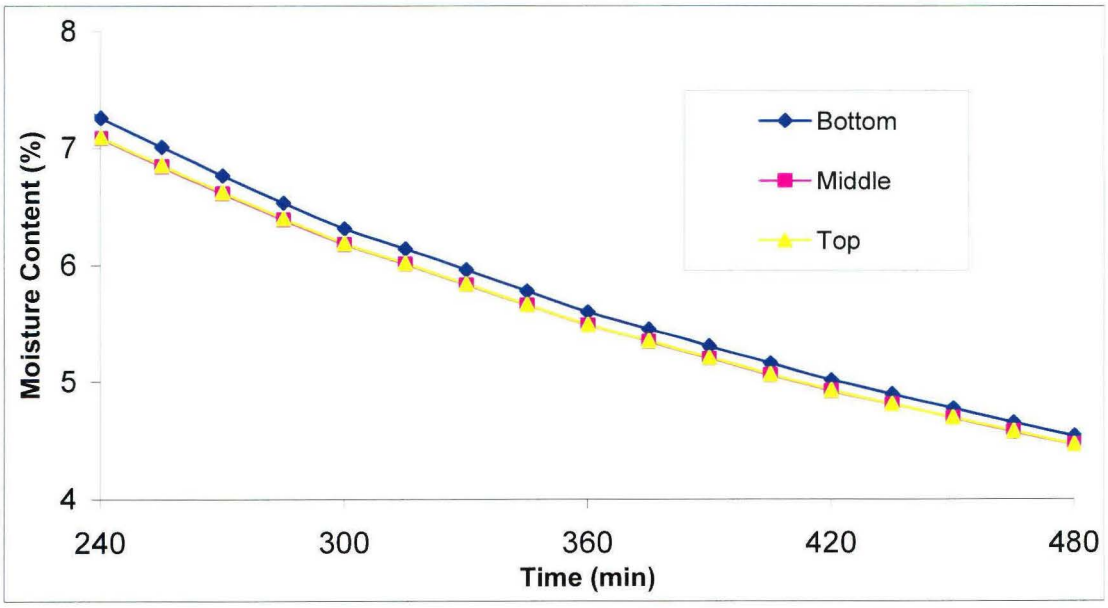

Figure 6.18 *Wood Moisture Content at the Bottom, Middle, and Top Wood Layers for The Second Period of Operation (4-8 hours)*

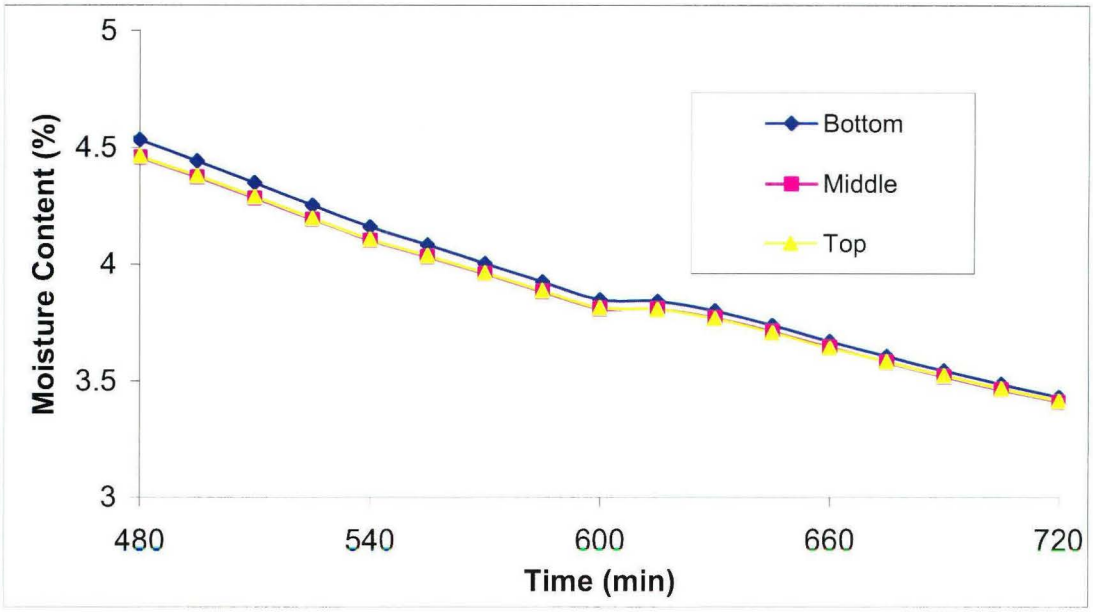

Figure 6.19 *Wood Moisture Content at the Bottom, Middle, and Top Wood Layers for The Third Period of Operation (8-11 hours)*

It is seen in the above figure that at 600min the mass content is not changing, this is only because of the operating (heating) conditions given in Figure 6.1.

Initial wood moisture content is changed from 13% to 23% as in the non-pretreated wood and the heat treatment is simulated. Figure 6.20 shows the change of wood moisture content with time during the operation at the bottom, middle, and top wood layers.

The wood temperatures at the bottom, middle and top for two different initial humidities are compared in Figures 6.21, 6.22, and 6.23 for different periods of operation. When the wood is more humid, more heat is needed to evaporate water; as a result, the wood temperature is lower.

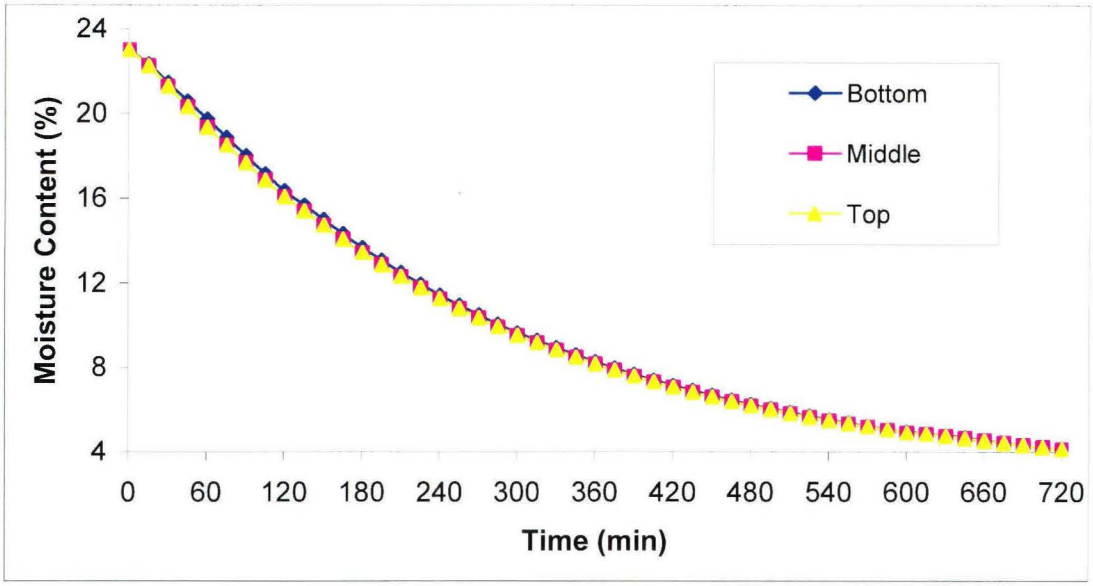

Figure 6.20 *Wood Moisture Content at the Bottom, Middle and Top Wood*

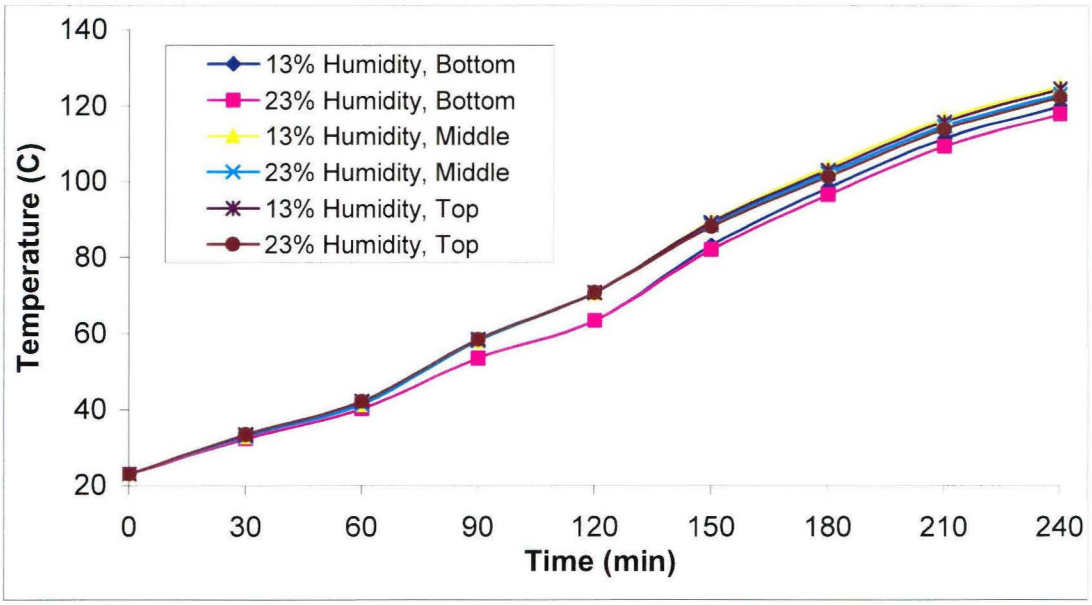

Figure 6.21 *Wood Temperature at the Bottom, Middle, and Top Wood for The First Period of Operation (0-4 hours) for 13%, and 23% Initial Moisture Content*

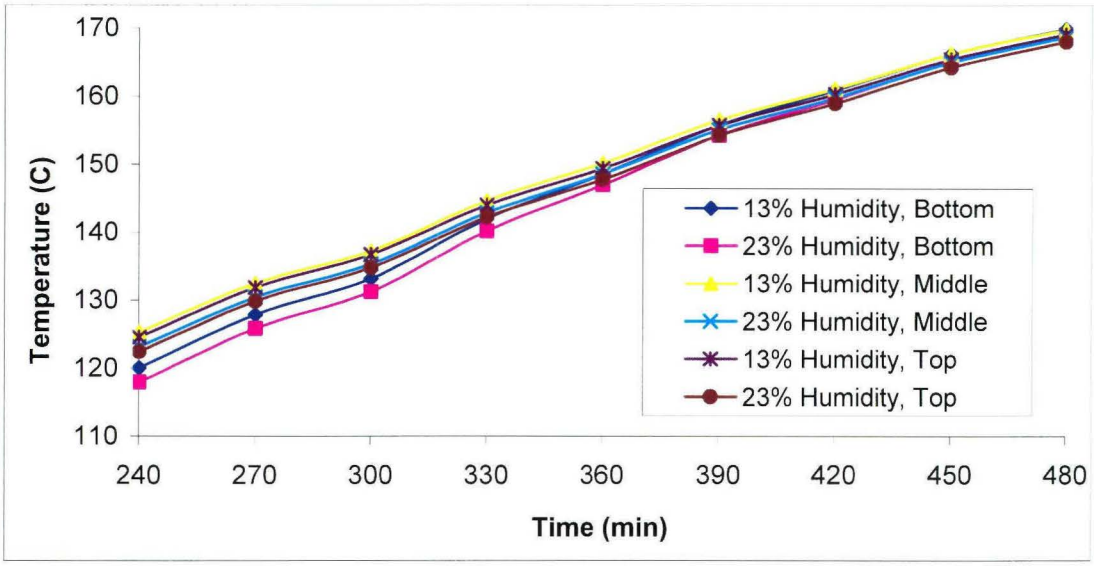

Figure 6.22 *Wood Temperature at the Bottom, Middle, and Top Wood for The Second Period of Operation (4-8 hours) for 13%, and 23% Initial Moisture Content*

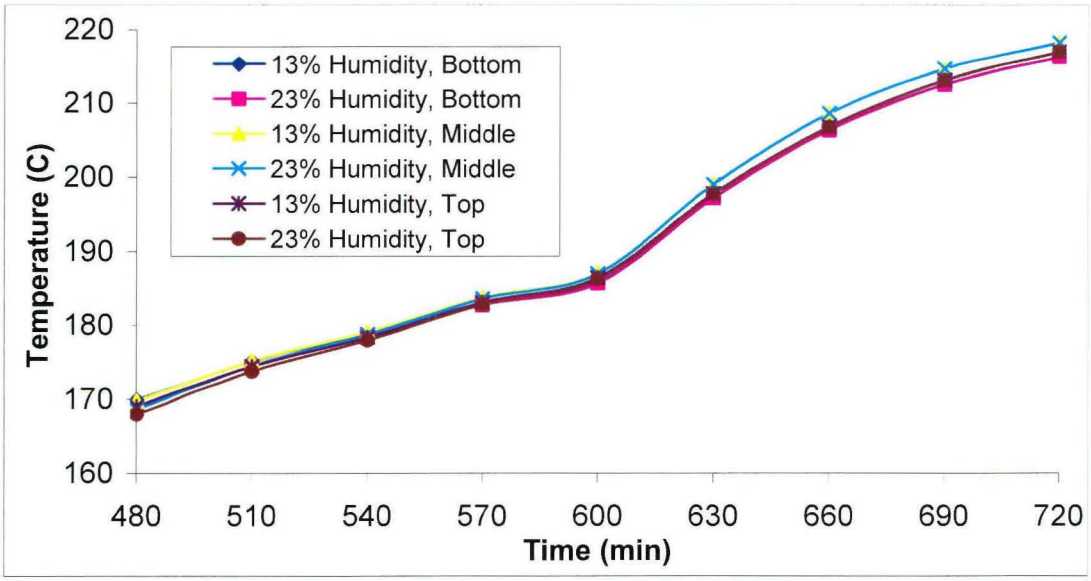

Figure 6.23 *Wood Temperature at the Bottom, Middle, and Top Wood for The Third Period of Operation (8-12 hours) for 13%, and 23% Initial Moisture Content*

6.11 Parametric Study and Results

6.11.1 Heating Rate and Holding Time

In this part, a parametric study was carried out. The heating rate shown in Figure 5.1 which represents 15˚C/h was changed to 10˚C/h and 20˚C/hour (see Figures 6.24 and 6.25).

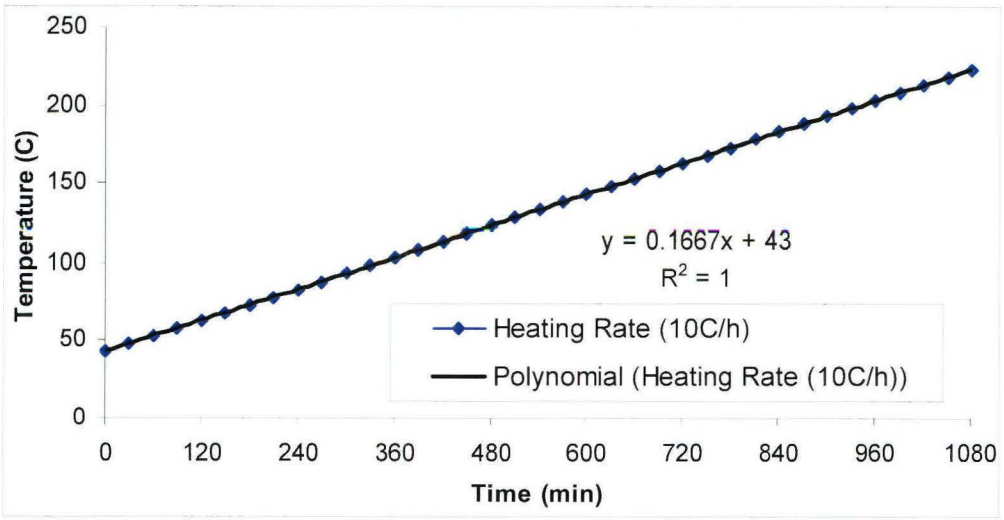

Figure 6.24 *Injection Gas Temperatures for a Heating Rate of 10˚C/h*

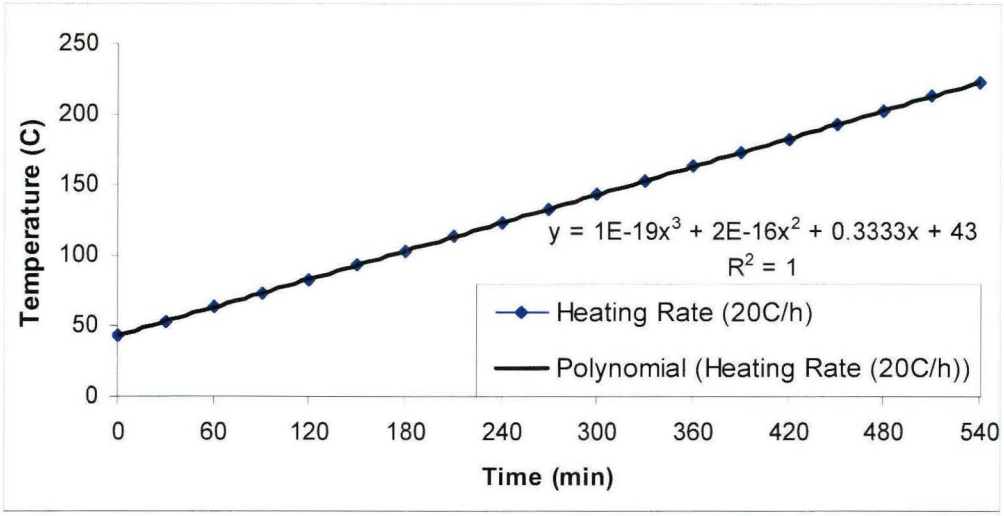

Figure 6.25 *Injection Gas Temperatures for a Heating Rate of 20˚C/h*

The heating rates were represented in the model using a polynomial fit given in these figures (see Figures 6.24 and 6.25). Wood temperatures predicted for different heating rates are compared in Figures 6.26, 6.27, and 6.28 with plant data.

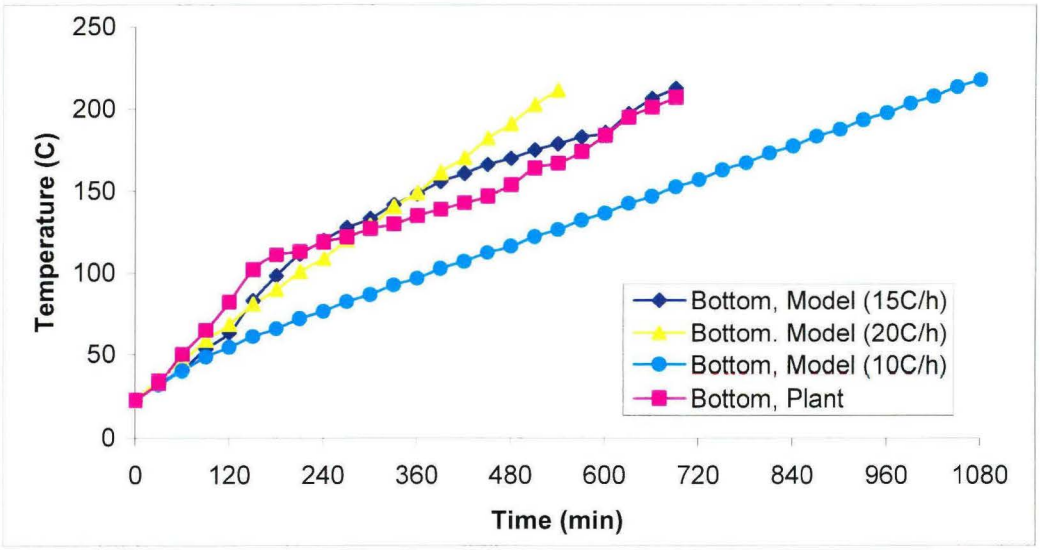

Figure 6.26 *Comparison of Predicted Temperatures with the Plant Data for Bottom Wood Layers for a Heating Rate of 15˚C/h, 10˚C/h, and 20˚C/h*

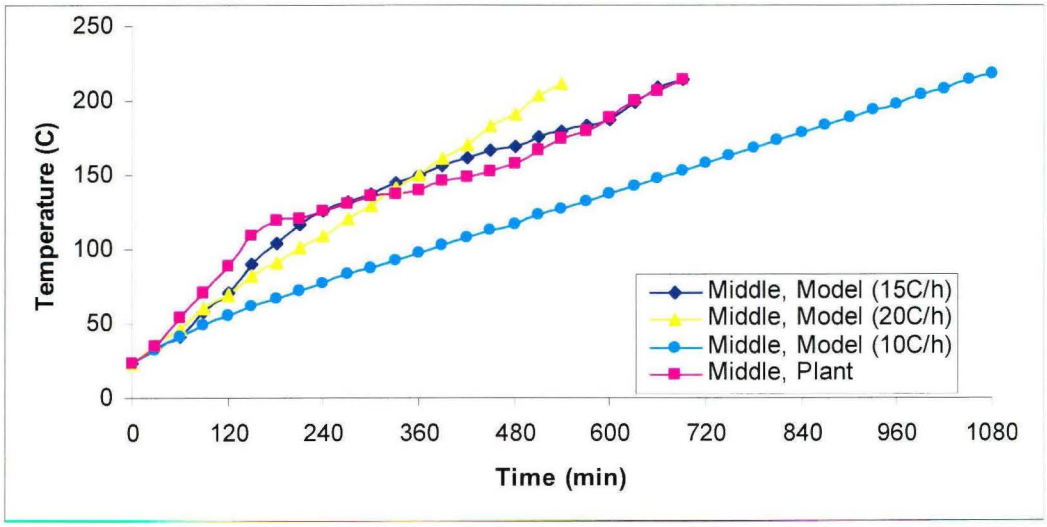

Figure 6.27 *Comparison of Predicted Temperatures with the Plant Data for Middle Wood Layers for a Heating Rate of 15˚C/h, 10˚C/h, and 20˚C/h*

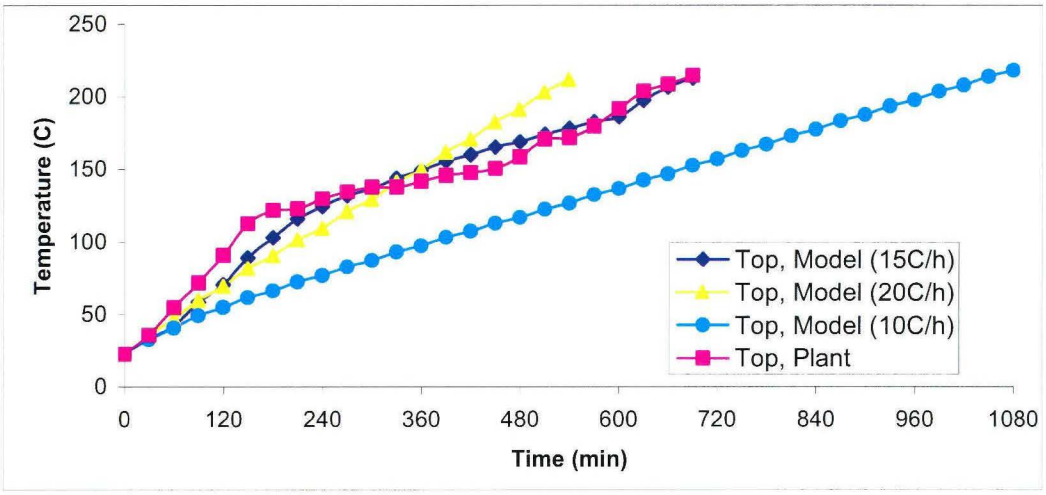

Figure 6.28 *Comparison of Predicted Temperatures with the Plant Data for Top Wood Layers for a Heating Rate of 15˚C/hr, 10˚C/hr, and 20˚C/hr*

In the above figures, it can be easily seen that the wood temperatures were changing according to the injection temperatures, the same heating trend is observed for the injection gas (see Figures 6.24, 6.25) and for wood temperatures (see Figures 6.26, 6.27, and 6.28). The moisture content change is shown in Figure 6.29.

There is a slight difference between the humidity during the operation (max 1.8 %); the major difference is the final humidity of the wood.

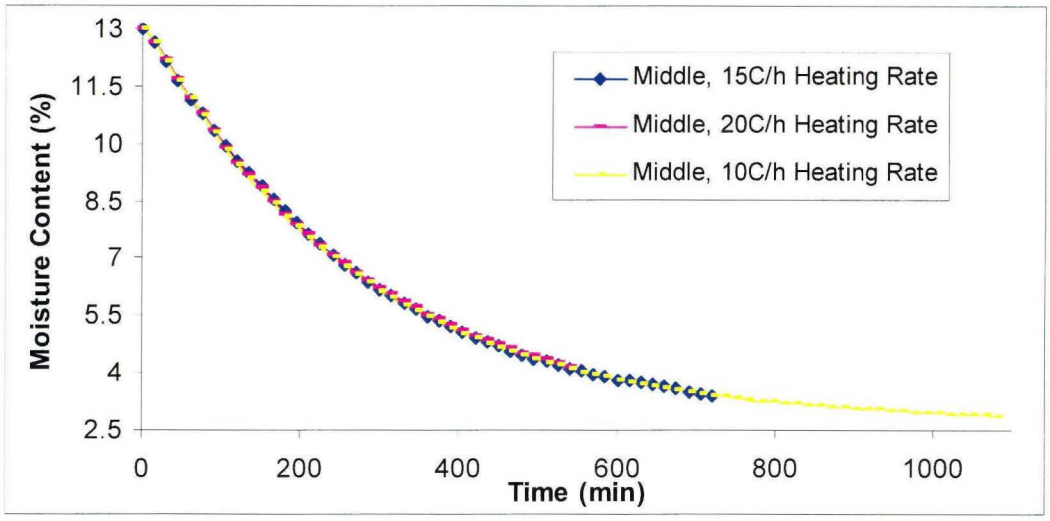

Figure 6.29 *Comparison of Predicted Humidity of Wood for a Heating Rate of 15˚C/h, 10˚C/h, and 20˚C/h*

The effect of holding time at the end of operation is studied. In the previous model and in the actual operation in the plant, the heating temperature is continuously changing with time. In the following simulations, the injection temperature is kept constant at the final value for 60 min, and for 120 min. The final temperature and moisture content of the simulations are summarized in Table 6.2.

Table 6.2 *Comparison of Holding Time Change in the Model*

	Holding Time	Initial Temperature and Moisture Content	Final Temperature and Moisture Content
Original Model	-	23˚C 13%	216~220˚C 3.40~3.43%
Case 1	60 min	23˚C 13%	220~222˚C 3.23~3.25%
Case 2	120 min	23˚C 13%	222~223˚C 3.10~3.12%

The final moisture content and temperature of the wood are different for each holding time as seen in table. However the significant difference comes from the distribution of temperatures and moisture content within the different wood layers at the end of operation, as seen in Figures 6.30 and 6.31. It seems that increasing the holding time improves the uniformity of the final temperature and moisture content of the wood.

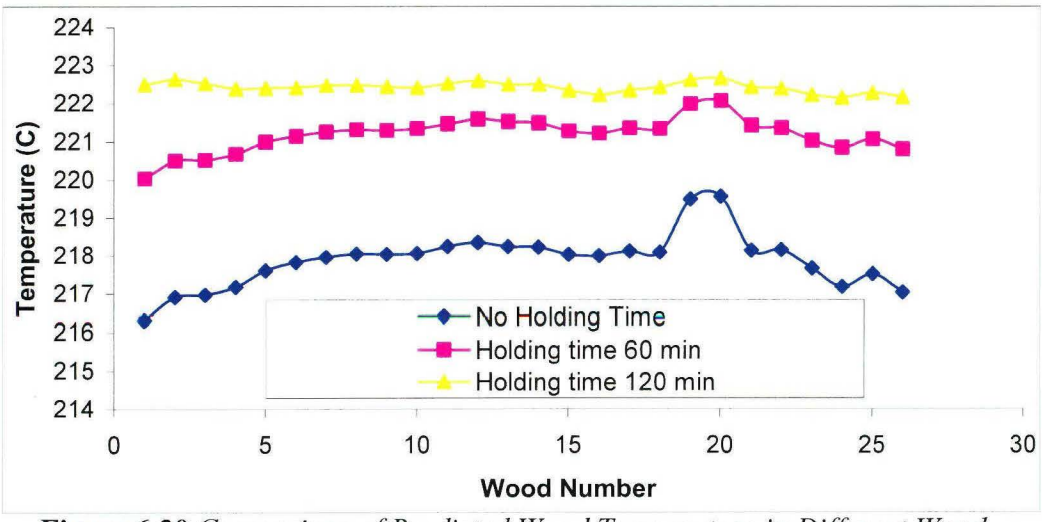

Figure 6.30 *Comparison of Predicted Wood Temperature in Different Wood Layers at the end of Operation.*

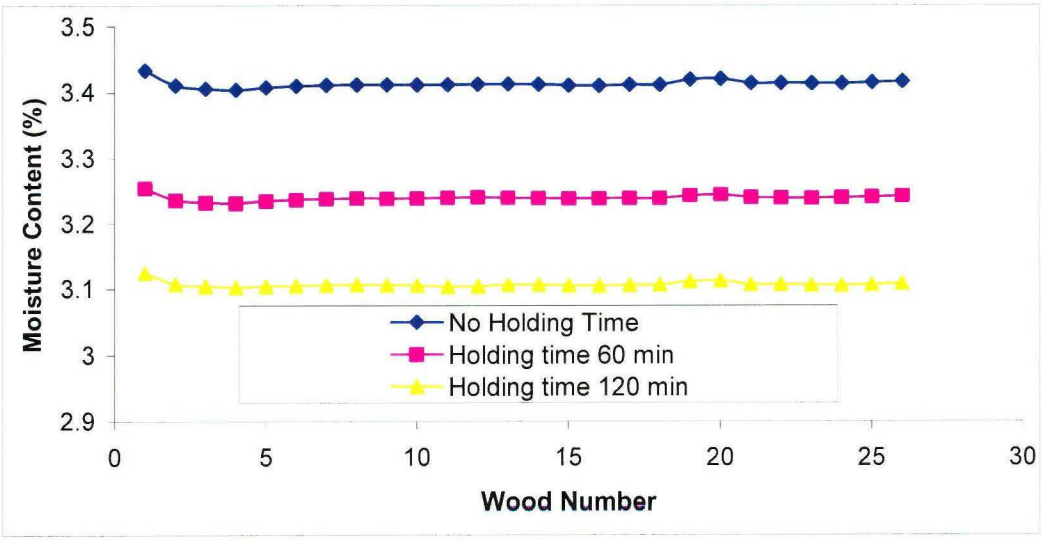

Figure 6.31 *Comparison of Predicted Wood Humidity in Different Wood Layers at the end of Operation*

6.11.2 Thermal Diffusivity

A parametric study was carried out by varying the thermal diffusivity in the Luikov coupled heat and mass transfer equations. The properties used as reference were obtained from the literature. Two different diffusivities were studied. The first variation represents the lower limit, while the second one represents the upper limit of the parameter. Figure 6.32 shows the variation of moisture content at the middle wood layers for the value of moisture diffusivity equal to 10^{-8}, 10^{-9}, and 10^{-10} (which corresponds to the upper limit, the value used in simulations, and the lower limit). The final wood moisture contents are 4.04%, 3.41%, 3.36% for diffusivities equal to 10^{-10}, 10^{-9}, and 10^{-8}, respectively. When the lower limit is used, the wood moisture content increases. The upper limit and the value used during the simulations result in similar wood moisture contents.

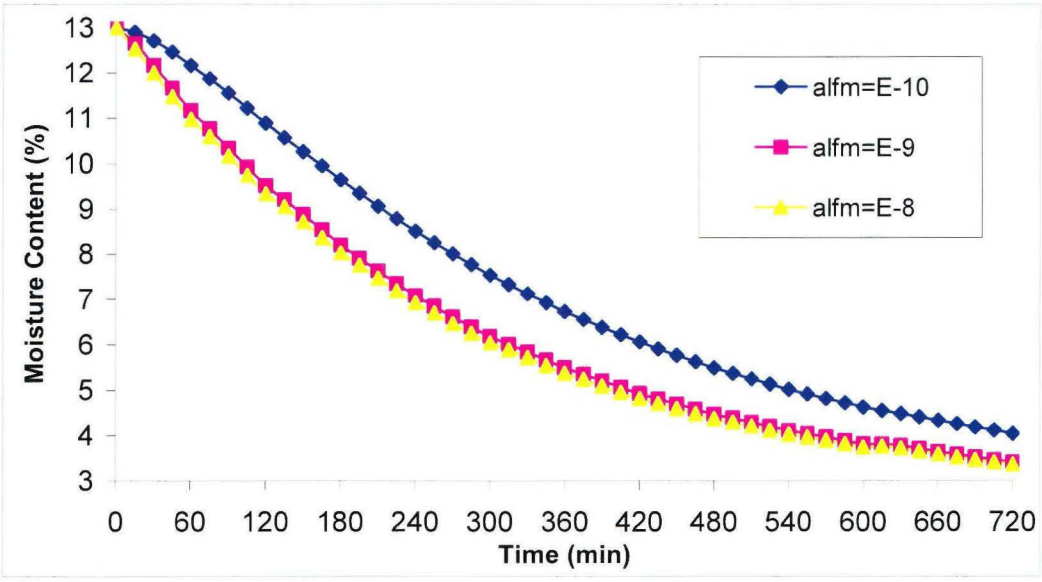

Figure 6.32 *Change of Moisture Content in the Wood during the Operation for Different Diffusivities (At the middle layer)*

6.12 Furnace Modifications and Results

The objective of this part is to study the effect of furnace dimension modifications on the wood and gas temperatures during the operation of the furnace. Similar study was already carried out with the heat transfer model and it was concluded that the furnace dimensions could be changed without affecting the product quality under given conditions. Here, the same exercise is repeated with the model which takes into account the mass transfer.

The conditions of the simulations are presented in Table 6.3; the furnace section was also given in Chapter 5 in Figure 5. Case 1 represents the industrial furnace as is now. In Case 2, the furnace dimensions are kept constant, but the wood charge is increased by decreasing the free distance between the wood pile and the top and bottom of the furnace (h_2 and h_3). The furnace height (h_1) is increased in Case3 whereas the furnace width (w) and charge width are increased in Case 4. The final two modifications are the increase of height and width together in Case 5, and the increase of width in Case 6.

In Cases 3 and 5, one row of inlet (on one side) and outlet (on the other side) are added to the top and the number of wood layers is increased to 38. In all cases, the distance between the wood pile and the side walls with gas inlet and outlets is kept constant, except in Case 6.

Table 6.3 *Simulation Conditions*

Case	h_1 (m)	h_2 (cm)	h_3(cm)	w (m)	w_c (m)	Comments
1	2.552	28.070	30.62	1.416	1.549	Actual dimensions
2	2.552	**7.656**	**5.104**	1.416	1.549	h_2 and h_3 are decreased, charge is increased.
3	**3.164**	7.656	5.104	1.416	1.549	h_1 (height) is increased by 0.612 m, h_2 and h_3 are kept constant
4	2.552	7.656	5.104	**1.924**	**2.057**	w (width) and w_c (width of the charge) are increased by 0.508 m
5	**3.164**	28.070	30.620	**1.924**	**2.057**	h_1 (height) is increased by 0.612 m. w (width) and w_c (width of the charge) are increased by 0.508 m.
6	2.552	28.070	30.620	1.416	**2.057**	w (width) is increased by 0.508 m, w_c (width of the charge) remains. Distance between the wood and furnace is increased.

The change of wood temperature with time predicted for the modified furnace geometries was compared in Figures 6.33, 6.34 and 6.35 for Bottom, Middle and Top Wood Layers at the Position 2, respectively. In general, it seems that the modifications do not have a significant effect on the temperature of middle and top layers of wood.

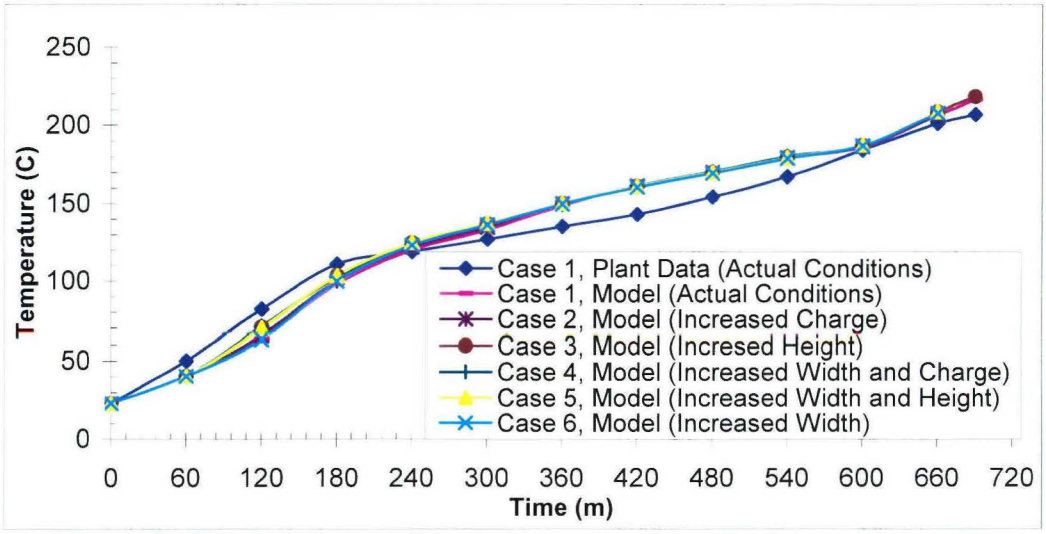

Figure 6.33 *Comparisons of Temperatures Predicted by the Model for Different Furnace Geometries at the Bottom Wood Layer*

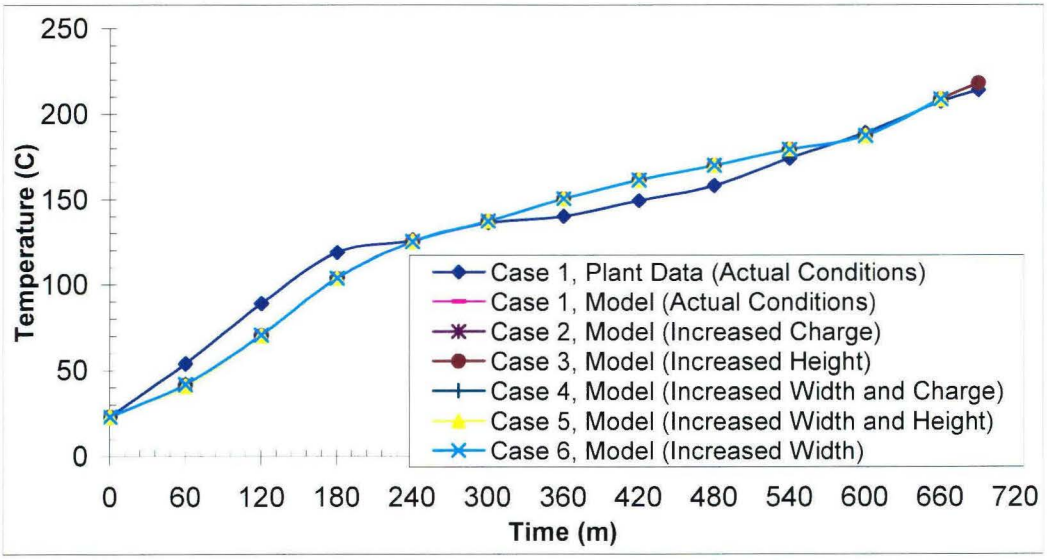

Figure 6.34 *Comparisons of Temperatures Predicted by the Model for Different Furnace Geometries at the Middle Wood Layer*

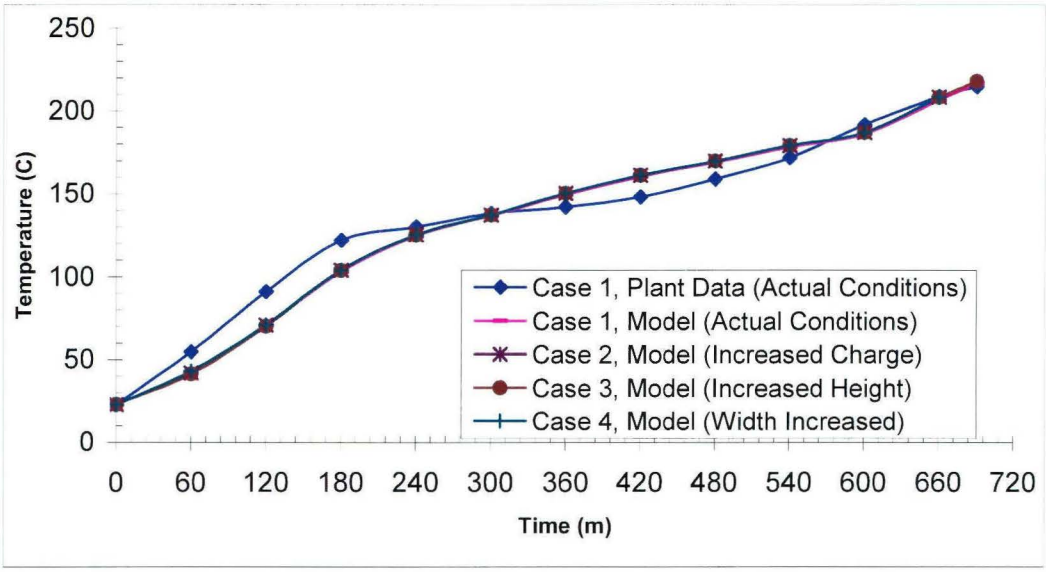

Figure 6.35 *Comparisons of Temperatures Predicted by the Model for Different Furnace Geometries at the Top Wood Layer (Position 2)*

The change in moisture content is shown in Figure 6.36 for different cases. Since the operation time and procedure does not change, the moisture content change is the same for the cases studied.

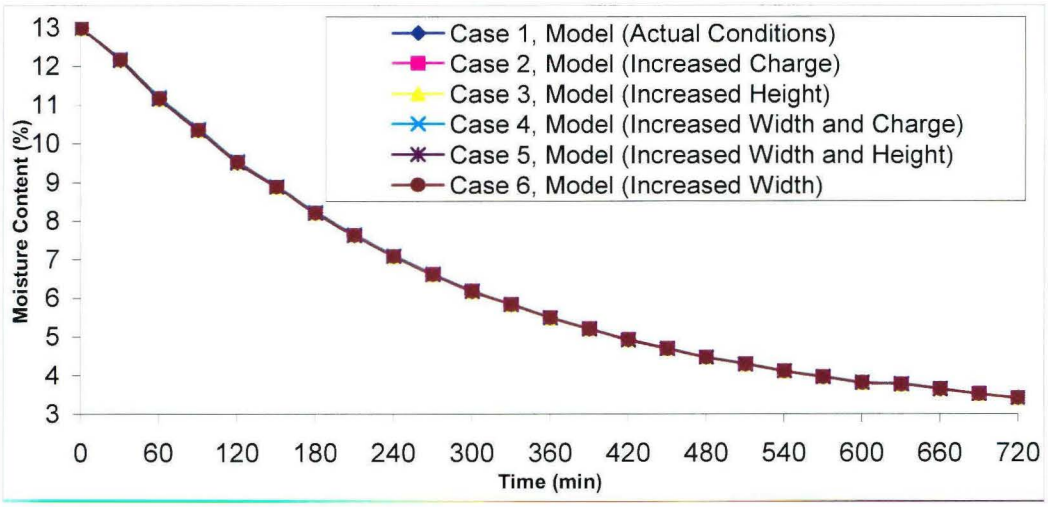

Figure 6.36 *Comparison of Moisture Content Predicted by the Model for Different Furnace Geometries at the Middle Wood Layer*

Figures 6.37 to 6.41 compare the temperatures of different wood layers predicted by the model for increased charge, width and height, respectively, at different times for position 2. Again, it can be seen from these figures that the model results differ only slightly (0.26%). The modifications do not seem to have a significant effect on the temperature, consequently, the quality of wood for the other layers.

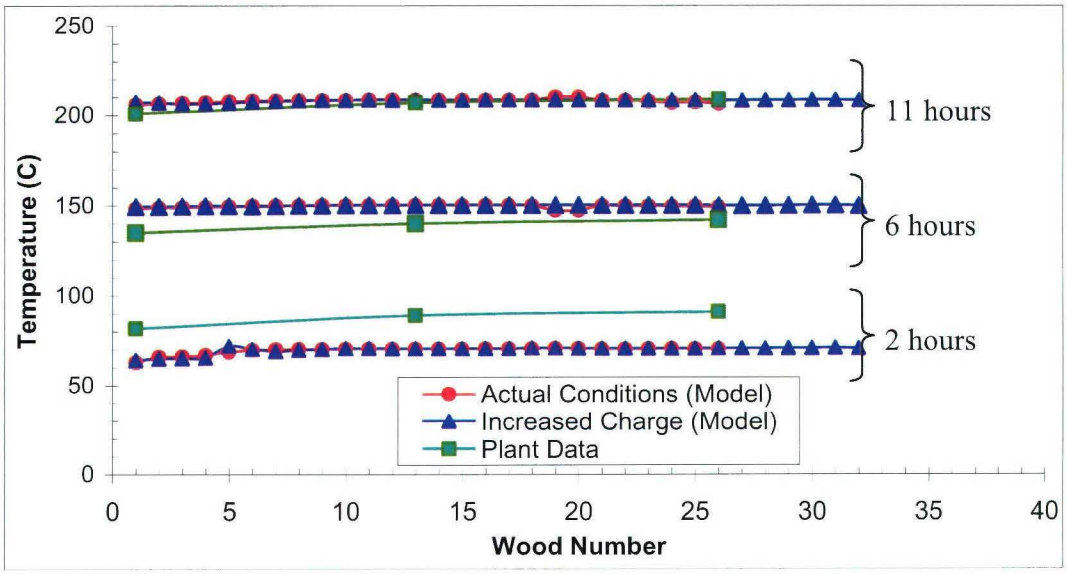

Figure 6.37 *Comparisons of Temperatures of Different Wood Layers Predicted by the Model for Increased Charge at Different Times*

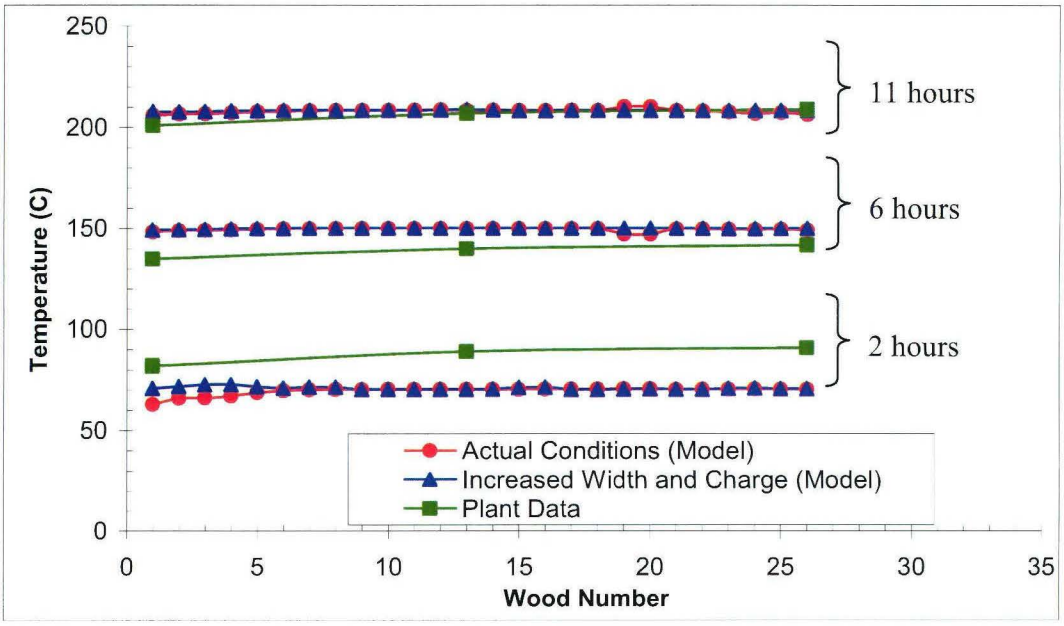

Figure 6.38 *Comparisons of Temperatures of Different Wood Layers Predicted by the Model for Increased Width and Charge at Different Times*

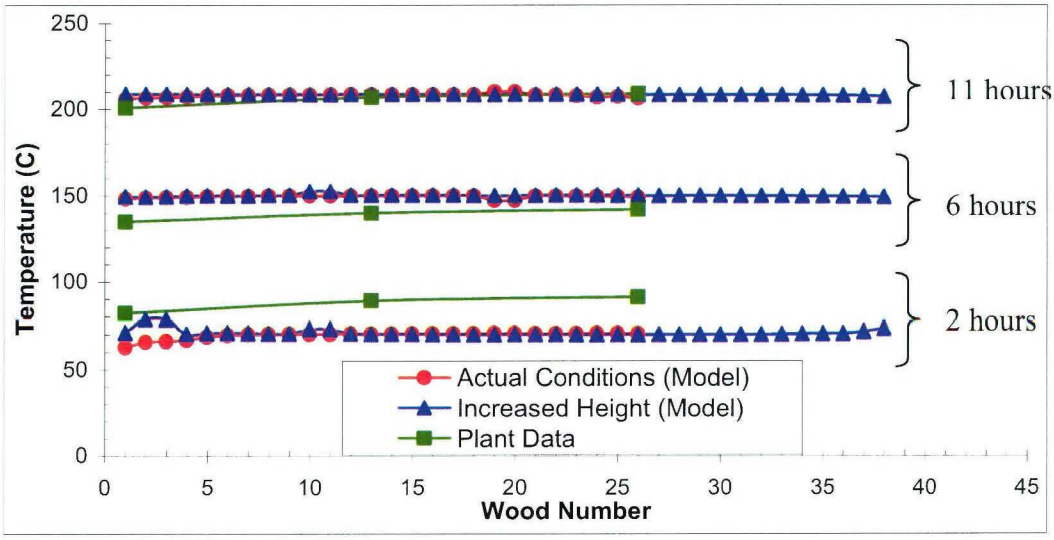

Figure 6.39 *Comparisons of Temperatures of Different Wood Layers Predicted by the Model for Increased Height at Different Times*

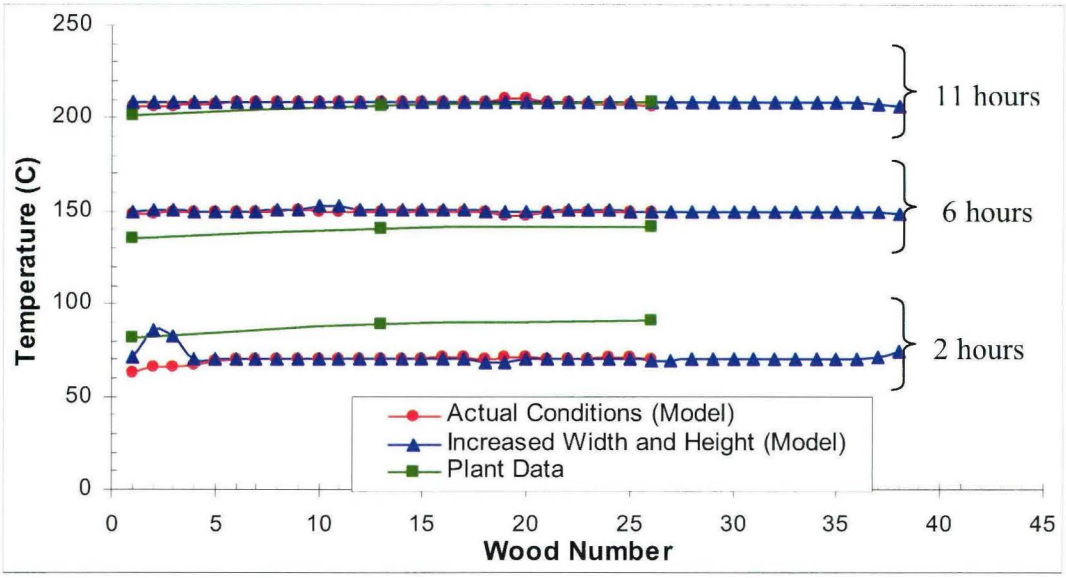

Figure 6.40 *Comparisons of Temperatures of Different Wood Layers Predicted by the Model for Increased Width and Height at Different Times*

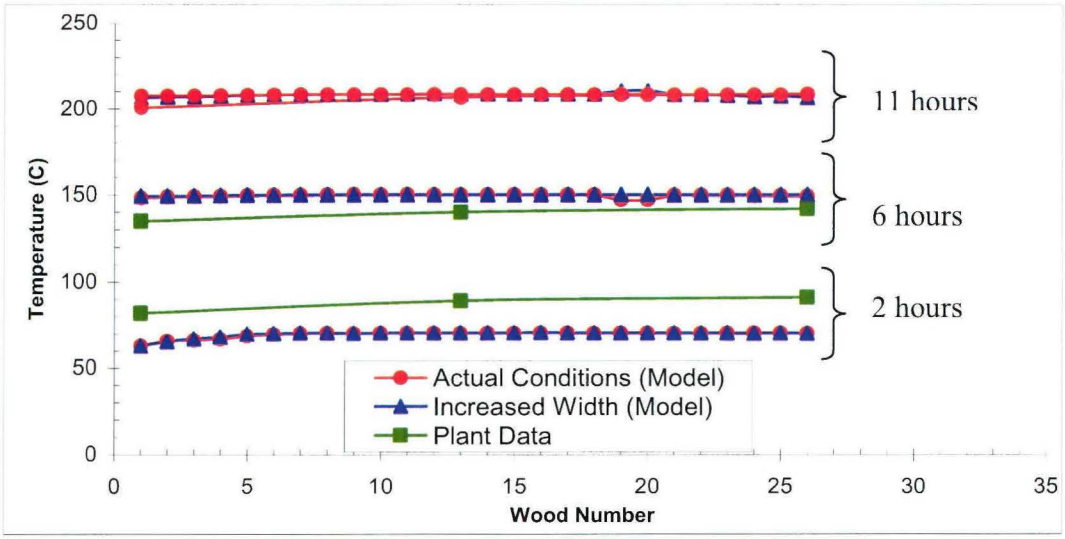

Figure 6.41 *Comparisons of Temperatures of Different Wood Layers Predicted by the Model for Increased Width at Different Times*

The temperatures of different wood layers are presented in Figures 6.42 and 6.43 after six and twelve hours of operation, respectively. These figures show that some differences between various modifications are observed. However, the differences are a few degrees and probably due to flow patterns created at the bottom of the furnace.

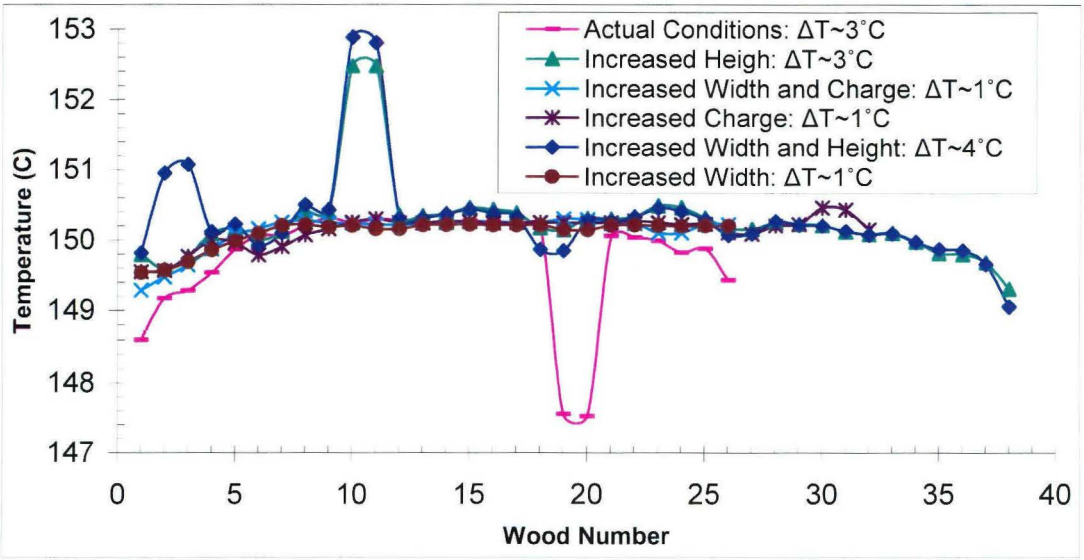

Figure 6.42 *Comparison of Predicted Wood Temperatures in Different Wood Layers after six Hours of Operation*

After six hours of operation, it is observed that the increase in width as well as the increase in charge in the furnace result in a more uniform temperature distribution in different wood slabs (ΔT~1°C). At the end of operation, there is still ~1°C difference between wood temperatures. The increase in width gives the most uniform temperature distribution at the end.

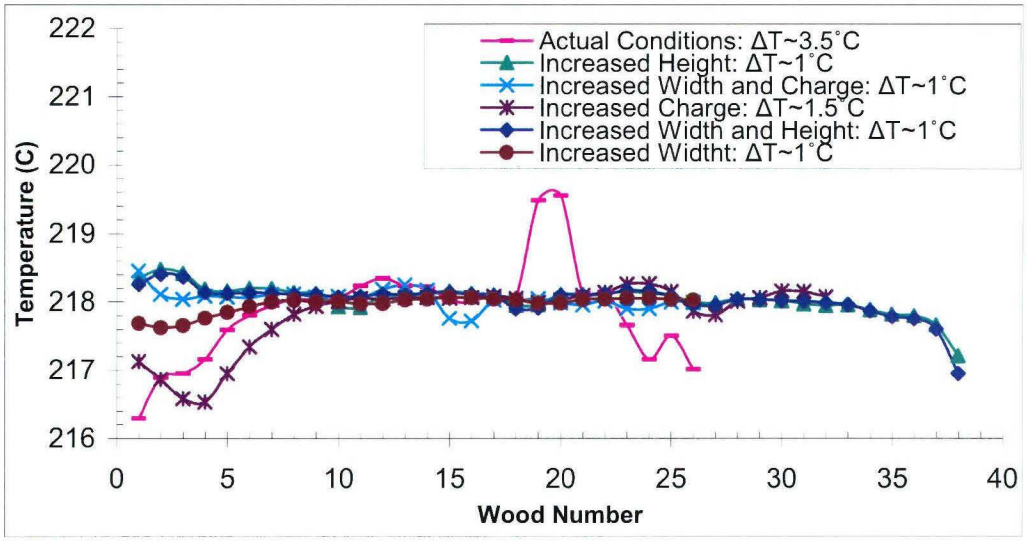

Figure 6.43 *Comparison of Predicted Wood Temperatures in Different Wood Layers at the end of Operation*

The temperatures in positions 1, 2, and 3 (see Figure 5.2) for the bottom and top wood layers after six and eleven hours of operations are presented in Figures 6.44 to 6.47. The differences between the wood temperatures of different modifications are greatest for the bottom layer for earlier times (see Figure 6.44). This difference decreases with increasing time (see Figure 6.45). At the top layer, the geometrical modifications do not affect the wood temperature as shown in Figures 6.46 and 6.47. Since the temperature differences at different points between the bottom and top wood layers are around ~1˚C, it is not easy to see the difference between Figures 6.44-6.46 and Figures 6.45-6.47.

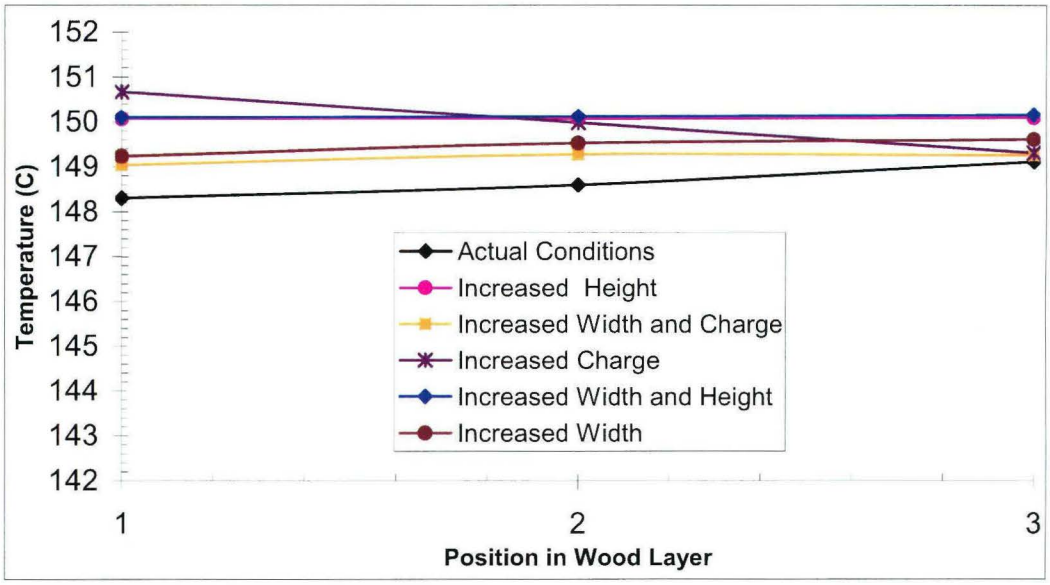

Figure 6.44 *Comparison of Predicted Wood Temperature in the Bottom Wood Layer after Six Hours of Operation.*

Figure 6.45 *Comparison of Predicted Wood Temperature in the Bottom Wood Layer after Eleven Hours of Operation.*

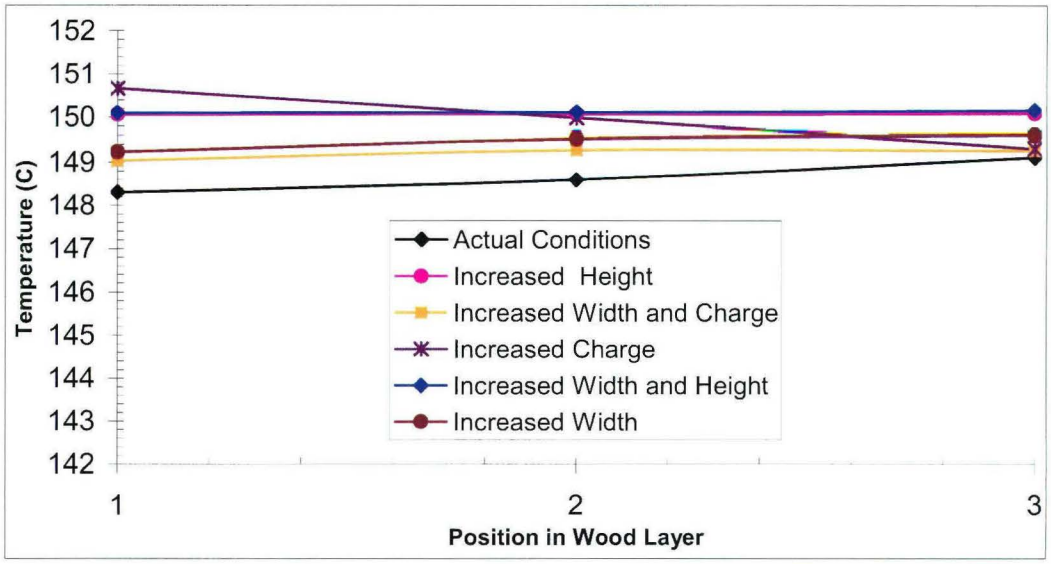

Figure 6.46 *Comparison of Predicted Wood Temperature in the Top Wood Layer after Six Hours of Operation.*

Figure 6.47 *Comparison of Predicted Wood Temperature in the Top Wood Layer after Eleven Hours of Operation.*

6.13 Conclusions

The model results, with a few degrees of difference give a good agreement with the plant data. The model results may be improved if more accurate material properties are used as a function of time, humidity and conditions.

The predicted and measured values of the initial and final humidity of the product give a good agreement. The change of humidity during the operation can not be measured for the time being in the plant; as a result, the change during the operation can not be compared.

Changes in two operational procedures were tested using the model. It is seen that a longer holding time at the end of the treatment yields a more uniform product.

Diffusivity parameter was changed to see the response of the mathematical model. As expected, decrease in diffusivity results in the low mass transfer.

Furnace dimensions were modified for five different cases. According to the mathematical model results, the furnace dimensions can be increased as shown in Table 6.3 without changing the quality of the product significantly. Increasing the distance between the wood and furnace wall by increasing the furnace width will help to have more uniform heating during the operation.

CHAPTER 7

CONCLUSIONS

This study was undertaken with the objective of developing a numerical model of the high temperature heat treatment furnace of Perdure Technology. The model was created to address the following issues: (1) study of flow, heat transfer and mass transfer, (2) investigate the humidity and temperature profile in the end product, (3) find geometry and conditions which will lead to better wood properties.

Many insights were gained from the research performed during this project. A 3D unsteady-state flow model of the heat treatment furnace was showed that the gas flow distribution is not uniform in the furnace. New injection conditions were investigated. It is observed that changing injection velocity and angles have a minor effect on the gas distribution and didn't prevent mass flow rate fluctuations in the channels between wood layers, blocking the upper and lower sides of the wood pile seems to force the gas to go through the channels between wood layers and leads a more uniform gas distribution, new injection design improves significantly the distribution of the gas in the channels. This design combined with the blockage of the empty regions below the wood pile gives the best result among the injections configurations presented. 1D unsteady-state heat transfer model

was introduced into 3D unsteady-state flow model in order to predict temperature distribution in the wood during the operation. The heat transfer model gave a good agreement with the plant data. Temperature fluctuations between different wood layers were observed. The furnace geometry was modified and the effect of the modifications on the wood temperature was predicted. The furnace modifications are increase of product charge, increase of furnace height, increase of furnace width. This study showed that the production can be increased by about 23% if the charge is increased, 24.5% if the furnace width is increased, and 42% if the furnace height is increased. However, these modifications do not have an effect on the product uniformity. As discussed previously, the modification of injection geometry is more effective in increasing the flow uniformity.

A 1D heat and mass transfer model coupled with a 3D gas flow and heat transfer model was developed. The results were in good agreement with the plant data. The model is likely to give better results when more accurate material properties as a function of temperature and humidity are used.

The initial and final moisture content of the product gives a good agreement with the model. The change of wood moisture content during the operation cannot be measured in the plant and, consequently, cannot be compared with the model results.

The present mathematical model proved to be a useful tool enabling detailed analysis of transport phenomena in high temperature heat treatment process. The model also enables

the analysis of the several process variables and suggested furnace modifications; thus, it allows the selection of appropriate changes that will lead to increased furnace performance and capacity. This saves industry a considerable amount of time and money.

REFERENCES

[1] www.perdure.com

[2] A.O Rapp, *Review on Heat Treatment of Wood,* Symposium Environmental Optimization of Wood Protection, Antibes, France 2001

[3] Centre de Recherche Industrielle du Québec, *Bois Traité à Haute Temperature,* Québec, Canada, 2003.

[4] http://patents1.ic.gc.ca, http://ep.espacenet.com

[5] www.21siecle.qc.ca/arsenic.htm

[6] Forest Products Laboratory, *Wood Handbook-Wood as an Engineering Material*, (Gen. Tech. Rep. FPL-GTR-113), Madison, Wisconsin, U.S. 1999.

[7] http://www.forestprod.org/Jermann2.pdf

[8] P. Gohar, R. Guyonnet, *Development of Wood Retification, Process at the Industrial Stage,* 4th Symposium Wood Preservation, Cannes, France 1998

[9] www.cartage.org.lb/en/themes/Sciences/BotanicalSciences/PlantsStructure/PlantsStructure/PlantsStructure.htm

[10] http://www.cfr.ncsu.edu/wps/k12activities/ppts/forest/

[11] Finnish ThermoWood Association, *ThermoWood Handbook,* Helsinki, Finland, 2003

[12] W.T. Simpson, J. Y. Liu, *An Optimization Technique To Determine Red Oak Surface And Internal Moisture Transfer Coefficients During Drying,* USDA Forest Service, Forest Products Laboratory, Madison, Wisconsin, U.S., 1997.

[13] J. Irudayaraj, Y.Wu, *Analysis and Application of Luikov's Heat, Mass, and Pressure Transfer Model to a Capillary Porous Media*, Drying Technology, 14(3&4), pp: 803-824, New York, 1996.

[14] A.V. Luikov, *Systems of Differential Equations of Heat and Mass Transfer in Capillary-Porous Bodies,* International Journal for Numerical Methods in Engineering, 18, pp: 1-14, 1975.

[15] J. Irudayaraj, K. Haghighi, R.L. Stroshine, *Non-Linear finite Element Analysis of Coupled heat and Mass Transfer Problems with Application to Timber Drying,* Drying Technology, 8(4), pp: 731-749, New York, 1990.

[16] H.R. Thomas, K. Morgan, R.W. Lewis, *A Fully Nonlinear Analysis of Heat and Mass Transfer Problems in Porous Media,* International Journal for Numerical Methods in Engineering, 15, pp: 1381-1393, 1980.

[17] G. Comini, R.W. Lewis, *A Numerical Solution of Two-Dimensional Problems Involving Heat and Mass Transfer,* International Journal for Numerical Methods in Engineering, 19, pp: 1387-1392, 1976.

[18] J.Y. Liu, S. Cheng, *Heat and Moisture Transfer in Wood During Drying,* Mechanics of Cellulosic and Polymeric Material, ASME, pp: 25-32, 1990.

[19] R.W. Lewis, W.J. Ferguson, *The Effect of Temperature and Total Gas Pressure on The Moisture Content in a Capillary Porous Body,* International Journal for Numerical Methods in Engineering, 29, pp: 357-369, 1990

[20] P. Horacek, *Modeling of Coupled Moisture and Heat Transfer during Wood Drying,* 8th International IUFRO Wood Drying Conference, 2003.

[21] H.R. Thomas, K. Morgan, R.W. Lewis, *An Application of The Finite Element Method to The Drying of Timber,* Wood and Fiber, 11(4), pp: 237-243, 1980.

[22] Juan C. Alvarez, *Evaluation of Moisture Diffusion Theories In Porous Materials*, Master Thesis, Virginia Polytechnic Institute and State University, Blacksburg, Virginia, August, 1998.

[23] C. Tremblay, *Détermination expérimentale des paramètres caractérisant les transferts de chaleur et de masse dans le bois lors du séchage,* Ph.D. Thesis, Laval University, Québec, Canada, 1998.

[24] Z. Benrabah, *Modélisation tridimensionnelle par éléments finis des phénomènes hygro-thermiques dans les milieux poreux : Application au séchage du bois à la dessiccation du bois,* Ph.D. Thesis, Laval University, Québec, Canada, 2002.

[25] Y.T. Keum, J.H. Kim, B.Y. Ghoo, *Computer Aided Design of Electric Insulator*, Journal of Ceramic Processing Research, 1(1), pp: 74-79, 2000.

[26] I.W. Turner, P. Perré, *The Use of Implicit Flux Limiting Schemes in The Simulation of The Drying Process: A New Maximum Flow Sensor Applied to Phase Mobilities,* Applied Mathematical Modelling, 25, pp: 513-540, 2001.

[27] Fortes, M., and M.R. Okos. 1981. A non-equilibrium thermodynamics approach to transport phenomena in capillary porous media. Trans, ASAE 24(3):756-760.

[28] F.P. Incropera, D.P. Dewitt, *Introduction to Heat Transfer,* third edition, New York, John Wiley & Sons, 2002.

[29] AEA Technology plc, *CFX-F3D Manual*, United Kingdom, 1995.

[30] J.N. Beard, H.N. Rosen, B.A. Adesanya, *Temperature Distributions and Heat Transfer during The Drying of Lumber,* Drying Technology, 1(1), pp: 117-140, 1983.

[31] J. Irudrayaj, Y. Wun, *Analysis and Application of Luikov's Heat, Mass, and Pressure Transfer Model to a Capillary Porous Media,* Drying Technology, 14(3&4), pp: 803-824, 1996.

[32] www.acadjournal.com/2004/v11/Part7/p3/

APPENDIX 1

Numerical Values of Parameters Used in Model Based on Mass Transfer Potential

Thomas *et al.* [16] given the numerical values of the thermo physical parameters used in their model for linear and nonlinear problems. These values were listed in Table A1.1.

Table A1.1 *Numerical Values of the Varying Parameters*

Thermo physical Parameter	Nonlinear Problem		Linear Problem
k_q	0.29 W/mK at 10°C	0.45W/mK at 60°C	0.35W/mK
c_q	1163 J/kgK at 10°C	1405 J/kgK at 60°C	1284 J/kg.K
a_m	$0.6*10^{-9}$ m^2/sec at 12% mc (db)	$1.54*10^{-9}$ m^2/sec at 12% mc (db)	$1.00*10^{-9}$ m^2/sec
δ	0.01/°C at 12%mc	0.02/°C at 12%mc	0.02/°C
ε	0.1 at mc≥30%	0.1-1 at mc<30%	0.3

The constant parameters were tabulated in Table A1.2.

Table A1.2 *Numerical Values of Constant Parameters* [16]

Thermo physical Parameter	Constant Value
λ	$2.5*10^6$ J/kg
ρ	500 kg/m^3
c_m	0.003 $kg_{moisture}/kg_{drybody}$ °M

In another study Irudayaraj *et al.* **[15]** used the following convective heat and mass transfer coefficients shown in Table A1.3.

Table A1.3 *Materials Properties*

Property	Value
α_m	$1.67*10^{-6}$ $kg_{moisture}/m^2s$ M
α_q	22.5 $W/M^{2\circ}K$

Beard *et al.* **[30]** obtained heat transfer coefficient in his study in a range of 42-63.8J/sm^2K.

Thomas *et al.* **[21]** were used in another study the values for the thermo physical properties of spruce listed in Table A1.4.

Table A1.4 *Numerical Values of Some Parameters*

Property	Value
k_q	0.65 W/mK
k_m	$2.2*10^{-8}$ kg/ms°M
c_q	2500 J/kgK
c_m	$0.01kg_{moisture}/kg_{dry\ body}$ °M
δ	2.0°M/K
ε	0.3
ρ	370 kg/m^3
α_m	2.5 kg/m^2s
α_q	22.5 W/m^2 °K

Irudrayaj and Wun [31] simplified the Luikov's equations as follows and gave the values of the coefficients used for solving the system of equations (6)-(8) as in Table A1.5.

$$C_q \frac{\partial T}{\partial t} = K_{11}\nabla^2 T + K_{12}\nabla^2 M + K_{13}\nabla^2 P \quad \text{(A1-1)}$$

$$C_m \frac{\partial M}{\partial t} = K_{21}\nabla^2 T + K_{22}\nabla^2 M + K_{23}\nabla^2 P \quad \text{(A1-2)}$$

$$C_p \frac{\partial P}{\partial t} = K_{31}\nabla^2 T + K_{32}\nabla^2 M + K_{33}\nabla^2 P \quad \text{(A1-3)}$$

Table A1.5. *The Values of Coefficients*

Property	Value
C_q	5.25
C_m	10.5
C_p	21.0

Property	Value	Property	Value	Property	Value
K_{11}	4.0	K_{12}	2.0	K_{13}	1.0
K_{21}	4.0	K_{22}	2.0	K_{23}	1.0
K_{31}	4.0	K_{32}	2.0	K_{33}	1.0

APPENDIX 2

Furnace Geometry

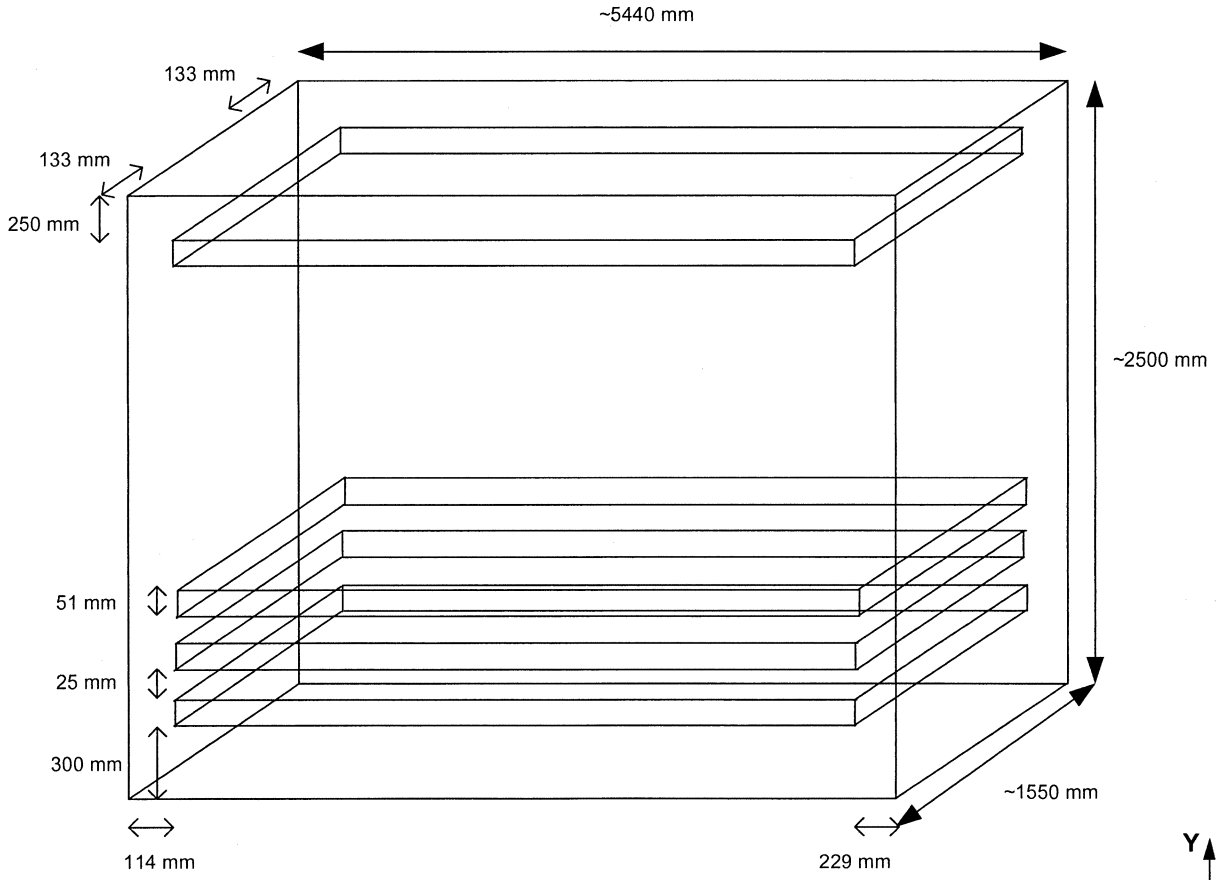

Figure A2.1 *Furnace Dimensions*

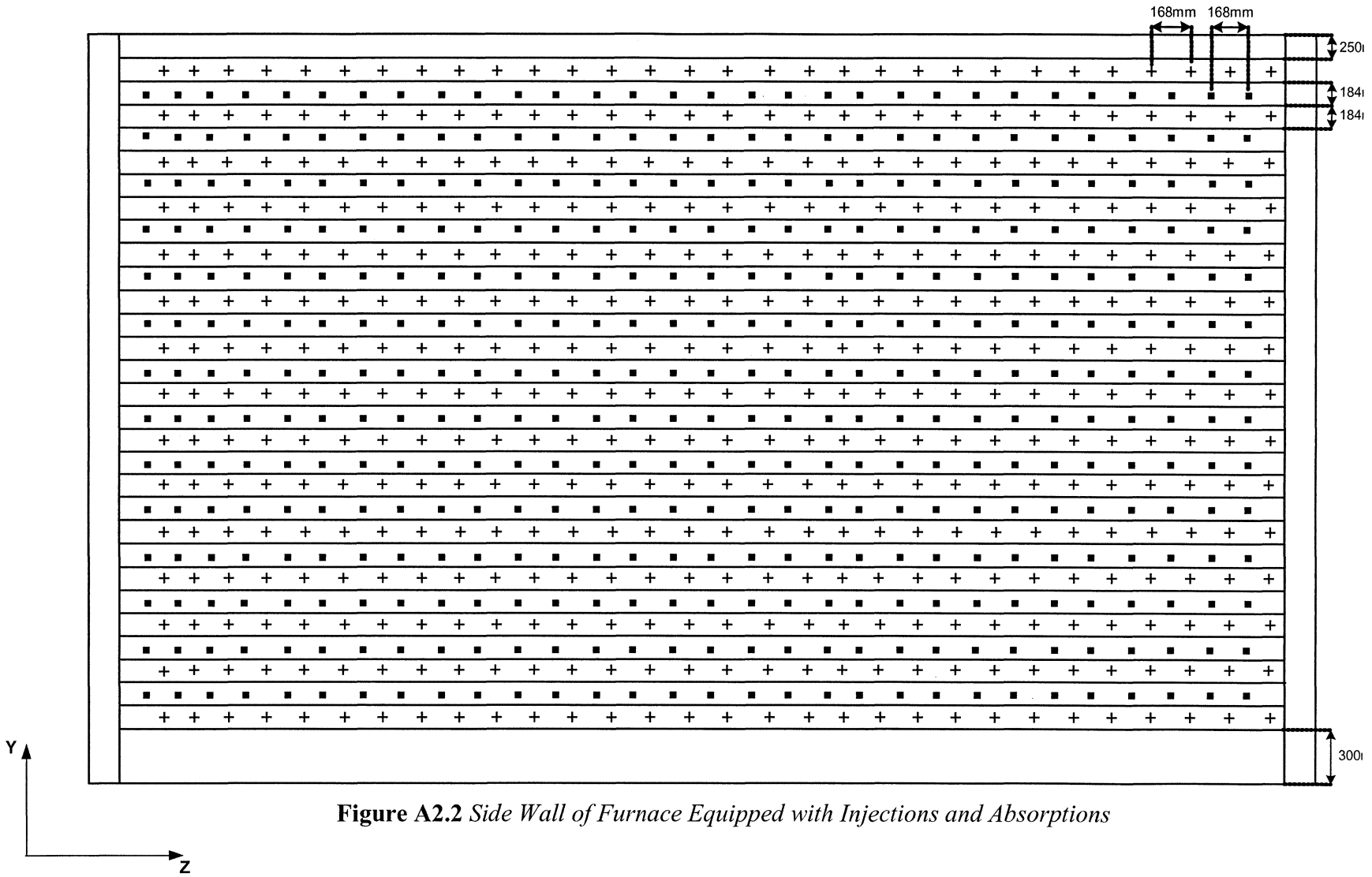

Figure A2.2 *Side Wall of Furnace Equipped with Injections and Absorptions*

+ Inlets (on side wall 1), outlets (on side wall 2)

■ Outlets (on side wall 1), inlets (On side wall 2)

On side wall 1, there are:

- 30 (horizontal axe) x 10 (vertical axe) inlets,
- 30 (horizontal axe) x 9 (vertical axe) outlets.

On side wall 2, it is vice versa.

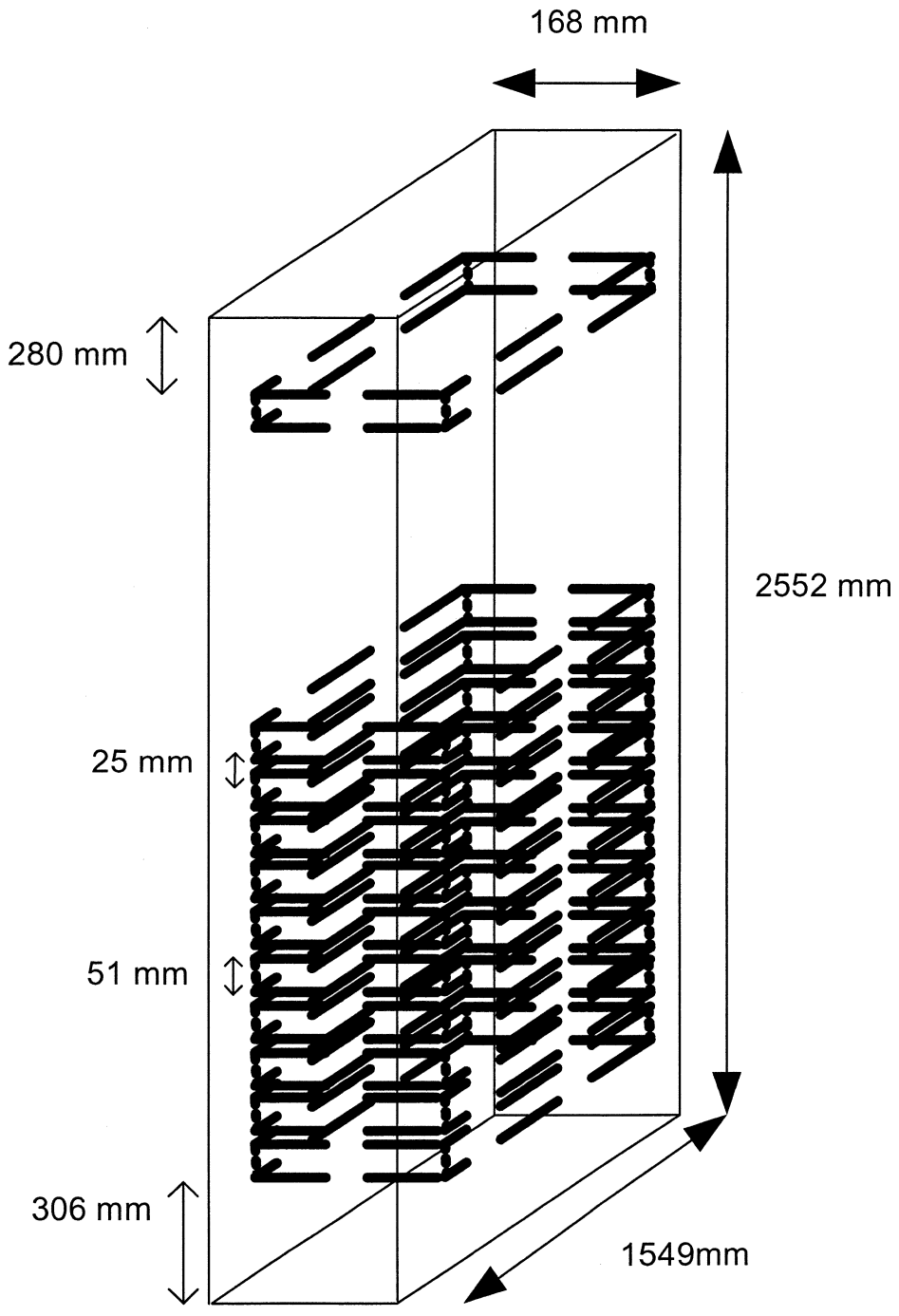

Figure A2.3 *Model Dimensions*

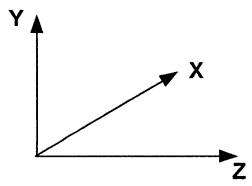

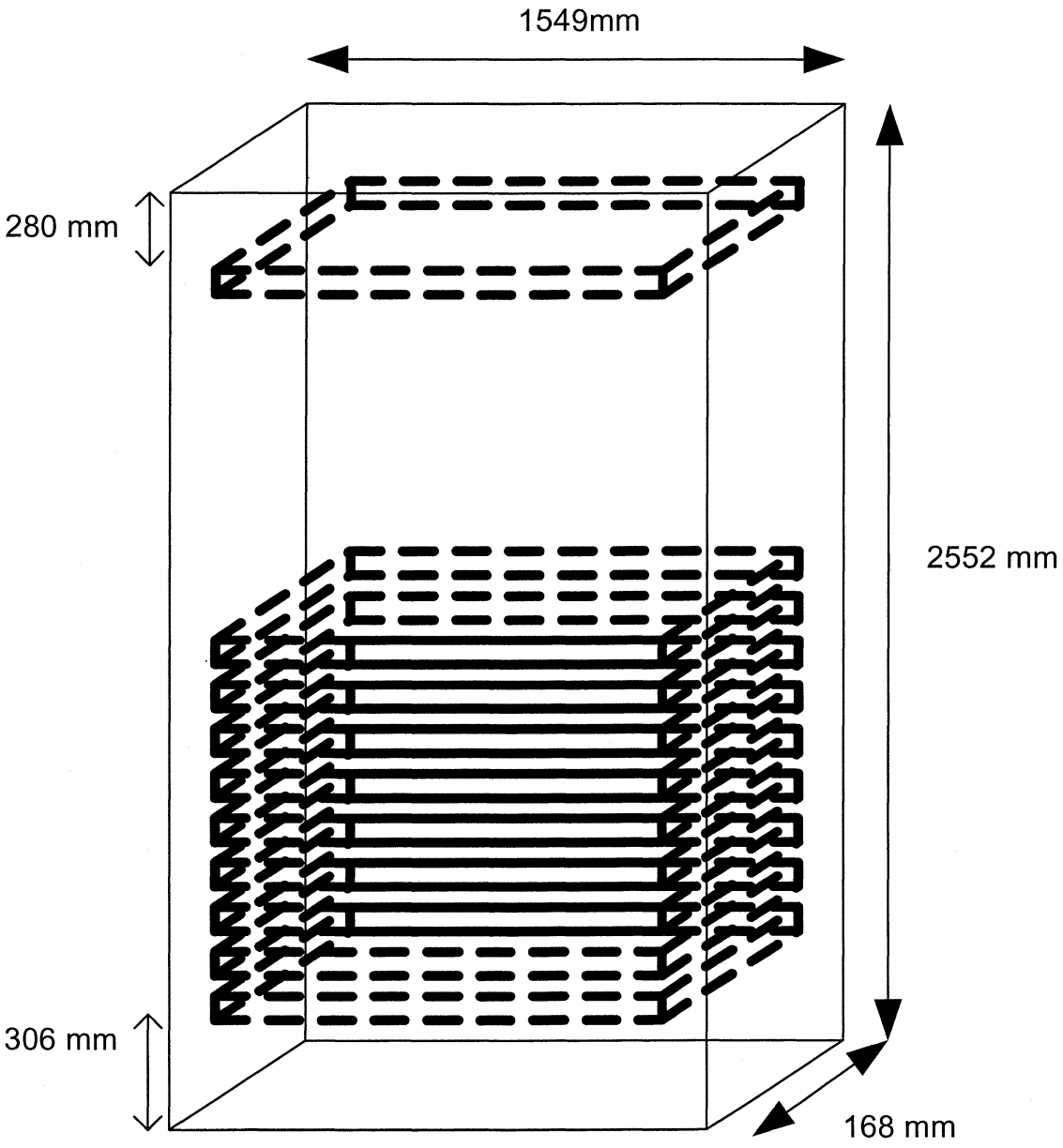

Figure A2.4 *Model Dimensions*

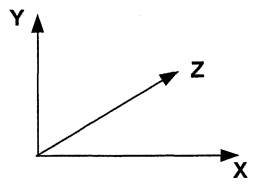

APPENDIX 3

Numerical Values of Parameters Used in Heat Transfer Model

The apparent conductivity is explained by Fotsing *et al.* [32] as follows and physical properties are given in Table A3.1;

$$\frac{1}{k_{\min}} = \frac{c}{k_g} + \frac{1-\chi}{k_w} \tag{A3-1}$$

$$k_{\max} = \chi k_g + (1-\chi)k_w \tag{A3-2}$$

$$k_{app} = \chi k_{\max} + (1-\chi)k_{\min} \tag{A3-3}$$

where χ : porosity of wood

k : conductivity

Table A3.1 *Physical Properties and Their Values* [32]

Property	Value
χ	0.2
k_g	0.035 W/m K
$k_{w\perp}$	0.130 W/m K
$k_{w\parallel}$	0.325 W/m K
k_{max}	0.267 W/m K
k_{min}	0.084 W/m K
k_{app}	0.120 W/m K

APPENDIX 4

Comparison of Heat and Mass Transfer Model Results and Plant Data

In the following figure, the results of the heat transfer model were compared whit the results of the model when the mass transfer is added and plant data.

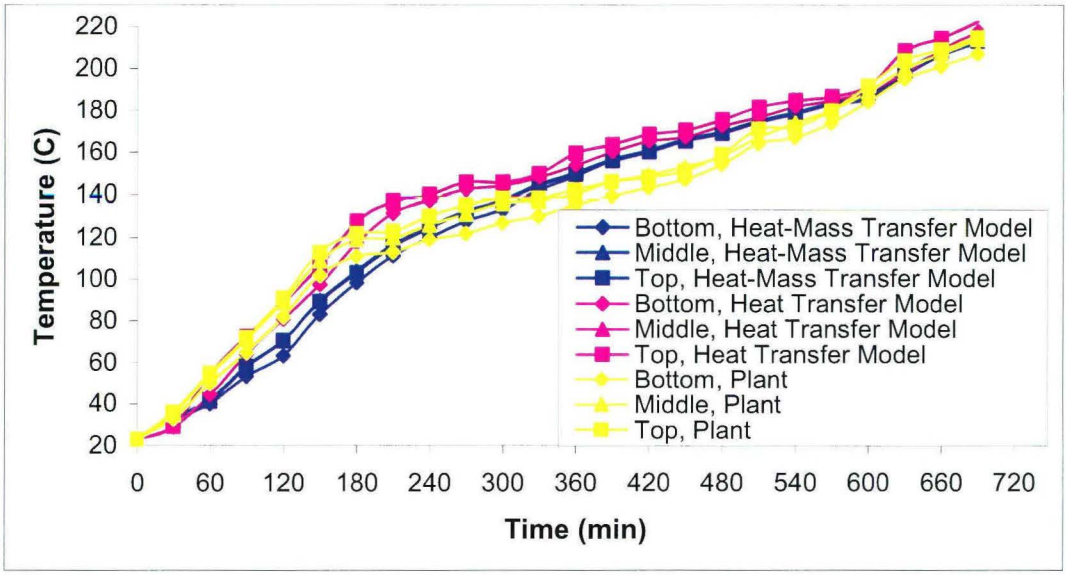

Figure A4.1 *Comparison of Heat and Mass Transfer Model Results and Plant Data*